A system-level, molecular-evolutionary analysis of mammalian phototransduction

Brandon M. Invergo

TESI DOCTORAL UPF / ANY 2013

DIRECTORS DE LA TESI
Jaume Bertranpetit and Ludovica Montanucci
Departament of Experimental and Health Sciences

For my family...

Acknowledgments

As I write this, I am sitting in an airplane, on my way to interview for a post-doctoral research position. Only now, with my thesis complete and the next steps in sight do I begin to realize that this chapter of my life is really coming to a close. It has been a goal of mine for some time to earn a PhD and so many people have helped me along the way. It will be difficult to express sufficiently my gratitude to everyone and I'm certain that I will leave someone out.

First and foremost, I must thank my two thesis supervisors, Jaume Bertranpetit and Ludovica Montanucci, for supporting me throughout this work. Somehow, I managed to convince them to let me take the project in a very uncertain direction, for which I am extremely grateful. To Jaume, I must also give thanks for your never-ending sources of cultural and historical knowledge; even the most casual conversation with you is an opportunity to learn. To Ludovica, I have to thank you for your patience with me through these years. I can be a stubborn, opinionated and argumentative person. As for your help with my writing, well, I am getting there slowly, I think.

I also have to give a deep acknowledgment to my collaborators Daniele Dell'Orco and Karl-Wilhelm Koch. Simply put, without your help and your profound knowledge of phototransduction, three out of the four manuscripts presented in this thesis would not have been possible. To Karl, I especially want to give thanks for hosting me in your lab in Oldenburg and for your excellent insights during the course of my research. To Daniele, you helped me go from not having any systems biology experience at all to having a good handle on what must be one of the bigger biochemical models available. Your long and thoughtful responses to my often confused e-mails were always much appreciated.

I also want to make a proper mention of those mentors who supported me on my path before earning this PhD. In particular, Larry Pinto at Northwestern University helped turn me around from a directionless twenty-something with naught but a bachelor's degree and a sense of apathy to a budding scientist with aspirations for a long career in the field. Bas Zwaan of Leiden University helped guide me through my first self-

designed research project, despite its disproportionately large scale for a master's thesis (and a special thanks to Vicencio Oostra and Maaike de Jong for making that research actually happen, despite 80 hour work-weeks and having to be at the lab at all hours of the night).

I'm grateful to the Bertranpetit group and the extended family of Bio-evo for the great times and good chocolates that we've had, both in the lab and out. I've made some amazing friends during my time here. I would name names, but then I would be naming everybody. I hope we all continue to run into each other in this small world of biology, no matter where we all end up.

To my family, thanks for supporting me, even when I decided that the best thing to do was to move to a different continent. More importantly, thanks for always encouraging me through every stage of my life. And finally, to Giouli, thanks for standing by me during this crazy time. I am in awe of your never-ending support and patience with me.

Thanks again to everyone.

Brandon Invergo
Somewhere over France
September 24, 2013

This research was supported by FI-DGR and BE-DGR grants from AGAUR, Generalitat de Catalunya (2011 F1 B1 00275)

Abstract

Phototransduction is the biochemical process by which a light stimulus is converted to a neuronal signal. The process functions through complex interactions between many proteins, which work in concert to tightly control the dynamics of the photoresponse. The primary aim of this thesis is to describe how the topology and kinetics of these interactions have given rise to detectable patterns of molecular evolution. To this end, a secondary aim is to develop a comprehensive mathematical model of mammalian phototransduction, first through the improvement of an existing model of the amphibian system and then through the re-tuning of that model to fit mammalian data. The results show a striking importance of the signal recovery-related proteins in shaping the photoresponse. This is reflected in relaxed evolutionary constraint on those proteins that exert the greatest dynamic influence. Meanwhile, the proteins most central to the process, while less important dynamically, are strongly constrained due to their essentiality in proper signal transduction.

Resum

La fototransducció és el procés bioquímic pel qual un estímul de llum es converteix en un senyal neuronal. El procés funciona a través d'interaccions complexes entre moltes proteïnes, que funcionen en conjunt per controlar estretament la dinàmica de la fotoresposta. L'objectiu principal d'aquesta tesi és descriure com la topologia i la cinètica d'aquestes interaccions han donat lloc a patrons detectables d'evolució molecular. Amb aquesta finalitat, un objectiu secundari és el desenvolupament d'un model matemàtic integral de la fototransducció en mamífers, primer a través de la millora d'un model existent del sistema d'amfibis i després a través de la refinament d'aquest model per ajustar-lo a les dades de mamífers. Els resultats mostren una importància notable de les proteïnes relacionades amb la recuperació del senyal en la fotoresposta. Això es reflecteix en una relaxació de les constriccions evolutives en les proteïnes que exerceixen la major influència dinàmica. Alhora, les proteïnes més centrals per al procés, tot i essent menys importants dinàmicament, es troben fortament limitades degut a la seva essencialitat en la correcta transducció de senyal.

PREFACE

The veritable explosion of data available to biologists in recent years has opened the doors to analyses of trends that would have been formerly unfeasible to address. In some ways, it represents a reversal from the predominantly reductionist approach of the previous century. Rather than considering a deep analysis of an individual gene or protein, the trend is now to rapidly assay a large number of them, possibly on the order of the entire genome or proteome. The field of evolution, for example, has seen broad, renewed interest thanks to the capabilities offered by comparative genomics techniques. These are exciting times, with Big Data promising big answers.

Nevertheless, one would hope that we are not so quick to abandon detailed characterization of individual biological units as an essential step in research. Computational and high-throughput approaches have quickly provided a swath of new data, however any such method necessarily carries with it a certain amount of error. Thus, careful verification of interesting findings remains necessary.

Early in the course of the research presented in this thesis, inaccuracies in computationally predicted data, such as protein interactions, were often encountered. Repeatedly, the answers to such uncertainties were to be found in the literature, having been resolved in a laboratory years ago. The existence of this thesis is indebted to the decades of careful biochemical assessment that have been performed until now, and due respect must be given to the researchers who have made the countless discoveries that might otherwise be taken for granted. An attempt was thus made to straddle the line between using novel computational approaches and

keeping a firm footing in the long-established knowledge of the field. I hope that this humble contribution to the field not only successfully builds upon past research but can also offer novel insights that will lead to future discoveries.

And yet of all the organs of sensation,
the eye, methinks, bears the closest
resemblance to the sun.

Republic
PLATO

Contents

List of Figures

List of Tables

Part I

Introduction

> . . . In that Empire, the Art of Cartography attained such Perfection that the map of a single Province occupied the entirety of a City, and the map of the Empire, the entirety of a Province. In time, those Unconscionable Maps no longer satisfied, and the Cartographers Guilds struck a Map of the Empire whose size was that of the Empire, and which coincided point for point with it.
>
> ---
>
> *On Exactitude in Science*
> JORGE LUIS BORGES

Chapter 1

BACKGROUND

1.1 From Phenotype to genotype and back again

Since the modern synthesis of evolutionary theory in the twentieth century, our understanding of the genetic nature of phenotypic change and the influence of natural selection on it has gradually improved. Pioneering theoretical work by J.D.S. Haldane, R.A. Fisher and Sewall Wright clearly demonstrated that natural selection on a trait determined by a discrete genetic locus or multiple loci can affect rapid change in the frequency of the loci in a population, leading to evolution in the traits. Data from formerly disparate biological fields rapidly contributed to a picture of evolution that could explain both genotypic and phenotypic variation seen from the population level and the macroevolutionary processes seen in the fossil record.

By the 1970's, with these ideas firmly entrenched in the field, the nuances of the finer mechanics at play in evolution could begin to be addressed. Richard Dawkins, building on the work of George C. Williams, put forward the notion of a gene-centered view of evolution [1]. Whereas previously the organism as a whole was viewed as the target of selection, proponents of the gene-centered view of evolution argued that it was, in fact, the genes themselves that were the smallest target of selection. Under this evolutionary paradigm, genes are "selfish," in that their own propaga-

tion is more important than the success of the other genes in their cohort, and the organism is relegated to the status of merely a "survival machine" of the genes [1]. In order to study their evolution, one would consider all of the copies of a given gene, across all individual organisms, as a population; those alleles that best promote the propagation of the gene will be selected to survive further generations. Thus, the theory gave a strong explanation for the otherwise difficult notion of altruism: relatives are more likely to carry the same alleles of a gene, and thus those alleles that promote altruism will better ensure their own survival, be it in their own "host" organism or in a closely related one. It also resolves counter-intuitive mechanisms such as intragenomic conflict, in which one gene promotes its own replication even to the detriment of the rest of the genome.

This view was not without its opponents, such as Stephen Jay Gould and Ernst Mayr. A primary objection was that it is the phenotype that is exposed to the environment and thus it is the phenotype, not the genotype, that is the interface to natural selection. Indeed, while the products encoded by the various genes in the genome each contribute their own particular functionality, the survival of the organism is dependent upon the proper interaction of all of these molecules in order to produce a viable phenotype. Thus, selection on the phenotype results in selection on the genome as a suite. Furthermore, the gene-centric view of evolution fails to properly account for phenomena such as epistasis. If two genes together affect the phenotype in a nonlinear way, then any hypothetical selection directly on either gene would be inexorably linked to the other. Thus it is difficult to reconcile the gene-centric view of evolution with the sheer complexity of the biochemical systems present in even the simplest organisms and the apparent prevalence of epistasis that emerges from them [2]. If the phenotype is an emergent property of the nonlinear combination of the effects of all of the genes in the genome and it is the phenotype that is subject to natural selection, then one would expect to see system-level evolutionary patterns. A purely gene-centric view of evolution, on the other hand, would predict largely independent evolution of the genes.

Much effort has been spent in recent years to detect the existence of

system-level patterns of molecular evolution. This has primarily resulted in two lines of investigation. In the first, research groups choose particular biochemical systems of interest in order to gain insight into their specific evolutionary histories [3–16]. In the other, attention is given to the entire interactome, that is, the set of all molecular interactions comprised by the organism, in order to detect universal patterns of evolution [17–28]. Despite the extreme differences in scope, the methodologies are similar: perform an evolutionary analysis of the system's proteins, encode biochemical knowledge of the system into a suitable structure for mathematical use and map the evolutionary data onto the system structure to detect patterns of selection.

1.2 Quantifying molecular evolution

1.2.1 Selective forces in molecular evolution

Genes evolve when sequence variation is introduced into the population and those novel variants are maintained and eventually fixed via evolutionary forces. The primary sources of genetic variation are mutations during DNA replication, recombination during meiosis and gene flow from other populations. Multiple processes then exert influence on the evolution of allele frequencies. Natural selection is the process by which alleles that impart positive fitness effects rise in frequency in a population, while deleterious alleles are removed. In the field of molecular evolution, the former event is referred to as "positive" or "adaptive" selection, while the latter is "negative" or "purifying" selection. In the absence of natural selection, simple genetic drift, arising from the random sampling of alleles during reproduction, will also lead to change in allele frequencies from generation to generation [29].

The question of the extent to which general trends in molecular evolution are the result of selection or of neutral processes such as drift has remained an open question. Beginning in the 1960's and formalized by Motoo Kimura in his book *The Neutral Theory of Molecular Evolution*, the dominant notion for a time was that, in fact, nearly all molecular evo-

lution is neutral and the action of natural selection is limited to purifying selection [30]. This was taken in contrast to phenotypic evolution, which was assumed to still proceed in a Darwinian manner. However, aside from environmental effects, all phenotypic variation has its roots in genetic processes; thus, adaptive selection must still occur to some degree at the molecular level. With knowledge of demonstrable cases of adaptive molecular evolution, such as that of the color-vision opsin receptors in primates [31], the current view may be summarized as natural selection having a role in both molecular and phenotypic evolution, with mutation being the major force for both [32].

1.2.2 Estimating molecular evolutionary rates

The most commonly used method for determining the nature of the selective forces acting on a gene is the calculation of the ratio d_N/d_S (sometimes referred to as ω). Given orthologous gene sequences for two or more species, d_N is calculated as the rate of nonsynonymous nucleotide substitutions that have occurred per nonsynonymous site in the sequence and d_S is the rate of synonymous substitutions per synonymous site. Their ratio may then be taken as an indication of the degree of non-neutral selective forces acting on the sequence during the divergence of the phylogeny. When $d_N = d_S$, the gene is said have evolved neutrally, based on the assumption that synonymous substitutions are largely neutral in nature. $d_N < d_S$ indicates that the gene has been under purifying selection, such that non-synonymous substitutions have been removed from the population at a greater rate than synonymous substitutions. $d_N > d_S$ would thus imply that adaptive selection has occurred, with more non-synonymous substitutions having been fixed than what would be expected under the assumption of neutrality.

Several methods have been developed for estimating d_N/d_S. Early methods, typified by that of Nei and Gojobori [33], are simple in their dependence on basic counting methods but they are nevertheless illustrative of the task. First, the numbers of synonymous and nonsynonymous sites per codon are counted. For each position, i, in a codon, the fraction f_i of

synonymous changes is computed; the numbers of synonymous (s) and nonsynonymous sites (n) are then given by $s = \sum_{i=1}^{3} f_i$ and $n = 3 - s$. For example, for the codon TGT, $f_1 = 0$ (no possible synonymous substitutions), $f_2 = 0$ and $f_3 = \frac{1}{3}$ (one possible synonymous substitution: T $\rightarrow$ C). Therefore, $s = \frac{1}{3}$ and $n = \frac{8}{3}$. The total number of synonymous (S) and nonsynonymous (N) sites in a sequence are the sum of s and n, respectively, across the whole sequence. The number of synonymous (s_d) and nonsynonymous changes (n_d) per codon between two sequences are then counted, treating multiple mutational paths between two codons as being equally likely, and calculating the resulting counts as the average between all possible paths. The counts are then summed to give the total number of synonymous (S_d) and nonsynonymous (N_d) changes across the sequence. Proportions of synonymous (p_S) and nonsynonymous (p_N) differences can be estimated by $p_s = S_d/S$ and $p_n = N_d/N$. Finally, the number of synonymous substitutions (d_S) and nonsynonymous substitutions (d_N) may be calculated by the formula [34]:

$$d = -\frac{3}{4} log_e \left(1 - \frac{4}{3}p\right) \tag{1.1}$$

where p is either p_S or p_N. Modern methods integrate more biologically meaningful parameters, such as transition/transversion bias and chemical differences between amino acids. Additionally, more sophisticated statistical methods are now used in the estimation of d_N and d_S, such as the Markov-process model of Goldman and Yang [35] or the Bayesian approach of Seo et al. [36].

1.2.3 Tests of adaptive selection

Using neutral evolution as a null hypothesis, it is possible to statistically test for the occurrence of adaptive selection at specific codon sites during phylogenetic divergence. Two main classes of tests exist: the individual site (IS) and the pooled site (PS) methods. The former method was first proposed by Suzuki and Gojobori [37] and is performed by constructing a phylogenetic tree and then counting the total number of synonymous

and nonsynonymous substitutions across all branches of the tree. If the number of nonsynonymous substitutions is significantly greater than the number of synonymous substitutions at a given codon, then that codon is taken to have been under positive selection. This class of tests has since been improved through likelihood- and Bayesian-based methods [38–40].

The PS method, on the other hand, fits a sequence alignment with two nested models, allowing for a likelihood-ratio test of significance. In the null model, all sites in the alignment are assumed either to have $d_N/d_S < 1$ or $d_N/d_S = 1$, that is, all sites are either evolving neutrally or are under purifying selection. In the alternative model, another site class is added, such that some proportion of sites are fit by the model to have evolved with $d_N/d_S > 1$ [41, 42]. For example, in the test between the so-called models M7a and M8, the sequences are first fit with model M7a, under which they are partitioned into seven site classes (one with $d_N/d_S = 1$ and six with $d_N/d_S < 1$) with d_N/d_S values for the sites following a β distribution. Next, the same data is fit to model M8, which adds an eighth site class allowing for $d_N/d_S > 1$. A likelihood ratio test of the models then determines whether adding adaptive selection to the model can explain the data significantly better. Complementary Bayesian methods have also been proposed to make *a posteriori* inferences about the specific codons that have been under adaptive selection [41–43].

The advantage of these tests over the simple calculation of d_N/d_S is that they allow individual sites to evolve at different rates; calculating a single d_N/d_S ratio for all sites requires a very strong trend of adaptive selection to produce a value greater than one. Nevertheless, these methods of detecting adaptive selection still tend to have low power in general [44]. In particular, they require sustained, strong adaptive selection to have been acting on a codon during phylogenetic divergence, which may be a rare event. Indeed, brief episodes of adaptive selection are more likely to be the common case. In order to detect episodic adaptive selection, multiple methods have been developed which allow evolutionary rates to vary not only between codons but also between phylogenetic branches [45–47]. These methods have proven to have more power in detecting adaptive selection and suggest that previous methods have led to a

significant underestimation of the number of sites undergoing adaptation [47, 48].

1.3 Mathematical representations of biological systems

1.3.1 Networks

The most common tool in evolutionary research for the mathematical representation of a system is the network, which is a structure that consists of "nodes" and the "edges" that connect them. In biology, proteins are typically encoded as the nodes and edges represent physical interactions between them. Depending on the system in question, a variety of types of interactions might be used: physical, protein-protein interactions; shared metabolites; or regulatory relationships, for example. In a graphical representation of the network, the nodes will often be circles and the edges will be drawn as lines connecting them (Figure 1.1). Importantly, representing a system in this way allows a quantitative characterization of both the topology of the network as a whole and of the position of individual nodes in the network.

Of particular interest in the study of molecular evolution are the node-specific properties. Several node metrics exist. Perhaps the most commonly encountered measurement is node connectivity, also known as "degree", which is simply a count of the number of edges associated with a node. In biological terms, this measures the number of interactions in the system that include a given protein. Other useful properties include a variety of different measurements of centrality, particularly closeness centrality and betweenness centrality. Both depend on the notion of a shortest path, which is a minimal sequence of nodes that connect two nodes of interest.

Betweenness centrality is calculated as the number of shortest paths that pass through a node [49]:

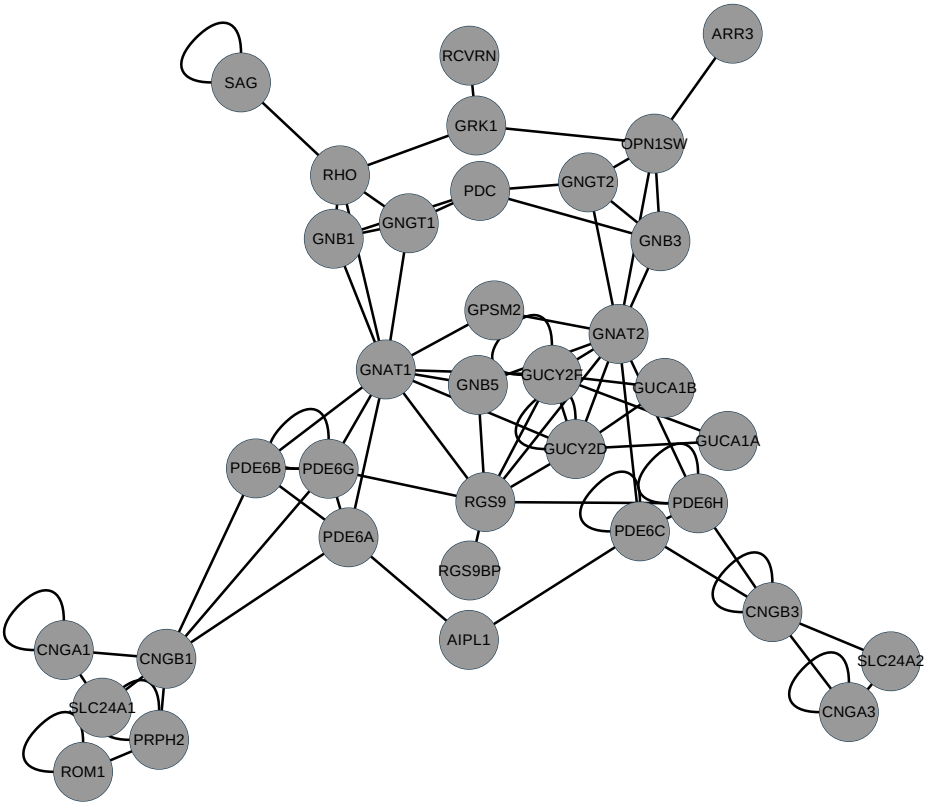

Figure 1.1: A typical network representation of a molecular system, in this case the visual phototransduction system (Chapter 3). Nodes (circles) represent proteins and edges (lines) represent interactions between the proteins.

$$c_B(v) = \sum_{s,t \in \mathbf{N}} \frac{\sigma(s,t|v)}{\sigma(s,t)} \tag{1.2}$$

where v is the node of interest, s and t are two other nodes in the network $\mathbf{N}$, $\sigma(s,t)$ is the total number of shortest paths between s and t, and $\sigma(s,t|v)$ is the total number of shortest paths between s and t that pass through v. A high betweenness centrality score indicates that the node acts as a sort of "information bridge" in the network.

Closeness centrality, on the other hand is the reciprocal of the sum of the shortest path distances between a node and all the other nodes in the network [49]:

$$c_C(v) = \frac{n-1}{\sum_{u=1}^{n} d(v,u)} \tag{1.3}$$

where n is the number of nodes in the network and $d(v,u)$ is the shortest path distance between nodes v and u. Closeness centrality may be thought of in terms similar to the common-language usage of the word "central", in that a central node is on average closer to most of the other nodes.

1.3.2 Dynamic models

Less commonly used in the study of evolution are dynamic models of biochemical systems. Under this paradigm, a mathematical model is constructed that can simulate known system dynamics. It can thus serve as a test of the breadth of knowledge of a system: a model is built to include known reactions and if the simulations it produces are accurate, it is likely that the primary mechanisms of the system are well-understood. Where a model falls short, it points to potential gaps in our knowledge or shortcomings in the mathematical implementation.

A primary choice in building a model is whether to aim for deterministic or stochastic simulation of molecular activities. In the former case, reactions are described by a system of differential equations that track the concentrations of the various molecules in the system. At any time point

in the simulation, it is possible to calculate the exact concentrations at the next instant. Stochastic simulation, on the other hand, is performed by considering the probability of molecular events and randomly determining the time and nature of the next reaction to occur. Thus, at any time point, one can only know what concentrations are likely at the next instant. Stochastic models are necessary for accurately simulating dynamics at low molecular counts, where the probability of encounter between two molecules becomes significant. For considering large-scale dynamic trends across a system, deterministic models are often sufficient. In this thesis, attention will be given to deterministic modeling, thus stochastic modeling will not be addressed further.

In building a deterministic model, the specific chemical rate law used will determine the mathematical formulation of a reaction. A common rate law is the law of mass action, in which a reaction occurs at a rate proportional to the product of the concentrations of the participating molecules. Thus, the reversible reaction $\mathrm{A} + \mathrm{B} \rightleftharpoons \mathrm{A} \cdot \mathrm{B}$ would occur at a forward rate of $k_f[A][B]$ and at a reverse rate of $k_r[AB]$ for some rate constants k_f and k_r. A mathematical model of this reaction would track the concentrations of A, B and $\mathrm{A} \cdot \mathrm{B}$ via a system of differential equations:

$$\begin{aligned} \frac{d[A]}{dt} &= -k_f[A][B] + k_r[AB] \\ \frac{d[B]}{dt} &= -k_f[A][B] + k_r[AB] \\ \frac{d[AB]}{dt} &= k_f[A][B] - k_r[AB] \end{aligned} \tag{1.4}$$

Were the system to include more reactions, particularly others that produce or consume reactants A, B or $\mathrm{A} \cdot \mathrm{B}$, the above equations would include terms for each reaction in which the specific molecule participates. Therefore, a general equation for the change in the concentration of some molecule X over time is [50]:

$$\frac{d[X]}{dt} = \text{synthesis} - \text{degradation} - \text{phosphorylation} + \text{dephosphorylation} - \text{binding} + \text{release, etc.} \tag{1.5}$$

1.4 Network analyses of molecular evolution

1.4.1 System-level analyses

To date, studies of molecular evolution in the context of complex systems have focused on the use of networks. While relationships between molecular evolutionary histories and system topology have been routinely described, the particular patterns appear to vary from system to system. Much of the past research has utilized systems with largely linear structures, which permits the notion of "upstream" and "downstream" proteins. Several studies on plant metabolic pathways suggested that genes encoding upstream proteins tend to be under stronger evolutionary constraint (low d_N/d_S ratios) [3, 4, 7, 8, 10]. When similar methods were used to characterize linear signaling pathways, the results were contradictory: while the case of the Ras-mediated signal transduction pathway in *Drosophila* species confirmed past results that upstream proteins are more evolutionarily constrained [5]; multiple studies on the insulin/TOR pathway, on the other hand, found d_N/d_S ratios to decrease along the upstream-downstream axis in both *Drosophila* [11, 51] and across several vertebrate species [13]. A similar trend in the strength of purifying selection at downstream proteins was also described for the primate N-glycosylation pathway [12].

Branch points in metabolic pathways have also been shown to be sites of differential targeting by natural selection. In particular, they have been described to be both under stronger purifying selection [9] and more likely to be targets of adaptive selection [6]. Results from a study of patterns of evolution in the N-glycosylation pathway of humans lent further support to the notion that branch points are likely targets of adaptive selection [15].

Finally, measurements of network topology have been implicated in defining patterns of molecular evolution as well. In the previously described study of primate N-glycosylation, it was found that the correlation between d_N/d_S and pathway position was confounded by a correlation between d_N and node connectivity, a covariate of position [12]. In an investigation into the evolution of the insulin/TOR signaling pathway in human populations, it was found that genes encoding proteins with higher connectivity, closeness centrality and betweenness centrality were more likely targets of adaptive selection, while position in the pathway had no effect [14].

1.4.2 Interactome-level analyses

Results on molecular evolutionary patterns on the interactome level have been similarly controversial. An initial study on the interaction network of *Saccharomyces cerevisiae* described a negative correlation between the connectivity of proteins and evolutionary rates [17]; thus, it was concluded tht the well-connected "hubs" of the network are more constrained in their evolution. These results were quickly called into question and they were shown to be strongly dependent on a small percentage of highly connected, highly conserved proteins [18]. This criticism prompted the original authors to expand the network and the phylogeny used in order to reconfirm their findings [19]. A strong bias in the method towards counting more interactions for abundant proteins was later described, which once again eliminated any correlations between evolutionary rates and interactome network measurements [21].

Later research into the relationship between interactome topology and molecular evolution proved more promising. In a comparison of the protein-protein interaction networks for three eukaryotic species, it was found that connectivity and centrality, particularly betweenness centrality, were both significant, negative correlates of d_N/d_S [22]. This result was corroborated in a later study using the *Arabidopsis thaliana* interactome [26]. Furthermore, it was found that proteins at the periphery of the human protein-protein interaction network were more likely to be targets

of positive selection [23]. Thus, it would appear that central proteins are strongly conserved while innovation occurs at the periphery.

In addition to protein-protein interaction networks, other systems were considered. Two investigations into the influence of the structure of the whole metabolic network found that central and highly connected enzymes are more evolutionarily constrained in yeast [24] while enzymes residing at metabolic branch points were under stronger purifying selection in *Drosophila* species [25]. Finally, the hierarchical nature of cellular signaling was considered and it was found that d_N/d_S values decrease downstream along the signal flow from the extracellular space to the nucleus [27, 28], however this effect disappears when accounting for confounding factors such as expression level and connectivity [27].

1.4.3 Summary of evolutionary network studies

Taken together, these results clearly indicate that there is, indeed, a relationship between the topology of biochemical interactions in the cell and molecular evolutionary patterns, however universal patterns remain elusive. A particularly interesting question is whether the interactome- or system-level perspective is more relevant to address these questions. It can be argued that, because it ostensibly includes all of the protein interactions occurring in the organism, the interactome should be more relevant in drawing a connection between molecular and phenotypic evolution. However, the very fact that there are several published studies, in which effectively the same overall methodologies were used, but from which different results were found, indicates a fundamental problem with this line of research. Namely, such research is highly dependent upon having accurate whole-proteome interaction networks in order to make consistent conclusions. Nevertheless, the concordance between the more recent interactome-level studies indicates that robust, universal patterns of molecular evolution are likely to be found.

System-level studies, on the other hand, offer high-confidence networks derived from detailed biochemical knowledge rather than from high-throughput methods. Unfortunately, it would appear that no gen-

eral principles are to be found in such systems due to the unique selective pressures imposed on each by the environment. Nevertheless, it remains important to characterize the molecular evolutionary patterns in many systems in order to understand the full suite of patterns to be found. Ideally, interactome-scale patterns of molecular evolution will be found that can also account for the varied results from studies on individual systems; this depends upon an ever-higher resolution of the molecular interactions that occur within the organism and a clearer understanding of their modular organization.

1.5 Visual phototransduction

The particular system of interest in this thesis is the visual phototransduction pathway. Phototransduction is the biochemical process by which a light stimulus is converted into a neuronal response. In vertebrates, it occurs in the rod and cone photoreceptor cells of the retina. These two cell types mediate different aspects of vision. The highly sensitive rod cells are primarily active under scotopic, or low-light, conditions, owing to their ability to detect and amplify a response from even a single photon of light. However, rods saturate and become unable to generate further responses during prolonged, bright stimuli. Cone photoreceptors, on the other hand, do not saturate in bright light and thus mediate vision under photopic, or bright-light, conditions. Rods and cones are differentiated by their morphology, their electrophysiology, their opsin receptors, and the proteins associated with their phototransduction cascade [52].

1.5.1 Biochemical description

A long history of research into the chemical mechanisms of phototransduction, beginning in the 1870's with the first description of rhodopsin and flourishing from the 1970's through the present, has resulted in a highly detailed body of knowledge [53]. Signal transduction proceeds in a similar manner in both rod and cone cells, however most of the pro-

teins involved have rod- and cone-specific isoforms. Of the two, the rod-specific pathway is particularly well-studied. Research on cone phototransduction, on the other hand, has been hampered by the relatively low cone-to-rod ratio of mammalian retinas and the fragility of the cone cells [53]. In recent years, however, the zebrafish (*Danio rerio*) has emerged as an excellent model for the study of cone vision, due not only to its cone-dominated retina but also to the late onset of rod-mediated vision during development [54]. Thus, our knowledge of the mechanisms of cone phototransduction is quickly expanding.

Phototransduction is a prototypical G-protein signaling pathway and the rod-specific pathway is perhaps one of the best studied pathways of this class (Figure 1.2). For a detailed description of the mechanisms of the pathway, see the reviews by Pugh Jr and Lamb [55] or Yau and Hardie [56]. In short, the response is initiated by the absorption of a light stimulus by a visual chromophore associated with an opsin receptor, converting the receptor into an active form (R^*). R^* next binds the heterotrimeric G-protein transducin (G_t) and catalyzes the release of GDP from G_t. G_t is then free to bind GTP, which causes the dissociation of the the GTP-bound, active α subunit ($G^*_{t\alpha}$) from the heterotrimer [57]. $G^*_{t\alpha}$ binds and activates phosphodiesterase (PDE), causing it to hydrolyze cyclic GMP (cGMP) to GMP [58, 59]. Decreasing cGMP concentrations result in the closure of cGMP-gated ion channels that are open in the darkness, preventing the influx of calcium (Ca^{2+}) and sodium (Na^+) ions through the channels. Meanwhile, Ca^{2+} and potassium (K^+) ions are constantly extruded in exchange for Na^+ ions by a Na^+/Ca^{2+} K^+ ion exchanger [60, 61]. This leads to a drop in the cytoplasmic Ca^{2+} concentration and the subsequent hyperpolarization of the cell, initiating the neuronal response.

Several concurrent processes act to deactivate the pathway, in order to prepare it to transduce another stimulus. Falling Ca^{2+} concentrations induce a conformational transition in the protein recoverin (Rec) [62], causing it to dissociate from rhodopsin kinase (RK) [63, 64]. Free RK binds R^* and phosphorylates it, with each R^* supporting multiple phosphates [65–67]. The sequential addition of phosphates to R^* induces a step-wise reduction in the affinity of both G_t [68] and RK [69] for it

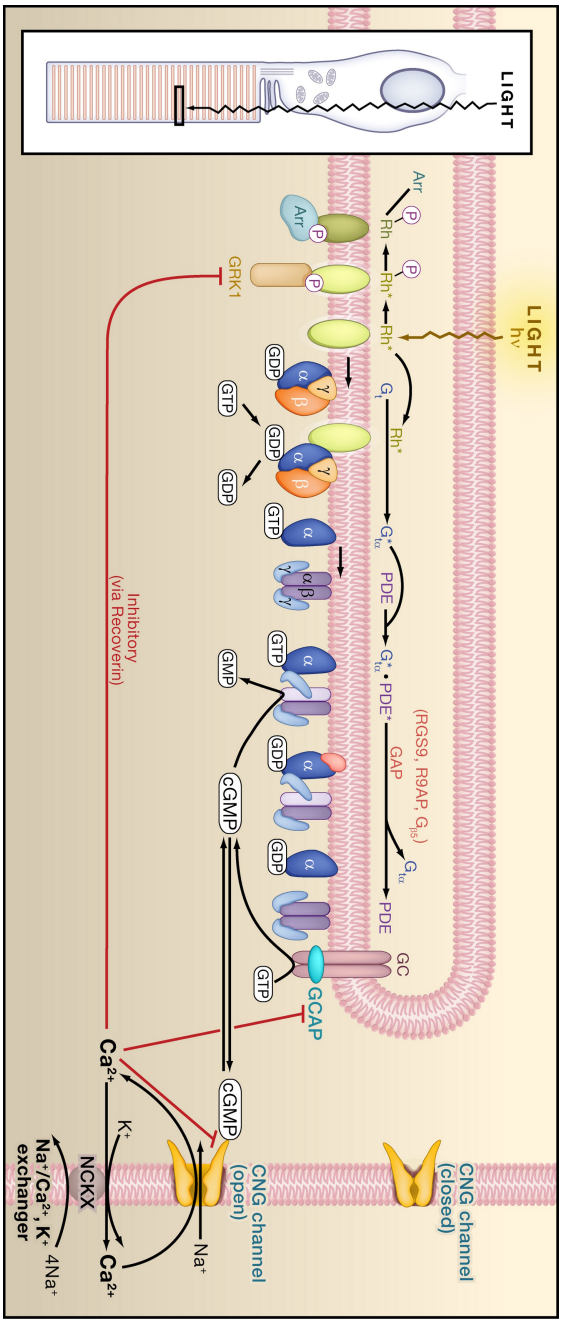

Figure 1.2: Schematic of rod phototransduction (from Yau and Hardie [56]).

while increasing the affinity of arrestin (Arr) for it [68, 70]. Arr dissociates from homodimeric and homotetrameric storage forms to bind R^*, capping it and preventing the further activation of the pathway [71–73]. The light-sensitive chromophore is released from R^* and carried out of the photoreceptor for recycling. Meanwhile, a regulator of G-protein signaling (RGS9-1) binds the $G^*_{t\alpha} \cdot$ PDE complex and accelerates the innate GTPase functionality of $G^*_{t\alpha}$, leading to the deactivation of the complex and the reformation of the G_t heterotrimer [74]. Finally, low Ca^{2+} concentrations cause the activation of guanylate-cyclase activating proteins (GCAPs), inducing rapid resynthesis of cGMP by guanylate cyclases and the subsequent re-opening of the cGMP-gated ion channels [75].

1.5.2 Dynamic models

The wealth of biochemical data available on phototransduction has resulted in a rich history of mathematical modeling of the photoresponse. An early effort by Forti et al. [76] included the basic mechanisms of signal amplification as well as a detailed representation of Na^+, Ca^{2+} and cGMP dynamics. Modeling of the second messenger dynamics was further employed by Pugh Jr and Lamb [77] to confirm contemporary hypotheses about the system. Lamb and Pugh Jr [78] also developed a much more detailed account of the activation steps of the signaling pathway. Additionally, efforts were made to stochastically simulate the initial interactions between R^* and G_t and the generation of activated PDE, which provided a more realistic view of the molecular interactions, particularly under the single-photon response paradigm [79, 80]. By 1996, the amplification dynamics were largely resolved [81], however the recovery mechanisms remained elusive. A seminal book chapter by Pugh Jr and Lamb [55] served to compile the previous modeling efforts, accurately covering signal amplification and second messenger dynamics, while also providing basic signal deactivation mechanisms.

Building upon the stochastic work of Lamb [79] and Felber et al. [80] a more comprehensive model of the pathway was built to include RK-mediatated deactivation of R^* that could accurately reproduce the single

photon response [82]. The model eschewed the previous models' two-dimensional protein diffusion in favor of more detailed reactions occurring in a well-mixed substrate. The model also explicitly linked PDE activation to the downstream Ca^{2+} and cGMP dynamics. This model was later adapted to further simulate responses to bright flashes in addition to the stochastic dim-light responses [83]. Dell'Orco et al. [84] significantly extended the model of Hamer et al. [83] to include accurate PDE deactivation via RGS9-1; a reaction for the reformation of G_t from the separate subunits; a reaction for the reconstitution of deactivated rhodopsin; and reactions for the slow activation of the cascade by the deactivated, chromophore-free receptor (Figure 1.3). The model was then used to perform robust simulations of light-adaptation, including the simulation of a variety of mutant conditions. The model of Dell'Orco et al. [84] has been further expanded in this thesis in Chapter 4 and converted to fit mammalian biochemical and electrophysiological data in Chapter 5.

Recently, attention has been given to modeling the influence of the spatial structure of the photoreceptor on the dynamics of the photoresponse. Initial work produced a detailed model of the diffusion of the second messengers cGMP and Ca^{2+} during a single-photon response, which demonstrated the importance of local changes to cGMP concentration and localization of the membrane current [85–87]. The modeled structure of the photoreceptor was further refined to include incisures in the rod outer segment disk membranes where phototransduction occurs, demonstrating that these features both act as cytoplasmic tunnels for the diffusion of the second messengers as well as to limit the diffusion of signaling proteins along the disk, effectively localizing the single photon response to a limited region of the photoreceptor [88].

1.5.3 Molecular evolution

A primary focus in the study of the evolution of the proteins of the phototransduction system has been on the evolution of the opsins [89–93]. Particularly, the specific repertoire of expressed opsins has evolved to vary between vertebrate lineages. Five families of opsins have been described:

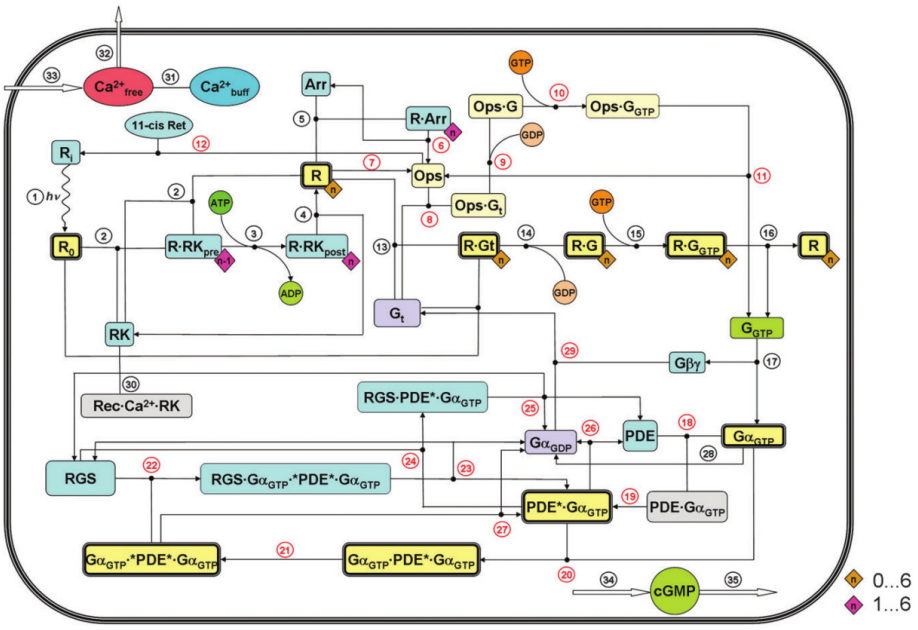

Figure 1.3: The reaction network of a comprehensive dynamic model of phototransduction as implemented by Dell’Orco et al. [84].

RH1, RH2, SWS1, SWS2 and M/LWS [52]. Opsin suites that include representatives from all five known families have been found in some, but not all, species of teleost fish, amphibians, reptiles and birds [52]. Mammalian species are therefore notable in their distinct lack of opsins. Most mammalian species only carry three opsins: rhodopsin (from the RH1 family), one M/LWS ("red/green") opsin and one SWS1 ("blue") opsin and are thus dichromats (capable of interpolating between two colors) [52]. It is thought that, because of the nocturnal nature of early mammals, two opsin genes were lost due to a lack of selective pressure to maintain them [93]. A duplication event in the M/LWS opsin gene during the divergence of Old World apes and the subsequent functional divergence of the copy resulted in a fourth opsin type and trichromatic vision for these species [31]. When considering the sequence evolution of opsins, the most frequently cited sites of adaptive selection events are those that determine the spectral tuning of the receptor, that is, the wavelength of light that causes maximal absorption of the stimulus. To date, a great number of studies have been published describing selection at spectral tuning sites, particularly at amino acids near the retinylidene Schiff's base counterion [94–103].

Less attention has been given to the molecular evolution of the downstream phototransduction proteins. Hisatomi and Tokunaga [104] constructed phylogenetic trees of eight phototransduction gene families aside from the opsins, and demonstrated that most of the trees show two clades, representing the rod and cone isoforms. They speculated that the difference in dynamic characteristics of the cone and rod phototransduction pathways were likely due to the molecular differences that have evolved between these isoforms and that these proteins have evolved as a system. This work was later expanded upon to include thirteen gene families [105]. The existence of cone and rod isoforms of the proteins was attributed to two whole-genome duplications (tetraploidizations) that occurred early in the vertebrate divergence. It was found that ten out of the thirteen families gained new members during these tetraploidization events. The other three families also underwent duplication events around the same period, however it is less clear that these were due to the genome

doublings. Finally, in a recent study, human SNP genotyping data for twenty phototransduction genes was used to detect signatures of adaptive selection [106]. Of the twenty genes considered, six showed significant signals: *RGS9*, encoding RGS9-1; *GNB1*, encoding the β subunit of rod G_t, $G_{t\beta}$; *GNAT1*, encoding rod $G_{t\alpha}$; *RHO*, encoding rhodopsin; *PDE6G*, encoding the γ subunit of rod PDE, PDE_γ; and *SLC24A1*, encoding the Na^+/Ca^{2+} K^+ ion exchanger.

In summary, while it is clear that the spectral tuning of the opsins presents a trait that is of evolutionary relevance, past results indicate that the other proteins comprised by the phototransduction pathway deserve closer attention. In particular, though we now have a clear picture of the phylogenetic diversity of these proteins in vertebrates, we have less information on recent evolutionary trends. Furthermore, while Hisatomi and Tokunaga [104] speculated that the specific dynamic properties of the proteins and their participation in the system have influenced their evolution, no further analysis of these hypotheses was done. In this light, this thesis presents a comprehensive dataset of recent molecular evolutionary rates in phototransduction genes as well as results explaining the system determinants of these rates in Chapters 3 and 6.

Chapter 2

OBJECTIVES

This work has two main objectives. The primary aim is to gain a better understanding of the evolutionary forces that have acted on the proteins of the phototransduction pathway during the mammalian divergence, particularly with regard to their evolution as a system. In order to accomplish this aim, robust system-level descriptions of the pathway were required. Thus, a second objective arose to contribute to and improve an existing mathematical model of phototransduction.

2.1 System-level evolutionary analysis of phototransduction

A thorough analysis of the evolutionary histories of the proteins of the phototransduction pathway was performed in order to fill an important gap in our understanding of these proteins, especially given the dearth of evolutionary data on the downstream phototransduction proteins. In addition to giving a more complete understanding of the evolution on vision, these results will also provide general insight into the selective constraints acting on proteins of signaling pathways, particularly of the G-protein signaling cascades.

While several analyses of system-level patterns of molecular evolu-

tionary rates have been performed, the focus has been predominantly on linear and branched pathways. The phototransduction pathway, on the other hand, has a more complex structure given by its parallel recovery and feedback processes. Thus, a network-based, molecular evolutionary analysis of phototransduction would be an excellent contribution to the field. To this end, the pathway was encoded as a protein-protein interaction network and the relationship between the evolutionary rates and the network topology was described (Chapter 3).

The phototransduction process is highly dynamic. It is easy to conceive of the fitness advantages of effective signal amplification and efficient signal recovery. One would expect that the proteins that have the potential to greatly disrupt these dynamics would be strongly constrained in their evolution. In order to test this hypothesis and to determine how these dynamics have influenced natural selection, a novel method for analyzing the system-level determinants of molecular evolutionary rates is presented in Chapter 6. Whereas the network method captures the topology of the interactions between proteins, the method presented herein employs a mathematical model of the system in order to ascertain the influence of these interactions on the dynamics of the system.

2.2 Modeling of the phototransduction system

As evidenced by the model-based evolutionary research presented in Chapter 6, a robust, comprehensive mathematical model of the phototransduction pathway can be an useful tool in the study of this system. To this end, the amphibian phototransduction model of Dell'Orco et al. [84] was further extended in Chapter 4 to include more recent biochemical findings. The chief purpose of this model was to provide the most comprehensive coverage of the phototransduction reaction network in a dynamic model to-date, to be used in biochemical research. As a proof of principle, this model was used to compile and verify what is known about the complex dynamics of the recovery phase of the photoresponse, which, as seen in Chapter 6, have the greatest influence on the overall shape of the response.

While much of the past comprehensive modeling efforts have been based on amphibian biochemical and electrophysiological data, a majority of modern vision research is performed using mammalian species, particularly mice. Previous amphibian models were shown to produce qualitatively accurate simulations of the mouse photoresponse, however a quantitatively predictive model of the murine response would be extremely useful. To this end, the updated amphibian model was then converted to fit mammalian data in Chapter 5. While an immediate purpose of this mammalian model was its use in the evolutionary analysis of Chapter 6, it is also intended to be an important tool in the biochemical investigation of phototransduction.

The comprehensive nature of the models allows them to be used in hypothesis formation for future biochemical research. To demonstrate this, they have been shown to robustly predict the effects of several mutant conditions and thus may be used to explore probable phenotypic effects of mutations before the expensive generation and maintenance of experimental animal lines. Additionally, as demonstrated in Chapter 4, the models can assist in the prediction of the system effects of molecular mechanisms that may be difficult to detect in the laboratory.

Furthermore, it is quite common for research articles on specific mechanisms of phototransduction to include small, purpose-built models of the mechanisms in question (*e.g.* [107, 108]). While these often perform well for the limited scope of the article, they "average out" potentially interesting interactions with other parts of the system by simplifying the other reactions. The inherently modular nature of the models presented in this thesis allows new mechanisms to be inserted without disrupting the overall model behavior. Thus, a goal is to provide these models to other researchers to simulate specific functions of interest without the need to re-develop a redundant model of the rest of the pathway.

Lastly, the maintenance of a comprehensive model of the phototransduction system provides an ongoing, quantitative assessment of the breadth and depth of our knowledge of its underlying mechanisms. When the model fails to predict a known behavior, it points to a shortcoming in the implementation. By being confident that all known reactions are present

in the model and that all parameter values are realistic, we can be reasonably sure that this shortcoming represents a gap in our knowledge of the system. We aimed to use these models in such a way to identify potentially unknown mechanisms of phototransduction. This can help determine future directions of research. As new reactions are uncovered and physiological parameter values are measured, the model can be updated and retested. It is thus intended that these models be continually developed as new data on the phototransduction system is presented.

Part II

Results

Then the dark began to go in smooth,
bright shapes…

The Sound and the Fury
WILLIAM FAULKNER

Chapter 3

A SYSTEM-LEVEL, MOLECULAR-EVOLUTIONARY ANALYSIS OF MAMMALIAN PHOTOTRANSDUCTION

Brandon M. Invergo, Ludovica Montanucci, Hafid Laayouni and Jaume Bertranpetit

---

Reformatted from:
Invergo BM, Montanucci L, Laayouni H, Bertranpetit J. A system-level, molecular evolutionary analysis of mammalian phototransduction. *BMC Evolutionary Biology*, 13:52, 2013. doi:10.1186/1471-2148-13-52.
https://www.biomedcentral.com/1471-2148/13/52/

Chapter 4

EXPLORING THE RATE-LIMITING STEPS IN VISUAL PHOTOTRANSDUCTION RECOVERY BY BOTTOM-UP KINETIC MODELING

Brandon M. Invergo, Ludovica Montanucci,
Karl-Wilhelm Koch, Jaume Bertranpetit
and Daniele Dell'Orco

Reformatted from:
Invergo BM, Montanucci L, Koch K-W, Bertranpetit J, Dell'Orco D. Exploring the rate-limiting steps in visual phototransduction by bottom-up kinetic modeling. *Cell Communication and Signaling*, 11(1):36,2013.doi: 10.1186/1478-811X-11-36.
http://www.biosignaling.com/content/11/1/36/

Chapter 5

A COMPREHENSIVE MODEL OF LIGHT ADAPTATION IN MAMMALIAN ROD CELLS

Brandon M. Invergo, Daniele Dell'Orco,
Ludovica Montanucci, Karl-Wilhelm Koch,
and Jaume Bertranpetit

Manuscript in preparation

Abstract

Vertebrate visual phototransduction is perhaps the most well-studied G-protein signaling pathway. A wealth of available biochemical and electrophysiological data has resulted a rich history of mathematical modeling of the system. However, while the most comprehensive models have relied upon amphibian biochemical and electrophysiological data, modern research typically employs mammalian species, particularly mice, which exhibit significantly faster dynamics. In this work, we present an adaptation of a previously published, comprehensive model of amphibian phototransduction that can produce quantitatively accurate simulations of the mammalian photoresponse. We demonstrate the ability of the model to predict responses to a wide range of stimuli and under a variety of mutant conditions. Finally, we discuss features of the photoresponse that the model fails to accurately simulate and the possible sources of these discrepancies.

5.1 Introduction

Visual phototransduction is the biochemical process by which a light stimulus is translated into a neuronal signal. The response is triggered by the absorption of photons of light by visual pigments, which then activate a prototypical G-protein signaling cascade [53, 55]. The first steps of phototransduction involve the binding of the heterotrimeric G-protein transducin (G_t) to the activated receptor, rhodopsin (R^*). R^* catalyzes the exchange of GTP for GDP bound to G_t, which results in the dissociation of the $R^* \cdot G_t$ complex and the further dissociation of the $G_{t\alpha}$ subunit from the G_t heterotrimer. $G_{t\alpha}$ is then free to bind and activate a phosphodiesterase (PDE), resulting in the hydrolysis of intracellular cGMP. This leads to the closure of cGMP-gated ion channels and a subsequent drop in the intracellular Ca^{2+} concentration, and a consequent hyper-polarization of the cell membrane.

Deactivation of the pathway consists of several concurrent mechanisms. Decreasing Ca^{2+} concentrations induce a change in conformation of the protein recoverin (Rec), causing it to dissociate from rhodopsin kinase (RK). The kinase is then free to bind and phosphorylate R^*. Increasing phosphorylation levels of R^* lead to decreased binding affinities of both RK and G_t for it, while the affinity of Arrestin (Arr) for R^* increases. Arr dissociates from its homo-dimeric and homo-tetrameric storage form to bind R^*, preventing further activation of the pathway and effecting the release and recycling of the light-sensitive chromophore from the receptor. Meanwhile, the regulating protein RGS9-1 binds the activated $G_{t\alpha} \cdot$ PDE complex and stimulates the innate GTPase activity of $G_{t\alpha}$, resulting in the deactivation and dissociation of the complex. Finally, decreasing Ca^{2+} concentrations trigger the activity of two guanylate cyclase activating proteins (GCAPs), which cause guanylate cyclases (GCs) to synthesize cGMP at higher rates. This leads to the re-opening of the cGMP-gated ion channels.

The rod photoreceptor exhibits the ability to respond to stimuli across several orders of magnitude of intensity, including the detection of single photons. At low light intensities, activation requires efficient and effec-

tive signal amplification. Saturating stimuli, on the other hand, necessitate rapid recovery to allow the continued detection of light. Overly effective recovery mechanisms, however, would threaten to quench dim-light responses before they are sufficiently amplified. Thus, recovery is tightly controlled by parallel negative-feedback mechanisms, including Ca^{2+}-mediated feedback on GCAPs activity [75, 174–176] and on Rec regulation of RK [63, 64, 142, 143, 145, 158]. These serve to ramp up signal recovery to more intense stimuli without extinguishing dim-light responses. The result is an exquisitely balanced, but dynamically complex system.

In the past decade, an ongoing effort has been made to produce a comprehensive model of visual phototransduction in rod photoreceptor cells [82–84, 177]. The model to-date has been built to include nearly all of the known mechanisms involved in phototransduction. It has been constructed according to a bottom-up strategy, in which detailed representations of the underlying reactions are implemented according to the law of mass-action, eschewing high-level, empirical kinetic models [152]. This model has proven to be very successful in reproducing a variety of mutant conditions in many of the underlying proteins [84, 177]. Furthermore, it has been used to make novel predictions of the dynamical role of a homo-oligomerization mechanism of Arr [177].

Although the model parameters were fit using biochemical and electrophysiological data culled from experiments on amphibians, it was found to produce qualitatively accurate simulations of experiments originally performed in mice, despite the approximately ten-fold slower dynamics in amphibians [84, 177]. Because modern vision research most commonly employs the mouse visual system, it would be valuable to have a model that can also produce quantitatively accurate simulations of it. To this end, we have adapted the most recent version of the amphibian model by Invergo et al. [177] in order to simulate murine electrophysiological data. This was accomplished both through the integration of previously published parameter values and through the use of informed tuning and estimation techniques for unknown values. The resulting model provides accurate reproductions of the mouse visual response under a range of con-

ditions and stimuli, while pointing to potential gaps in our knowledge of the phototransduction system.

5.2 Methods

5.2.1 Model Implementation

The unaltered reaction network of Invergo et al. [177] was used to construct the model (Table S5, page 193). It consists of a system of ordinary differential equations for 96 reactions, deterministically tracking the time evolution of 76 molecular species using 62 parameters. It was implemented using SBTOOLBOX2 for MATLAB (`http://www.sbtoolbox2.org`) [171]. Model files in SBTOOLBOX2 or SBML formats are available upon request. All numerical simulations and parameter estimation were carried out in this framework. Deterministic simulations were run from automatically generated and compiled C-code models, based on the CVODE integrator from SUNDIALS [172]. Simulated light stimulus intensities in units of R^*/s were approximated from published values described in units of photons μm^{-2} using a collecting area of $0.43\,\mu m^2$ [154].

5.2.2 Parameter Determination

Parameters values were retrieved or approximated from the literature when possible. In cases where the true parameter values were unknown, they were either manually tuned to meet experimental expectations or they were estimated through parameter optimization techniques. Parameter estimation was done using a combination of the Nelder-Mead Simplex method for local optimization and a particle swarm method for global optimization [170]. Optimization was performed against published electrophysiological data of the responses of a three-month-old mouse of the B6D2F1/J strain, which is a F1 hybrid between the C57BL/6J and DBA/2J strains [178]. After estimation, parameter values were held fixed in all subsequent simulation experiments.

Amplification parameters

The model parameters related to the $Gt \cdot R^*$ interaction required significant modification to adapt the model to mammalian data (Table S6, page 195). The parameters controlling the $G_{t\alpha}$-PDE interaction, on the other hand, were left unchanged due to their insignificant effect on the model dynamics (see Dell'Orco et al. [84] for a global parameter sensitivity analysis). Because the true values of the G_t-R^* rate parameters are unknown, they were manually tuned to result in the expected rate of $G_{t\alpha}$ production per R^* per second, as was done in the original formulation of the amphibian model [83]. This rate can be estimated according to the following relationship [55]:

$$A = v_{RG}\, c_{GE}\, \beta_{sub}\, n_{cG} \tag{5.1}$$

where A is the amplification constant, estimated to be 5 to $10\,\mathrm{s}^{-2}$; v_{RG} is the rate of $G_{t\alpha}$ production per R^* per second, to be estimated; c_{GE} is the coupling efficiency of $G_{t\alpha}$ to PDE, which, due to the relative insensitivity of the PDE-activation-related parameters, is approximately unity; n_{cG} is the Hill coefficient of the cGMP channel activation, which was manually tuned to 3.8; and β_{sub} is the rate constant of cGMP hydrolysis per activated PDE subunit. β_{sub} may be approximated as follows [78]:

$$\beta_{sub} = \frac{\frac{1}{2} k_{cat}/K_m}{N_{Av}\, V_{cyto}\, B_{cG}} \tag{5.2}$$

k_{cat} is the turnover rate of a doubly-activated PDE holomer, estimated to be 1200 to $3500\,\mathrm{s}^{-1}$ [179]; K_m is the Michaelis constant of cGMP hydrolysis by PDE, estimated to be 17 to $23\,\mu\mathrm{M}$ [179]; N_{Av} is Avogadro's constant; V_{cyto} is the rod outer segment volume, calculated to be approximately $0.039\,16\,\mathrm{pL}$ for the mouse used in the model fitting [178]; and B_{cG} is the buffering power of the cytoplasm for cGMP, which is approximately 2 [55].

It was determined that an amplification constant of $10\,\mathrm{s}^{-2}$ was required to fit the data. The ratio k_{cat}/K_m was maximized according to the

reported ranges for the two parameters, resulting in a β_{sub} of $2.1826 \times 10^{-3}\,\mathrm{s}^{-1}$ and a v_{RG} of $1206\,\mathrm{s}^{-1}$. The maximal rate of $G_{t\alpha}$ production per activated receptor has been reported to be approximately $1290\,/\mathrm{R}^*\mathrm{s}$ [180]. Therefore, this estimate of v_{RG} is reasonable. The G_t-related parameters in the model were then manually tuned to approximate this rate of $G_{t\alpha}$ production (Table S6).

Recovery Parameters

The basal binding rates of RK and Arr to R^* required re-tuning to fit mammalian recovery dynamics (Table S7, page 197). It was previously reported that a linear decrease in the affinity of RK for R^* provided a better, less sensitive fit to the amphibian electrophysiological data [177]. In the present model, it was found that such a linear relationship resulted in a poor prediction of the signal responses of a Rec-knockout animal. In particular, it resulted in RK out-competing G_t for binding R^* and the subsequent full phosphorylation of the receptor before G_t could bind and activate the pathway; this was manifested as a significantly delayed and attenuated peak signal response. By reverting the $RK \cdot R^*$ relationship to an exponential one and by setting the exponent to a greater value than was previously used (see Dell'Orco et al. [84]), this problem was alleviated.

The basal rate of RK-R^* binding was tuned according to the original estimation by Hamer et al. [83], such that $RK_{dark}\ kRK1_0 = 100s^{-1}$, or $100\,/\mathrm{R}^*\mathrm{s}$, where RK_{dark} is the quantity of free RK molecules in the dark. According to a steady-state analysis, RK_{dark} is 580, thus $kRK1_0$ was set to $0.1724\,\mathrm{s}^{-1}$. The rates of phosphorylation and the following dissociation of the RK-R^* complex were required to be approximately ten-fold faster than in the amphibian model (Table S7). Parameters determining the rate of the RK-Rec interaction required no changes.

The Arr-R^* interaction required significant re-tuning (Table S7). In particular, the binding and dissociation rates were required to be several orders of magnitude faster than in the amphibian model. Hamer et al. [83] predicted the basal rate of Arr-R^* binding to be $0.25\,/\mathrm{R}^*\mathrm{s}$ ($Arr_{tot}\ kArr = 0.25s^{-1}$). In the present model, with a initial, steady-state Arr monomer

quantity of $1\,260\,760$ molecules, determined by the parameters $kA4$ and $kA5$, the resulting $kArr$ of $1.9829 \times 10^{-7}\,\mathrm{s}^{-1}$ was much too slow to fit mammalian recovery times. A value of $9.9147 \times 10^{-6}\,\mathrm{s}^{-1}$ ($12.5\,$/R*s) was determined to be sufficient through initial estimation and subsequent manual tuning.

The rate of dissociation of the Arr-R* complex prior to R* deactivation was manually tuned to approximate the equilibrium affinity constant of $10\,\mu\mathrm{M}^{-1}$ reported by Gibson et al. [68]. Similarly, the rate of increase of the affinity of Arr for R* with increasing phosphorylation of R* was manually tuned to approximate the reported rate [68]. The equilibrium constants may not accurately represent the physiological rate, however they provided a good fit and were thus retained. The self-association rate of Arr was also found by parameter estimation, while the self-dissociation rate was manually tuned to approximate the measured equilibrium dissociation constant of $60\,\mu\mathrm{M}$ of the reaction [72].

Finally, RGS9-1-mediated deactivation of the $G_{t\alpha} \cdot$ PDE complex was found to require a significantly faster rate, two orders of magnitude faster than that of the amphibian model (Table S7). The rate constant for the hydrolysis and dissociation of $G_{t\alpha} \cdot$ PDE was set to $98\,\mathrm{s}^{-1}$ according to Skiba et al. [181].

Ca^{2+} and cGMP regulation

The model was modified to accommodate the action of the two distinct GCAPs, as previously implemented [75]. The rate of cGMP production was changed to:

$$vf = \frac{\alpha_{max}}{1 + \left(\frac{Ca^{2+}_{free}}{Kc_1}\right)^{m_1}} + \frac{\alpha_{max}}{1 + \left(\frac{Ca^{2+}_{free}}{Kc_2}\right)^{m_2}} \tag{5.3}$$

where α_{max} is the maximal rate of cGMP production by GC, $60\,\mu\mathrm{M}\,\mathrm{s}^{-1}$ and is assumed to be the same for the activity of both GCAPs [182]; Kc_1 ($139\,\mathrm{nM}$) and Kc_2 ($59\,\mathrm{nM}$) are the Ca^{2+} concentrations at which the GCAPs activity is half maximal, for $GCAP_1$ and $GCAP_2$, respectively

[176]; and m_1 and m_2 are Hill coefficients for $GCAP_1$ and $GCAP_2$, respectively, both with a value of 1.7 [176]. β_{dark}, the dark rate of cGMP hydrolysis, was given a value of 4.1 according to Gross et al. [108] and $cGMP_{dark}$, the concentration of cGMP in the dark, was found by steady-state analysis (Table S8, 199).

Ca^{2+} regulation-related parameters were either culled from the literature or estimated by parameter estimation. See Table S8.

5.3 Results

5.3.1 Model validation

Model fitting was performed against single-cell recordings from a three-month-old mouse of the B6D2F1/J strain of photoresponses to stimuli ranging from 1.7 to 4630 photons μm^{-2} [178]. The resulting model successfully reproduces the primary characteristics of the photoresponse to both dim and saturating light flashes (Figure 5.1) and overall closely corresponds to the experimental data. In order to test the accuracy of the model in reproducing the mechanisms of light adaptation, we simulated and compared light flashes in the presence and in the absence of a steady, non-saturating background illumination (Figure 5.2). Consistent with *in vivo* experiments, we found a shortening of the saturation time in the presence of the steady illumination.

To further test the performance of the model, we simulated a variety of mutant conditions that were previously used for model verification [177]. Overall, simulations produced with the model provide good correspondence to experimental data. Decreasing RK activity via underexpression results in the expected slowing of recovery to a dim flash stimulus (Figure 5.3 A) and the increase in saturation time (T_{sat}, the time spent at at least 90% of the peak amplitude) after a bright stimulus (Figure 5.3 B; compare to Figure 4 in ref. [155]). Overexpression of the kinase did result in a slight decrease in T_{sat}, which is not seen in experimental data [155], however the exact reason for this discrepancy remains unclear [177].

The model also produces excellent predictions of the values of τ_{rec}

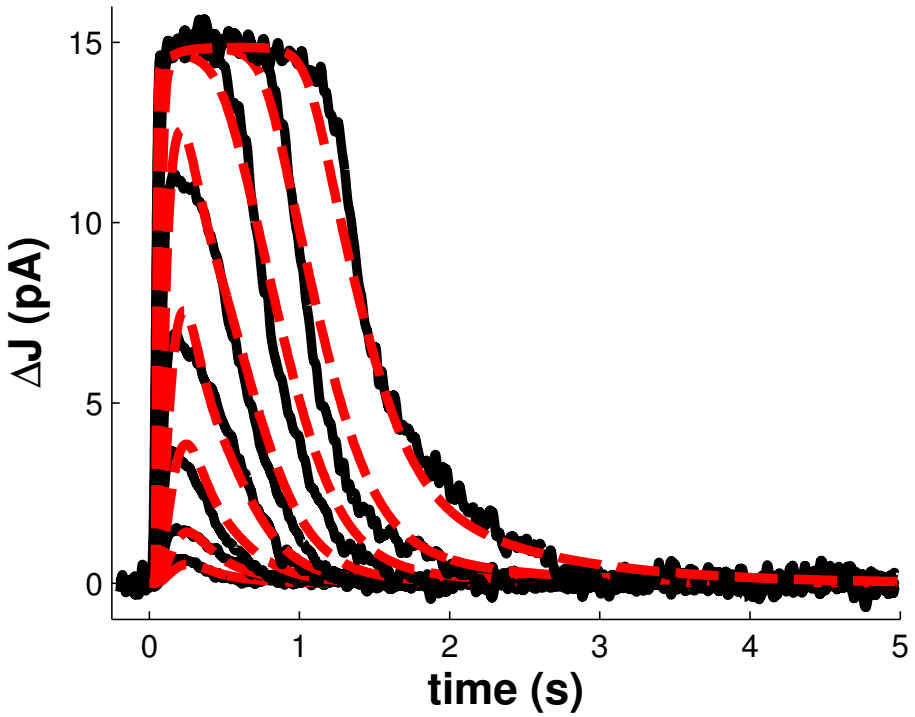

Figure 5.1: Simulations of flash responses generated by a three-month-old B6D2F1/J mouse. 20 ms flash stimuli were delivered at time $t = 0$, with intensities of 1.7, 4.8, 15.2, 39.4, 125, 444, 1406 and 4630 photons μm^{-2}. Black traces are of experimental data from Kolesnikov et al. [178]. Red traces are of simulations using our model.

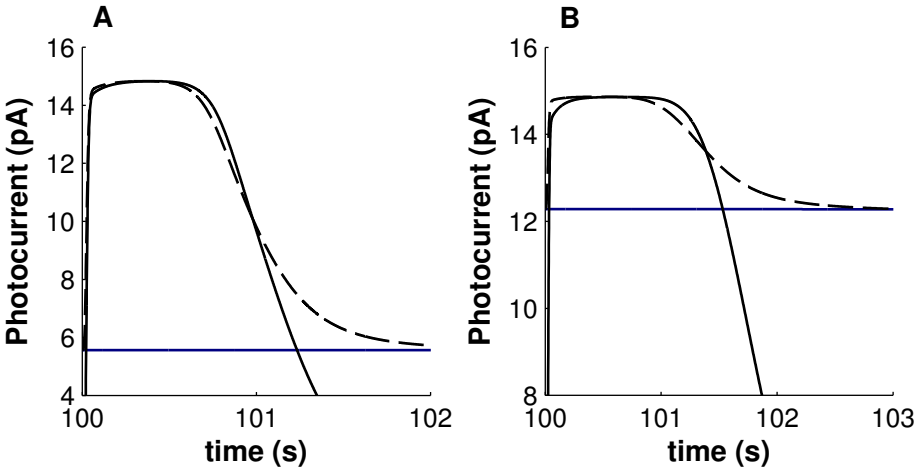

Figure 5.2: Simulated responses to a saturating flash stimulus in the presence (dashed traces) and the absence (solid traces) of a steady, background stimulus. Background stimuli were 81 photons μm^{-2} and resulted in the stable, non-saturating currents indicated by blue, horizontal traces. Flashes of 1590 photons μm^{-2} were delivered at $t = 100$. A) Wild-type simulations. B) Simulated GCAPs knock-out, implemented by setting the parameters m_1 and m_2 to zero. The background stimulus results in a slight reduction in saturation time that is more pronounced in the mutant.

(the time constant of an exponential fit to the second half of the recovery from a dim flash stimulus) and τ_D (the slope of the increase in T_{sat} with flash stimuli of logarithmically increasing intensities) and their experimentally determined values (Figure 5.3 C & D) [155]. Both have been measured to be approximately 250 ms for wild-type mice [155]. Sakurai et al. [155] showed that τ_{rec} is slightly higher when RK is underexpressed and moderately lower with overexpression, which the model accurately captures. τ_D, on the other hand, is not expected to change with increasing RK expression (however, three-fold overexpression may result in a small decrease in τ_{rec}, as measured by Sakurai et al. [155] and reproduced by our model). In our simulations, RK underexpression resulted in an unexpected, small increase in τ_D (Figure 5.3 D).

Removing Ca^{2+} feedback on RK by simulating a Rec knock-out mouse results in lower peak amplitudes to dim flashes and a strongly reduced T_{sat}. (Figure 5.4). A slight decrease in τ_D from 242 ms in the wild-type to 193 ms in the simulated knock-out is similar in magnitude to the decrease seen *in vivo* of 184 ms to 154 ms [158]. The model captures well the sharp peak and slowing rate of recovery to non-saturating stimuli exhibited by the knock-out animals (see ref. [158] figure 2A). This effect is heavily dependent upon the relationship of the affinities of G_t and RK for R^* as a function of the number of phosphates attached to the receptor. While the amphibian model performed better with a linear decrease in affinity of RK for R^* [177], such a linear relationship in the mammalian model led to full phosphorylation of the activated receptor followed by delayed G_t binding at its minimal rate. In effect, RK would entirely out-compete G_t for binding R^*. By reverting to the previously implemented exponential relationship of RK affinity for R^* [84], this binding competition effect was eliminated. The true relationship between RK-R^* affinity and R^* phosphorylation level remains unknown and the sensitivity of the model to this relationship indicates that it is an important gap in the present understanding of phototransduction recovery dynamics.

Finally, it is currently understood that RGS9-1-mediated shutdown of the effector PDE is the rate-limiting step in phototransduction recovery, which previous simulations confirmed [177]. This was most convincingly

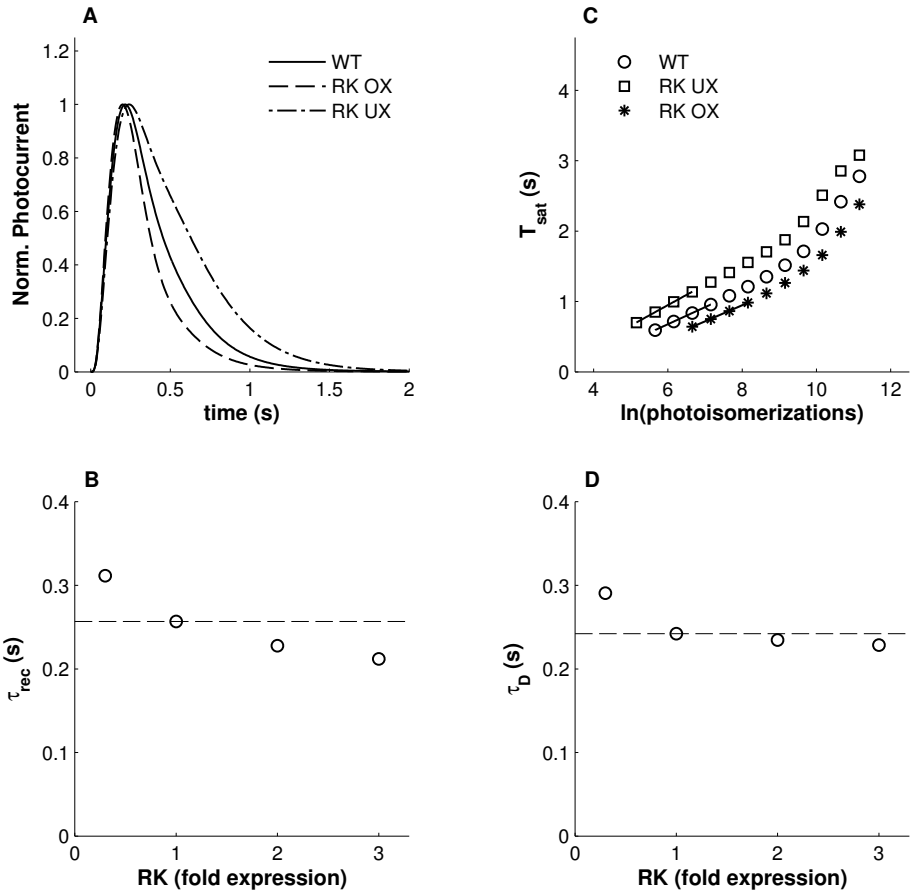

Figure 5.3: The effects of varying RK expression on the photoresponse. A) Normalized responses to a non-saturating flash (7 R*). 0.3x underexpression (dotted-dashed trace) results in a slowed recovery compared to wild-type (solid trace). 3x overexpression (dashed trace) has a marginal effect. B) The time constant of recovery, τ_{rec}, versus RK expression. C) Time spent in saturation (T_{sat}) as a function of logarithmically increasing stimulus intensities. RK underexpression (open squares) results in an increase in T_{sat} compared to wild-type (open circles). RK overexpression (stars) leads to a slight decrease in T_{sat}. The lines show the least-squares best fit of the first four points, used in the determination of τ_D D) τ_D, the slope of the relationship of T_{sat} with logarithmic stimulus intensity, versus RK expression levels. Underexpression results in a small increase in τ_D, while overexpression has no effect. Notice that τ_{rec} and τ_D are approximately equivalent for wild-type mice.

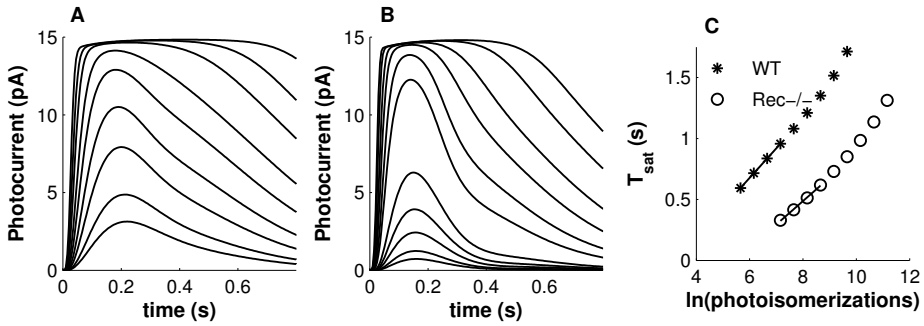

Figure 5.4: Simulated responses of mice lacking Rec. A) Wild-type responses to flash stimuli. Stimulus intensities were 11.8, 20.6, 42.8, 74.9, 139, 243, 504, 882 and 1690 photons μm^{-2}. B) Rec knock-out responses. Stimulus intensities were 12.8, 22.4, 46.5, 81.4, 151, 548, 960, 1840, 3230, 6700 and 11 700 photons μm^{-2}. C) Saturation time as a function logarithmically increasing stimulus intensities. Knocking-out Rec (open circles) results in a distinct shift in saturation time relative to wild-type (stars).

demonstrated by Burns and Pugh [107], who showed that varying the concentration of RGS9-1 has a strong effect on T_{sat} and τ_D influence on the recovery dynamics. When the experiments of Burns and Pugh [107] are simulated with our model, we find an excellent correspondence with the published results (Figure 5.5). In particular, underexpression of RGS9-1 leads not only to a strong increase in T_{sat} but it also results in a notable increase in the slope, τ_D. Conversely, overexpression results in a distinct drop in T_{sat} and a moderate decrease in τ_D.

5.3.2 Discrepancies with experimental data

A small discrepancy between the recovery dynamics of the dim and bright flash stimulus paradigms is noticeable (Figure 5.1). In particular, the peak amplitudes of dim-to-moderate intensity stimuli are slightly too high while the saturation times in response to bright flashes are slightly too short. It was determined that this is primarily affected by the shape of the Ca^{2+} dependency of GC, as moderated by the GCAPs. Naive param-

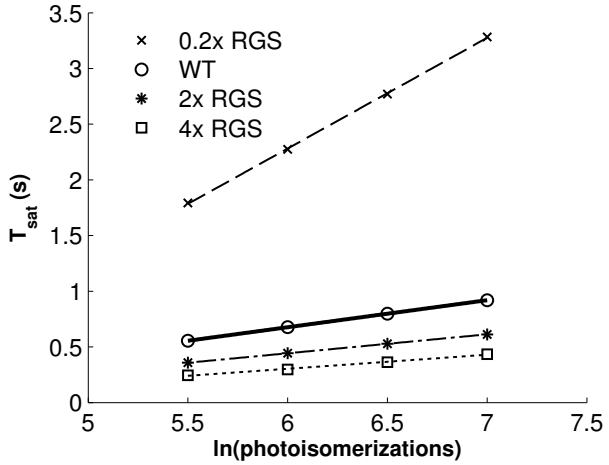

Figure 5.5: The relationship between saturation time and logarithmically increasing stimulus intensity varies strongly with RGS9-1 expression. 0.2x underexpression (X's, dashed line) results in a strong increase in both saturation time and the slope of the relationship compared to wild-type (open circles, solid line). 2x and 4x overexpression (stars, dotted-dashed line; open squares, dotted line, respectively) leads to a moderate drop in saturation time and the slope.

eter optimization showed that Kc_1, the concentration of Ca^{2+} at which $GCAP_1$-mediated GC activity is half-maximal, would have to be $0.2\,\mu M$ or higher in order to properly fit the full range of responses. Given a Ca^{2+} dark concentration of $0.25\,\mu M$, as described by Woodruff et al. [183], this value of Kc_1 seems unlikely. However, this dark concentration of Ca^{2+} may be underestimated; confirmation of the physiological concentration would resolve this. If a concentration of $0.25\,\mu M$ is accurate, then it is likely that the cGMP regulatory dynamics in the model are insufficient.

In measuring the effect of light adaptation on the photoresponse, we found a shortening of the saturation time in the presence of a steady background illumination. However, the simulated effect was not as strong as expected (Figure 5.2 A; see, *e.g.*, figure 7C in ref. [184]). To determine if cGMP regulation was responsible for this behavior, we performed the same simulations with a model of a GCAPs knock-out animal, implemented by setting the GCAPs Hill coefficients (parameters m_1 and m_2) to zero (Figure 5.2 B). The effect of the steady background was slightly stronger in the mutant, at least partially implicating the cGMP regulatory dynamics in the discrepancy. It was found through parameter manipulation that the R^* deactivation dynamics also have a strong effect on this characteristic of light adaptation. Slowing R^* deactivation, through decreased RK or Arr activity, results in a larger gap between dark-adapted and light-adapted saturation times for both wild-type and GCAPs knock-out mutants, in line with experimental expectations. However, doing so also results in these mechanisms having a stronger influence on the recovery parameters τ_{rec} and τ_D, disrupting the model's faithful reproduction of other mutant scenarios. A satisfactory and realistic combination of parameters to resolve this could not be found. This finding, along with the continued effect of RK overexpression on T_{sat} and the strong influence of the nature of the R^*-RK reaction affinity point to a possible unknown mechanism regulating RK activity.

5.4 Discussion

Visual phototransduction is a prototypical G-protein signaling pathway that encompasses a wide variety of protein-protein interactions and complex feedback mechanisms. To unravel its inner workings, a rich history of modeling efforts has arisen around it. Much of the past modeling work has been done through the integration of biochemical and electrophysiological data of amphibian species, while a majority of modern experimentation is done using the mouse visual system. We have adapted a previously published, comprehensive model of amphibian phototransduction to fit murine electrophysiological data. This was accomplished via the incorporation of parameter values that have been measured *in vivo* or *in vitro* in mice or other mammalian species. When parameter values were unknown, they were manually tuned to fit expected behavior or they were estimated by parameter optimization techniques.

The resulting model accurately simulates responses to light stimuli across several orders of magnitude. Furthermore, it has proven to predict the responses of mutant conditions without further parameter tuning, indicating that much of the model is well-resolved. Because it is constructed in a bottom-up manner using the known reactions comprising the pathway, cases in which the model performs poorly may point to gaps in our knowledge. Theoretically, if we know all of the reactions and we have reasonable estimates of the parameters, we can expect accurate simulations. Where the simulations deviate from experimental data, we can deduce that either some mechanisms are incomplete or missing, or some parameter values are grossly inaccurate. In this way, the bottom-up approach is a truer test of our mechanistic knowledge than traditional, empirical modeling: rather than employing high-level measurements and mathematical constructs to build a model that produces satisfactory simulations, we instead compile the "building blocks" of what we know about the pathway and verify whether they can sufficiently explain known system dynamics.

5.4.1 Missing or unknown mechanisms

Previous iterations of the amphibian model, as well as the present mammalian one, have seen inaccurate results of simulating RK overexpression [84, 177], such that it incorrectly results in a decrease in T_{sat}. The previous incorporation of a dynamic Arr-oligomerization mechanism partially eliminated this effect [177], however some discrepancy with the *in vivo* results remains. The model has been also found to be particularly sensitive to the affinity relationship of RK for phosphorylated R^* [177]. Furthermore, in the present work, we have found that the RK activity required to fit dark-adapted mammalian flash responses may be too fast to accommodate expected light-adaptation behaviors. No realistic, satisfactory combination of parameters could resolve this suite of inaccuracies. Thus, one might speculate that a yet unknown mechanism moderating RK activity exists. It is possible that further clarifying the effects of R^* phosphorylation and RK autophosphorylation on the R^*-RK interaction may resolve these discrepancies; our knowledge is currently limited to only the unphosphorylated and fully phosphorylated states [69], leaving the true relationship uncertain in a multi-step phosphorylation paradigm [67, 82].

Furthermore, it is clear that the cGMP-regulatory mechanisms in the model are insufficient, as evidenced by its short-comings presented herein. Only one of the two GC isozymes is present in the model, when in fact both exhibit different properties [176]. Unfortunately, we lack mechanistic information on the putative switch between GC_1 and GC_2 functionality in order to properly implement both cyclases in the model [75]. It is also worth noting that cGMP regulation remains implemented according to an empirical Hill equation rather than the desired, bottom-up representation of the underlying reactions. While a recent detailed model of cGMP kinetics in phototransduction using a similar Hill representation showed excellent performance in predicting local spatio-temporal kinetics, it was only used to simulate single-photon responses [108] and not a full range of stimuli as we present here. A more accurate model, capturing the complexities of the interactions of the two GCs and their Ca^{2+}-

sensitive regulation by the GCAPs, is necessary to improve the dynamics of this important signal recovery mechanism.

Finally, at very dim stimulus intensities, down to a single photon, the probability of two proteins encountering each other becomes an important factor in the phototransduction response, as does the local saturation of second messengers such as cGMP [108, 149]. Due to its deterministic nature, our model cannot accurately simulate the single photon response (SPR). Furthermore, the representation of the photoreceptor outer segment as a well-mixed substrate may omit important localized depletion of the second messengers [85–87]. A series of spatially accurate models of mouse phototransduction have been produced in order to more accurately simulate this scenario [85–87, 108, 185]. These models reproduce quite well the SPR and have revealed insights into the mechanisms underlying its variability, however they have not been demonstrated to also faithfully simulate light adaptation, limiting their utility. Additionally, they primarily give focus to the second messengers, while reducing protein activity to high-level, empirical parameters; thus, the intricacies of the inter-protein dynamics are lost. Ideally, the future will see a merging of the two techniques, allowing a detailed, spatially accurate model that can reproduce the full range of responses exhibited by a rod photoreceptor.

5.4.2 Conclusions

One of the chief aims of systems biology research is the production of quantitatively predictive models from which experimental hypotheses can be derived. It is hoped that our model will be a useful tool in guiding future research on phototransduction. By offering quantitatively accurate predictions across a range of conditions for the primary species used in vision research, it may be used to avoid costly lines of unproductive investigation. Meanwhile, its shortcomings may raise interesting questions regarding gaps in our knowledge of the phototransduction process. Furthermore, its modular structure allows for the easy integration of novel features without disrupting the existing network, allowing it to be expanded as research progresses.

Acknowledgments

We would like to thank Alexander V. Kolesnikov for kindly providing the electrophysiological data used in the model fitting. This research was funded by grant BFU2010-19443 (subprogram BMC) awarded by the Ministerio de Ciencia y Tecnología (Spain) and by the Direccío General de Recerca, Generalitat de Catalunya (Grup de Recerca Consolidat 2009SGR 1101). BMI is supported by FI-DGR and BE-DGR grants from AGAUR, Generalitat de Catalunya (2011 F1 B1 00275). LM acknowledges funding from the Juan de la Cierva Program of the Spanish Ministry of Science and Innovation (MICINN). DDO acknowledges funding from the Hanse- Wissenschaftkolleg Delmenhorst and from the Italian Ministry for Research and Education (Fur2011).

Chapter 6

A DYNAMIC MODEL OF MAMMALIAN PHOTOTRANSDUCTION REVEALS INSIGHTS INTO THE MOLECULAR EVOLUTION OF SYSTEMS

Brandon M. Invergo, Ludovica Montanucci, and Jaume Bertranpetit

Manuscript in preparation

Abstract

Determining the influence of the dynamics of complex molecular systems on the natural selection of proteins presents the significant challenge of characterizing the potential dynamic control of each protein in the system. We have employed a comprehensive mathematical model of mammalian phototransduction to predict the degree of influence that each protein in the system exerts on the high-level dynamic behavior. We then contrasted this data with molecular evolutionary rates for the proteins. We found that the proteins that have greater potential to disrupt system dynamics exhibited more relaxed evolutionary constraint, in the form of higher evolutionary rates. We also took advantage of the ability to rapidly simulate hundreds of perturbations to pairs of parameters, which revealed that non-additive interactions are pervasive in this system. The results suggest a role for dynamically sensitive proteins in the fine-tuning of the system. Furthermore, this work points to mathematical models of biochemical systems as useful tools in the study of molecular evolution.

6.1 Introduction

The flood of genomic and molecular data that has become available in recent years has permitted the investigation of high-level trends in molecular evolution, particularly in the context of whole biochemical systems. To date, studies on the patterns of molecular evolution across systems have largely focused on representing the systems as networks, calculating graph-topological properties of the proteins and then demonstrating correlations between these properties and molecular evolutionary histories [3, 4, 6, 8–16]. While correlations between network topology and molecular evolutionary histories were found by all, the observed relationships varied from system to system.

A shortcoming of the network approach is that it treats molecular systems as static entities, defined solely by the existence or absence of interactions between proteins. In reality, it is likely to be not only the existence of an interaction that is evolutionarily relevant but also the kinetics of that interaction will affect fitness. It is clear that a mutation that would cause an existing interaction to occur at a much slower rate or at a lower affinity would have potentially significant fitness effects. To this end, some recent studies on the evolution of metabolic pathways have considered the system dynamics via metabolic flux and flux control. Olson-Manning et al. [186] found that the first upstream enzyme in the alipathic glucosinolate pathway of *Arabidopsis thaliana* has higher flux control and that this protein is the only one to show evidence of selection. Colombo et al. [187] compared the metabolic flux coefficients of the erythrocyte core metabolic pathway with molecular evolutionary rates and found that enzymes that carry high fluxes have been more constrained in their evolution. Though these studies have greatly elucidated the evolution of molecular evolution in metabolic pathways, their methodologies are limited to the study of only this class of systems. Furthermore, while these methodologies certainly present a more dynamic view of the system than network-based methods would, the dependence of calculating flux coefficients or flux control on the steady-state of the system precludes a full view of the kinetics of the reactions, which may depend greatly on

the variable environment.

In order to consider the influence of system dynamics on molecular evolution, a robust mathematical model of the system would be of use. Many models of biochemical systems have been made publicly available; currently there are 460 models listed in the BioModels database (`http://www.ebi.ac.uk/biomodels-main`) [188]. To our knowledge no such dynamic model of a biochemical system has been employed in published evolutionary research. To investigate the utility of biochemical models in evolutionary research, we have used a comprehensive model of mammalian rod phototransduction to gain insight into how the dynamic properties of this system have influenced the evolution of the proteins that it comprises.

Phototransduction is the process by which a visual stimulus is converted to a neuronal response. Vertebrate phototransduction is a prototypical G-protein signaling cascade. In short, a light stimulus is absorbed by a visual pigment associated with the receptor, rhodopsin, triggering a conformational change. The G-protein transducin binds the activated rhodopsin, which catalyzes the exchange of GDP for GTP on the $G_{t\alpha}$ subunit of transducin, leading to the dissociation of the G-protein. $G_{t\alpha}$ is then free to activate the signal effector, a phosphodiesterase, resulting in the hydrolysis of cyclic GMP (cGMP). Falling cGMP concentrations lead to the closure of cGMP-gated ion channels, causing a drop in the cytoplasmic Ca^{2+} concentration and a subsequent hyper-polarization of the cell, which initiates the neuronal signal. Several parallel processes then act to recover from the signal, via deactivating the receptor and the effector and re-opening the ion channels, in order to prepare the cell to respond to further stimuli. Falling Ca^{2+} concentrations activate multiple feedback mechanisms, which tightly regulate the deactivation of the receptor, the re-synthesis of cGMP and the affinity of the ion channels for cGMP. For a detailed overview of the molecular mechanisms of phototransduction, see Pugh Jr and Lamb [55] or Yau and Hardie [56].

Recently, a comprehensive model of phototransduction has been developed to fit murine phototransduction (Figure 6.1) (Chapter 5). Using this model, we made an estimate of the overall sensitivity of the photo-

transduction response to functional variation in the system's proteins. To this end, we considered four common electrophysiological measurements of the photoresponse that may have been evolutionarily relevant during mammalian divergence: signal amplification, measured as the peak amplitude after a dim stimulus; the time constant of an exponential fit to the recovery from a dim stimulus, commonly denoted τ_{rec}; the total time spent in saturation after a bright stimulus; and the dominant time constant of recovery from bright stimuli, referred to as τ_D (Figure 6.2). It is expected that proteins to which these empirical measurements are the most sensitive will have been more constrained in their evolution. Thus, we investigated whether there exists any relationship between the evolutionary rates of phototransduction proteins and the dynamic sensitivity of the system to perturbations in them. Finally, we took advantage of the ability to rapidly simulate variation in multiple parameters in order to predict whether any epistatic interactions exist between genes of the phototransduction system.

6.2 Methods

6.2.1 Model Implementation & Simulations

A previously developed model of mammalian phototransduction was used for all simulations (Chapter 5). The model comprises a system of ordinary differential equations that deterministically track the time-evolution of 72 molecular species in 96 reactions and using 62 parameters. It was implemented using SBTOOLBOX2 for MATLAB (`http://www.sbtoolbox2.org`) [171]. Simulations were run from automatically generated and compiled C-code models, based on the CVODE integrator from SUNDIALS [172].

6.2.2 Simulated Electrophysiological Measurements

Four properties of the simulated electrophysiological response were measured for each simulated photoresponse: the peak amplitude of a dim-

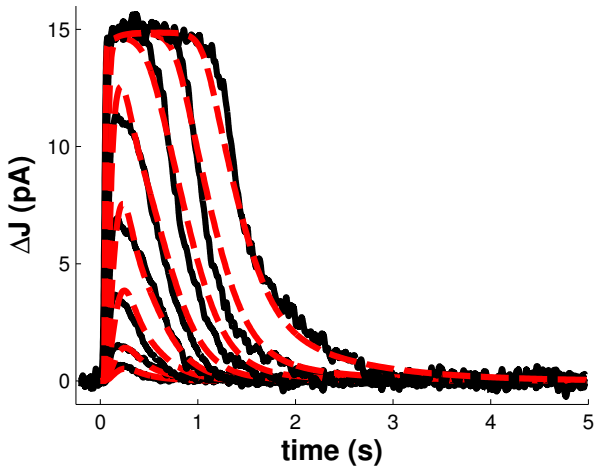

Figure 6.1: Simulations of flash responses generated by a three-month-old B6D2F1/J mouse. 20 ms flash stimuli were delivered at time $t = 0$, with intensities of 1.7, 4.8, 15.2, 39.4, 125, 444, 1406 and 4630 photons μm^{-2}. Black traces are of experimental data of Kolesnikov et al. [178]. Red traces are of simulations using the model.

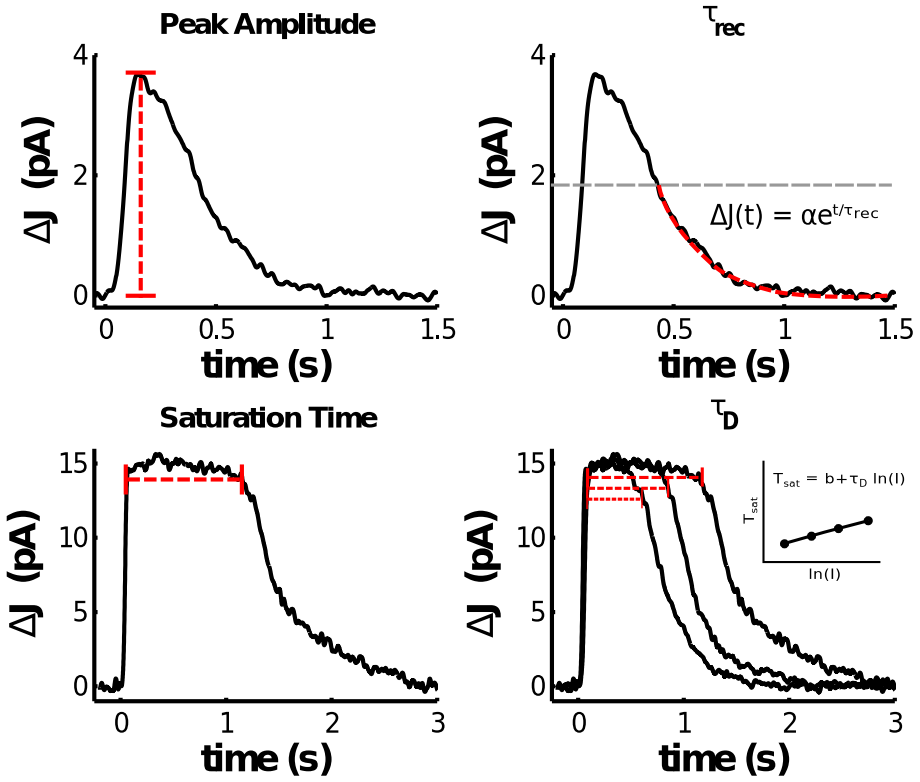

Figure 6.2: Illustrations of the four electrophysiological measurements of the photoresponse used in the present study. A) Peak amplitude after a dim stimulus. B) τ_{rec}, the time constant of a single exponential fit to the second half of recovery after a dim stimulus. C) Saturation time after a bright stimulus. D) τ_D, the dominant time constant of recovery, measured as the rate of increase of saturation time with logarithmically increasing stimulus intensities.

light response; the time constant of a single exponential fit to second half of the recovery (post-peak) phase of a dim-light response (τ_{rec}); saturation time, T_{sat}, measured as the total time the current spends at more than 90% of its peak amplitude during a saturating, bright-light response; and τ_D, measured as the change in T_{sat} with logarithmically increasing stimulus intensities [156] (Figure 6.2).

Dim-light responses were generated from a simulated stimulus causing 6.536 photoisomerizations per second (R^*/s). T_{sat} was determined for simulated responses to a flash generating $1808\ R^*$/s. τ_D was computed as the slope of a least-squares fit of the T_{sat} values measured for responses to stimuli resulting in 403.43 to $1808\ R^*$/s, increasing by half-log units. All flash stimuli had a duration of 0.02 s.

6.2.3 Parameter Sensitivity Analysis

6.2.4 Parameter Sensitivity Measurement

We chose local parameter sensitivity analysis as the most immediately relevant for an evolutionary study, owing to a common focus in the study of evolution on mutations of small phenotypic effect. Typically, local parameter sensitivity is computed as the absolute first-order partial derivative of a system output with respect to one of the parameters at a given point in parameter space:

$$S = \left| \frac{\delta M_i}{\delta P_j} \right|_{\mathbf{P}^0} \tag{6.1}$$

where M_i is a function describing an output measurement function (such as peak amplitude or τ_{rec} in the present model) and P_j is a parameter from the set of all parameters $\mathbf{P}$, at the point $\mathbf{P}^0$ in parameter space. $\mathbf{P}^0$ corresponds to a point of interest, in this case the point is defined by the physiological ("wild-type") values previously derived for this model. Thus, in biological terms, the local parameter sensitivity would approximate the magnitude of a system-level phenotypic effect due to a mutation

of small local effect.

Because the electrophysiological measurements were made empirically on simulated data, the derivatives could not be solved analytically. Instead, they were approximated numerically by producing a model with a parameter value increased by 1%, measuring the electrophysiological properties of simulations produced with the modified "mutant" model, and taking the ratio of the change in the measurement value to the change in the parameter, relative to the "wild-type". Since parameter values in the model span several orders of magnitude, sensitivity measurements would be dominated by the scale of the parameter. To remedy this and to produce comparable sensitivities for the four measurements, the resulting changes in measurement and parameter values were normalized according to the original, "wild-type" model values. Thus, the sensitivity was estimated as the percentage change in a measurement, i, for the percentage change in the parameter, j:

$$s_{i,\Delta P_j} = \left| \frac{(m_{i,\Delta P_j} - m_i)/m_i}{(\Delta P_j - P_j)/P_j} \right| = \left| \frac{(m_{i,\Delta P_j} - m_i)/m_i}{0.01} \right| \tag{6.2}$$

where m_i is the "wild-type" empirical measurement, $m_{i,\Delta P_j}$ is the "mutant" empirical measurement after a small change in parameter j, and P'_j is the "mutant" parameter value.

6.2.5 Parameter Selection

In order to ensure that all parameters carried similar meanings, only those defined according to the law of mass-action were included in the analysis. These included, for example, binding and dissociation rates, or catalytic rates of enzymes. Thus, parameters related to the homeostasis of Ca^{2+} (cGMP-gated ion channels, Na^+/Ca^{2+} K^+ ion exchanger, and cytoplasmic Ca^{2+} buffering) and cGMP (guanylate cyclases and guanylate cyclase activating proteins (GCAPs)) were excluded. Additionally, the exponential parameters ω and ω_G were excluded due to their inherently

sensitive nature. The final list of 32 parameters included in the analysis was: $kRK1_0$, $kRK2$, $kRK3_{ATP}$, $kRK4$, $kArr$, $kA2$, m_{Arr}, $kA3$, $kA4$, $kA5$, $kOps$, $kG1_0$, $kG2$, $kG3$, $kG4_{GDP}$, $kG5_{GTP}$, $kG6$, $kG7$, $kG_{shutoff}$, $kP1$, $kP2$, $kP3$, $kP4$, $kPDE_{shutoff}$, $kRGS1$, $kRGS2$, $kRec1$, $kRec2$, $kRec3$, $kRec4$, $beta_{dark}$ and $beta_{sub}$.

Some parameters influence steady-state molecular counts. When these parameters were modified, the model initial states were updated appropriately. For determining the sensitivity of the parameters $kA4$ and $kA5$, which define the self-association and self-dissociation rates of arrestin, the modified models were updated to set the initial states (molecule count) of the arrestin monomer (Arr), dimer (Arr_{di}) and tetramer (Arr_{tetra}) to their new steady-state values. Similarly, modifying $kRec1$ and $kRec2$, which define the rates of recoverin's Ca^{2+}-mediated conformation change, and $kRec3$ and $kRec4$, which determine the binding and dissociation rates of recoverin for rhodopsin kinase, required updating the model's initial states for Ca^{2+}-bound "relaxed" recoverin ($RecR\_Ca$), Ca^{2+}-free "tense" recoverin ($RecT$), rhodopsin kinase (RK) and recoverin-bound rhodopsin kinase ($RecR\_Ca\_RK$). Changes to the parameters $kG1_0$ and $kG2$ necessitated updating the initial states for rhodopsin (R), transducin (Gt) and the rhodopsin-transducin pre-stimulus complex (R_Gt) [151]. Finally, modifying the parameter $beta_{dark}$, the dark rate of cGMP hydrolysis, required retuning the parameter $cGMP_{dark}$, the cGMP concentration in the dark, and the initial concentration of cGMP (equal to $cGMP_{dark}$).

6.2.6 Gene Dynamic Sensitivity

For each gene, g, a set of associated parameters, $\mathbf{\Pi}_g$, was defined such that $\mathbf{\Pi}_g \subseteq \mathbf{P}$, where $\mathbf{P}$ is the set of all parameters. Genes were associated with parameters according to the reactions in which their encoded proteins participate (Table 6.1). For example, several proteins are involved in the following example reaction:

$$\text{RGS} + \text{PDE}^* \cdot \text{G}_{\alpha_{GTP}} \xrightarrow{kRGS1} \text{RGS} \cdot \text{PDE}^* \cdot \text{G}_{\alpha_{GTP}}$$

RGS exists as a heterotrimer comprising proteins encoded by the genes *RGS9*, *RGS9BP*, and *GNB5*; PDE is a tetramer that consists of proteins encoded by the genes *PDE6A* (one sub-unit), *PDE6B* (one sub-unit) and *PDE6G* (two sub-units); and $\mathrm{G}_{\alpha\mathrm{GTP}}$ is the GTP-bound, α subunit of the G-protein transducin, encoded by the gene *GNAT1*. Because all of these genes encode proteins that participate in this reaction, they would each have the parameter $kRGS1$ associated with them.

Table 6.1: Model parameters associated with each gene

Gene	Protein Name	Parameters
GNAT1	Transducin (α sub-unit; $\mathrm{G}_{\mathrm{t}\alpha}$)	$kG1_0$, $kG2$, $kG3$, $kG4_{GDP}$, $kG5_{GTP}$, $kG6$, $kG7$, $kP1$, $kP2$, $kP3$, $kP4$, $kPDE_{shutoff}$, $kRGS1$, $kRGS2$
GNB1	Transducin (β sub-unit; $\mathrm{G}_{\mathrm{t}\beta}$)	$kG1_0$, $kG2$, $kG3$, $kG4_{GDP}$, $kG5_{GTP}$, $kG6$, $kG7$
GNB5	$\mathrm{G}_{\beta 5}$	$kRGS1$, $kRGS2$
GNGT1	Transducin (γ sub-unit; $\mathrm{G}_{\mathrm{t}\gamma}$)	$kG1_0$, $kG2$, $kG3$, $kG4_{GDP}$, $kG5_{GTP}$, $kG6$, $kG7$
GRK1	Rhodopsin Kinase	$kRK1_0$, $kRK2$, $kRK3_{ATP}$, $kRK4$, $kRec3$, $kRec4$
PDE6A	Phosphodiesterase (α sub-unit)	$kP1$, $kP2$, $kP3$, $kP4$, $kPDE_{shutoff}$, $kRGS1$, $kRGS2$, β_{sub}, β_{dark}
PDE6B	Phosphodiesterase (β sub-unit)	$kP1$, $kP2$, $kP3$, $kP4$, $kPDE_{shutoff}$, $kRGS1$, $kRGS2$, β_{sub}, β_{dark}
PDE6G	Phosphodiesterase (γ sub-unit)	$kP1$, $kP2$, $kP3$, $kP4$, $kPDE_{shutoff}$, $kRGS1$, $kRGS2$, β_{sub}, β_{dark}
RCVRN	Recoverin	$kRec1$, $kRec2$, $kRec3$, $kRec4$

Table 6.1 – *Continued from previous page*

Gene	Protein Name	Parameters
RGS9	Regulator of G-protein Signaling 9 (RGS9-1)	$kRGS1$, $kRGS2$
RGS9BP	RGS9-binding Protein	$kRGS1$, $kRGS2$
RHO	Rhodopsin	$kRK1_0$, $kRK2$, $kRK3$, $kRK4$, $kArr$, $kA2$, m_{Arr}, $kA3$, $kG1_0$, $kG2$, $kG3$, $kG4_{GDP}$, $kG5_{GTP}$, $kG6$
SAG	Arrestin	$kArr$, $kA2$, m_{Arr}, $kA3$, $kA4$, $kA5$

A dynamic sensitivity score for each gene was then computed as the geometric mean of the sensitivities of the parameters associated with that gene. First, parameter sensitivity values calculated to be zero were set to 1×10^{-6}. Next, because the computed sensitivities ranged several orders of magnitude, they were log-transformed and inverted before calculating the mean (Figure 6.3). In order to preserve the conceptual correlation between high sensitivity and numerically high computed sensitivity values, the final averages were inverted again. Thus, the dynamic sensitivity of a gene, g, for a given electrophysiological measurement, i, was defined as:

$$s_{g,i} = -\left(\prod_{P_j \in \mathbf{\Pi_g}} -ln(s_{i,\Delta P_j})\right)^{1/|\mathbf{\Pi}_g|} \tag{6.3}$$

where $|\mathbf{\Pi}_g|$ is the cardinality of the set $\mathbf{\Pi}_g$. Finally an average sensitivity for each gene were calculated as the arithmetic mean of the gene's sensitivities for the four measurements.

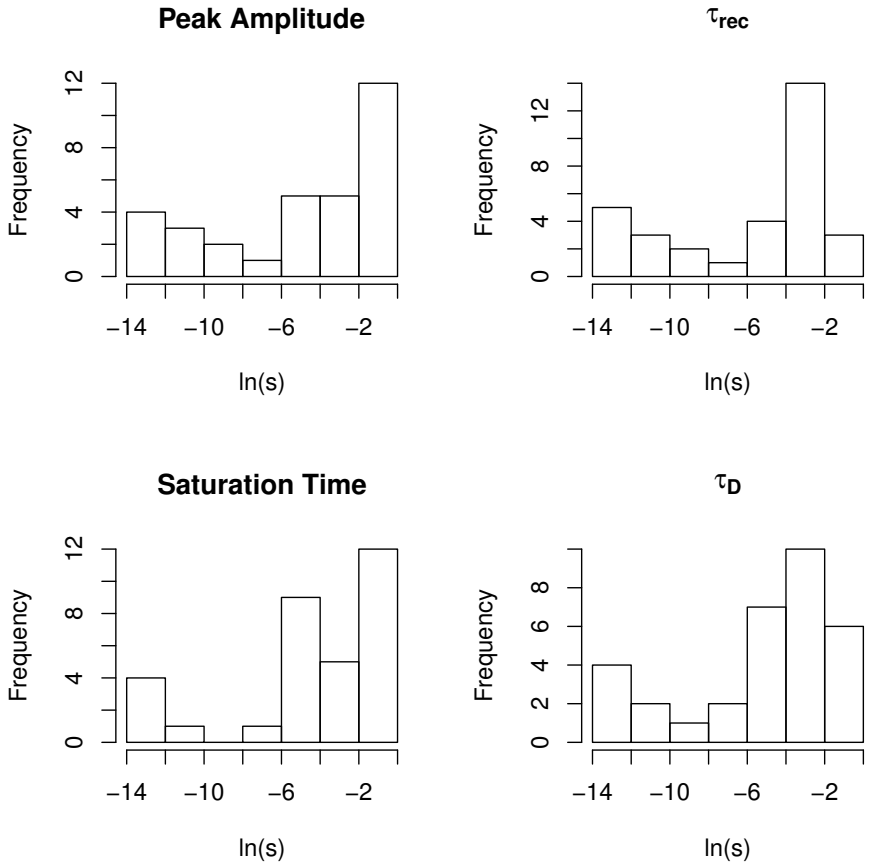

Figure 6.3: Distributions of parameter sensitivity values for the four electrophysiological measurements. Values spanned several orders of magnitude and were thus log-transformed in subsequent analyses.

6.2.7 Evolutionary Constraint

The evolutionary constraints acting on each gene were estimated according to the ratio of the rates of non-synonymous (dN) to synonymous (dS) substitution. d_N/d_S values for the genes in this study were retrieved from a previous publication [16]. In short, d_N/d_S values were computed for a phylogenetic tree of nine mammalian species: human, chimpanzee, gorilla, orangutan, macaque, marmoset, mouse, rat, and dog. Sequences were retrieved from the Ensembl database (release 60) or from DNA resequencing. Rates were computed using CODEML model M0 of the PAML package version 4.4c [111]. This model computes a single d_N/d_S ratio for the entire tree, treating all sites in the alignment as having evolved at the same rate. While the model is simple, it is relatively conservative and can be used to capture general trends in the evolutionary rates during a phylogenetic divergence.

6.2.8 Non-additive Phenotypic Effects

Non-additive dynamic effects between parameters were tested by first generating models with $1\,\%$ changes to two of the parameters used in the sensitivity analysis, for each combination of two parameters. Linear models were built to predict the double-mutant phenotype from a linear combination of the single-mutant phenotypic effects:

$$m_{i,\Delta P_j \Delta P_k} = \alpha + \beta \left(m_i + (m_{i,\Delta P_j} - m_i) + (m_{i,\Delta P_k} - m_i) \right) + \epsilon \quad (6.4)$$

where $m_{i,\Delta P_j \Delta P_k}$ is the electrophysiological measurement, i, for the double-mutant; $m_{i,\Delta P_j}$ and $m_{i,\Delta P_k}$ are the electrophysiological measurements for the single-mutants; α is the intercept of the model; β is the slope; and ϵ is the residual term. We then checked the externally studentized residuals of the models for points that were outliers according to the probability density function of the Student's t-distribution with 493 degrees of freedom.

6.2.9 Statistical Analyses

Correlations were tested by computing Spearman's ρ. Correction for multiple testing was performed using the method of Holm [138]. All statistical calculations were performed using R version 3.0.1.

6.3 Results

6.3.1 Parameter Sensitivity

We first investigated the local sensitivities of the model parameters. Sensitivity values spanned several orders of magnitude and, even after log-transformation, their distribution remained skewed towards higher sensitivity values (Figure 6.3). Next, we sought to determine whether the shapes of the empirical measurement functions are smooth, that is, whether they were monotonic in the neighborhood of the point in parameter space corresponding to the default model values. If the functions were not smooth, sensitivity measurements would be unreliable without knowledge of the true, physiological parameter values. For each parameter, we generated 39 models in which the parameter value was set between $5\,\%$ and $195\,\%$ of its default value. We then simulated flash responses to dim and bright stimuli with each model and measured the peak amplitudes, τ_{rec} values, saturation times and τ_D values for each one (for two examples, see Figures 6.4 and 6.5; for all parameters, see Figures S8 through S39). In most cases, the measurements changed monotonically with the parameter value. The parameter β_{dark}, the dark rate of cGMP hydrolysis, showed a sharp increase in τ_{rec} when decreased by more than 50%, with an apparent peak at 10% (Figure S32).

6.3.2 Gene Dynamic Sensitivity

When d_N/d_S ratios for the genes were plotted against their dynamic sensitivities for the four electrophysiological measurements, a strong positive relationship could be seen for three of the measurements: τ_{rec}, saturation

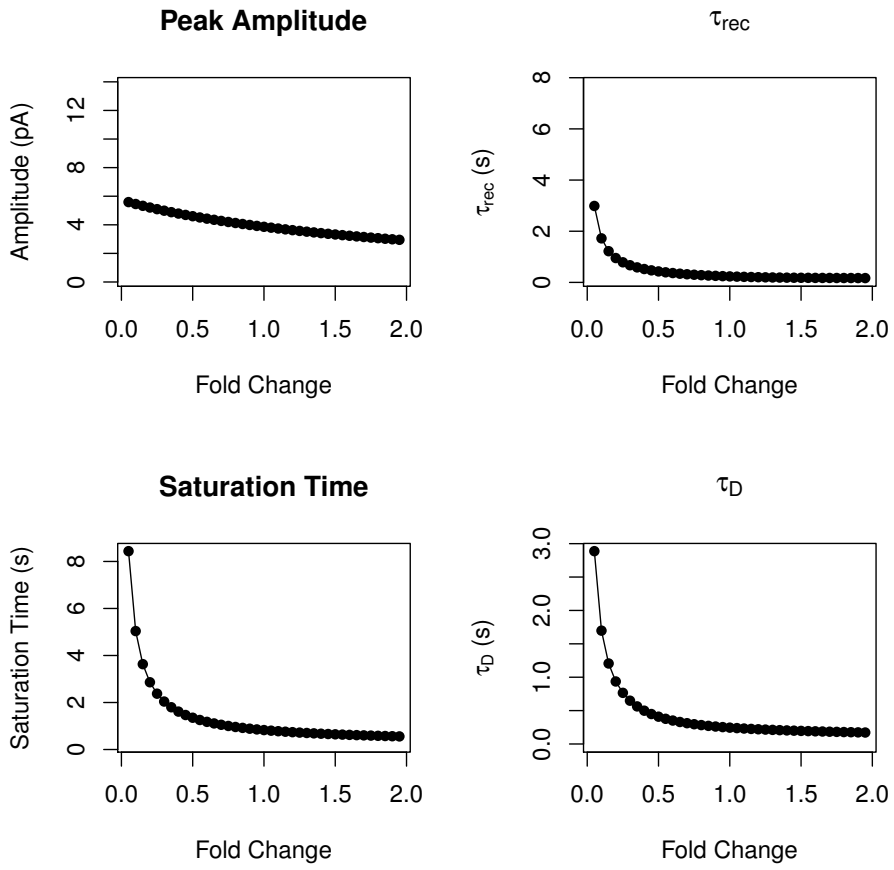

Figure 6.4: Electrophysiological measurements as functions of the parameter $kRGS1$.

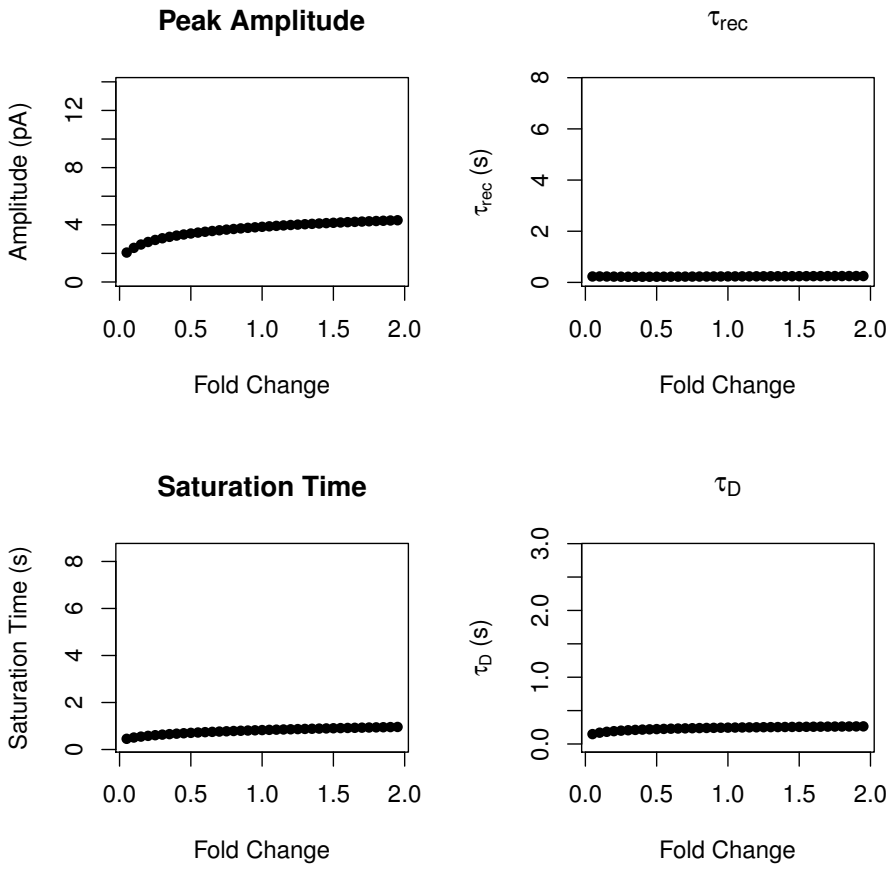

Figure 6.5: Electrophysiological measurements as functions of the parameter $kRec1$.

	$s_{g,i}$				
Gene	**Peak Amp.**	τ_{rec}	**Sat. Time**	τ_D	**Avg.**
GNAT1	-5.03	-5.82	-4.60	-5.26	-5.18
GNB1	-3.17	-5.28	-3.57	-4.53	-4.14
GNB5	-3.25	-1.46	-1.41	-1.37	-1.87
GNGT1	-3.17	-5.28	-3.57	-4.53	-4.14
GRK1	-2.78	-3.81	-2.62	-3.31	-3.13
PDE6A	-3.58	-4.93	-3.82	-4.90	-4.31
PDE6B	-3.58	-4.93	-3.82	-4.90	-4.31
PDE6G	-3.58	-4.93	-3.82	-4.90	-4.31
RCVRN	-1.71	-2.25	-1.51	-2.08	-1.89
RGS9	-3.25	-1.46	-1.41	-1.37	-1.87
RGS9BP	-3.25	-1.46	-1.41	-1.37	-1.87
RHO	-3.58	-4.18	-3.37	-3.88	-3.75
SAG	-4.00	-2.38	-2.49	-2.71	-2.89

Table 6.2: Dynamic sensitivities for the four electrophysiological measurements of each gene

time and τ_D (Figure 6.6). However, a clear statistical outlier could be seen in all three plots, corresponding to the gene *GNB5*. After removing this gene from the dataset, we performed tests of correlation and found significant results for these three measurements (τ_{rec}: $P = 0.0004906$, $\rho = 0.8481$; saturation time: $P = 0.003370$, $\rho = 0.7704$; τ_D: $P = 0.003370$, $\rho = 0.7704$). Peak amplitude did not significantly correlate with d_N/d_S ($P = 0.4383$). Additionally, we found that the average dynamic sensitivities for the genes also positively correlated with d_N/d_S ($P = 0.00337$, $\rho = 0.7704$) (Figure 6.7). After adjustment for multiple testing, the results remained significant ($P = 0.002453$ for τ_{rec} and $P = 0.01348$ for saturation time, τ_D and mean sensitivity). The similar results for τ_{rec}, saturation time and τ_D reflect a high degree of covariance between them ($\sigma(\tau_{rec}, sat.time) = 1.66,\ \sigma(\tau_{rec}, \tau_D) = 2.24,\ \sigma(sat.time, \tau_D) = 1.54$).

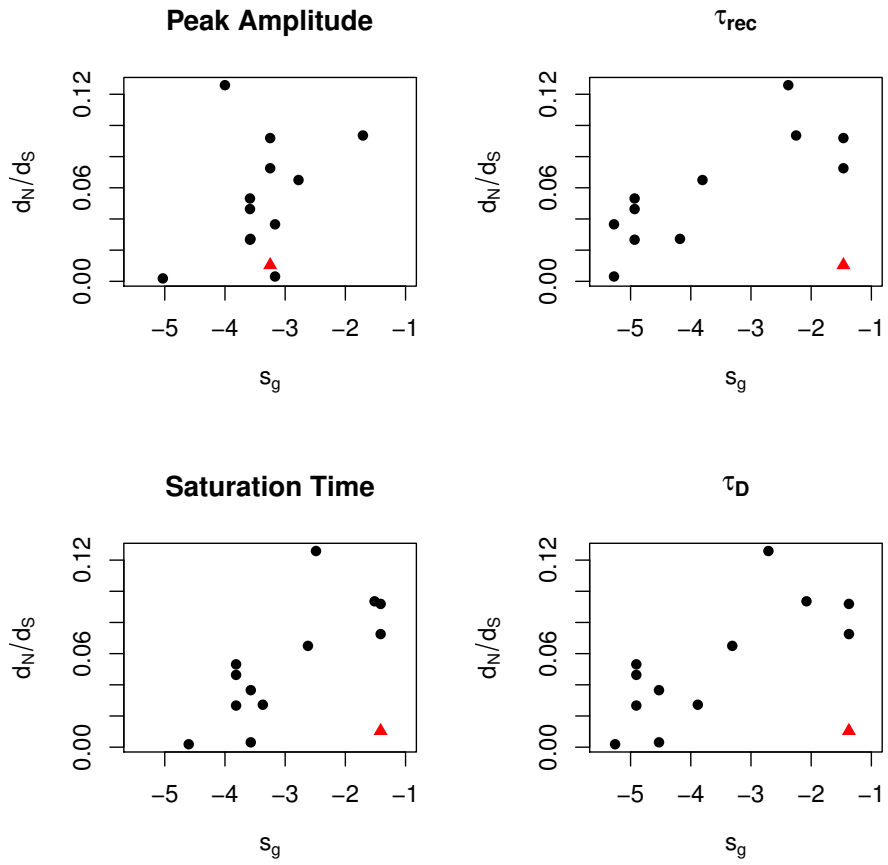

Figure 6.6: d_N/d_S plotted as a function of gene dynamic sensitivities for the four electrophysiological measurements. There was a clear statistical outlier (*GNB5*), indicated by a red triangle, which was removed from the dataset for tests of correlation.

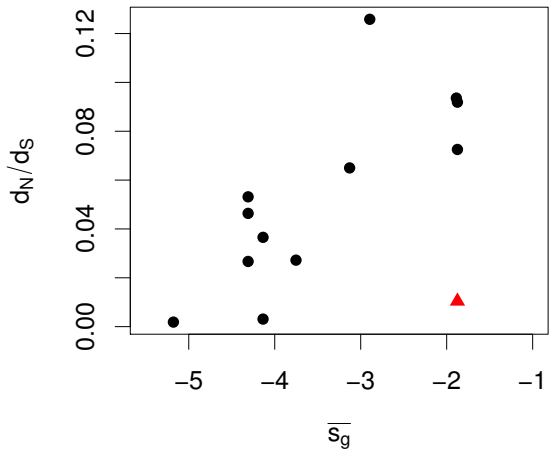

Figure 6.7: d_N/d_S plotted as a function of the average sensitivity for each gene. The statistical outlier (*GNB5*) is indicated as a red triangle.

6.3.3 Non-additive Phenotypic Effects

We used the model to determine whether any non-additive interactions exist in the dynamics. To investigate this, linear models were constructed to predict the effect of simultaneous perturbations to two parameters from the additive effects of individual changes in each of the two parameters alone. For each of the four electrophysiological measurements, the best-fit linear model had a slope of one, indicating a general trend of additive or near-additive interactions. The intercept of the linear model for saturation time also had an intercept that was significantly different from zero ($P = 0.00141$, $\alpha = 1.6 \times 10^{-4}$ s), suggesting at least a slight, positively multiplicative interaction for most parameter pairs, however the intercept is small relative to the scale of the simulated saturation times (approximately 0.8 s).

We next standardized the residuals and tested for values significantly different from zero (Figure 6.8). After correcting for multiple testing, several pairs of parameters were found to have significant residuals, indicating a strong, non-additive interaction between them. Both positive and negative epistatic effects were observed. Many of the parameters that we analyzied appeared in at least one of the significant pairs and all of the genes were associated with at least one non-additive interaction. These results indicate that the potential for epistasis through non-additive functional effects is strong in the phototransduction pathway.

6.4 Discussion

The phenotype, as it arises from the interactions of multitudinous proteins and other molecules, is exquisite in its sheer complexity. In order to truly understand how natural selection on the phenotype gives rise to evolutionary patterns at the genetic level, it is critical to understand how proteins contribute to the phenotype. While each protein taken independently has functionality that contributes to the survival of the organism, it is clear that the nature of that protein's interactions with others should also influence fitness. Indeed, the complex properties that arise out of molecular

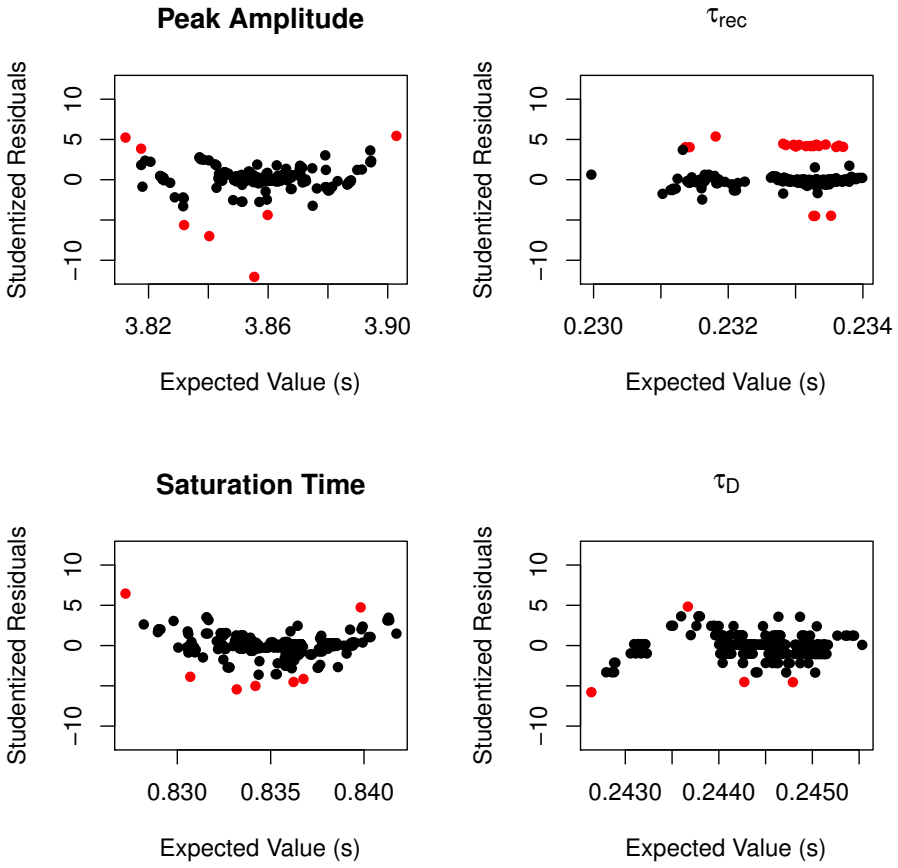

Figure 6.8: Standardized residuals of linear model predictions for parameter interaction effects. Pairs of parameters exhibiting strictly additive effects have a residual value of zero. Red points indicate parameter pairs that have a residual value significantly different from zero, indicating a strongly non-additive interaction between them.

systems are "closer" to the phenotype, the organism's interface with natural selection. Nevertheless, probing the influence of genetic variation on high-level system properties *in vitro* or *in vivo*, by testing the effects of functional changes in many interacting proteins, is a significant undertaking. To date, advances have been made in this direction only in the use of unicellular organisms [189]. For more complex organisms, however, it is possible to use *in silico* techniques to predict how functional changes will affect the phenotype.

Given the potential influence of system dynamics on survival, the question arises of whether proteins that have a greater influence on the dynamics have experienced more or less selective constraint. One would expect that these sensitive parts of the system would be strongly constrained in their evolution, due to their potential to greatly disrupt the normal dynamics. In order to address this, we employed a comprehensive model of mammalian visual phototransduction. We found that, in fact, the proteins that are more likely to have strong effects on system dynamics have shown less evolutionary constraint during mammalian divergence.

6.4.1 Gene dynamic sensitivity is a determinant of evolutionary constraint

While the d_N/d_S ratios of the genes in this study are relatively low, indicating that strong purifying selection has been the dominant evolutionary force acting on the genes, it is clear that the proteins to which the system is more sensitive have accumulated amino acid substitutions at a faster rate during mammalian divergence. While we cannot make predictions regarding the specific impact, if any, of those substitutions in such sensitive genes, we may speculate that, were any of them to be functional, they would be more likely to alter the system dynamics to a greater degree than substitutions in other genes. In this regard, their evolution may have resulted in a gradual fine-tuning of the system over time. The specific amino subtitutions could have resulted in such fine-tuning remain unknown, while we lack the power to test whether any of these changes were adaptive for most of the proteins [16]. Such functional characteriza-

tions are promising future investigations.

It is noteworthy that, of the three electrophysiological measurements used in the parameter sensitivity analysis, the three that are related to signal recovery (τ_{rec}, saturation time and τ_D) featured a correlation between gene sensitivity and evolutionary constraint, while peak amplitude, conceptually more related to signal amplification, saw no such correlation. This may indicate that, in the evolution of the phototransduction proteins, the ability of the system to recover quickly from a stimulus was a stronger adaptive pressure than the system's signal amplification needs. This is surprising, given the rod photoreceptor's role in scotopic (low-light) vision and its ability to produce a response to even a single photon of light. However, it appears that the peak amplitude of a response to a dim stimulus, in fact, can be moderately influenced by most of the proteins, given the similarity in sensitivity values for all genes for this measurement(Figure 6.6). It is possible that tuning the recovery-related proteins alone has been sufficient to moderate the evolution of signal amplification.

During the analysis, one gene, *GNB5*, was removed due to its appearance as a statistical outlier. This gene showed both high dynamic sensitivity and high evolutionary constraint. In the phototransduction system, the protein encoded by *GNB5* is an obligate partner of the regulator of G-protein signaling *RGS9* [190]. Mice lacking it show photoresponses that are indistinguishable from those of mice lacking *RGS9* [191]. It is possible that the system dynamics are not a strong source of selective pressure on this protein, but rather that simply its presence is essential. However, because it interacts with several proteins in the R7 RGS subgroup [192] and it is present in other retinal cells [193], it is likely that it is also strongly constrained in its evolution in order to maintain its functionality across multiple systems.

Previously it was shown that proteins that are topologically central in a network representation of the phototransduction pathway have been under stronger purifying selection [16]. Interestingly, we found no correlation between our gene sensitivity measurements and the topological network measurements described in that publication. Nevertheless, the

contrast between the two results is striking. This difference is likely due to the distinct attributes of the system captured by the two approaches, the static network and the dynamic model. The network was constructed according to the known physical interactions between the proteins. The central proteins may thus be seen as being important in the overall communication of the signal throughout the system. Because they tend to have many interacting partners, their loss would lead to a catastrophic failure to transduce the signal. The way in which we utilized the dynamic model does not capture this behavior; slightly modifying one of the parameters associated with such a protein may not, in fact, disrupt the system dynamics to any significant degree. However, if one were to disable that protein in the model altogether, the dynamics would be greatly affected. For example, the proteins comprised by the phosphodiesterase (PDE) heterotrimer have relatively high centralities in the network, while the model parameters associated with them were found to be extremely insensitive in the present study. Nevertheless, removing PDE from the model would result in cGMP not being hydrolysed and a subsequent lack of any response. Thus, a network representation is appropriate for capturing the essentiality of proteins, while a dynamic model can give information on the fine-tuning of the system.

A recent survey of adaptive selection on phototransduction-related genes in three human populations found significant signals of selection on six genes [106]: *RGS9*, *GNB1*, *RHO*, *PDE6G*, *GNAT1*, *SLC24A1*. In the present study, *SLC24A1* was not included in the analysis. *GNB1*, *RHO*, *PDE6G*, *GNAT1* were all found to have relatively low dynamic sensitivity, while *RGS9* has high sensitivity. This would appear to contradict our above findings. The original study that found evidence of adaptive in these genes used SNP genotyping data from the International HapMap Project [194]. In a re-analysis of these genes with statistics calculated for the same three populations using sequencing data from the 1000 Genomes project [195], only *RGS9* was found to show convincing evidence of adaptive selection (Pierre Luisi, personal communication). *RHO* and *GNAT* both showed significant F_{ST} signals for isolated SNPs but no significant signals were found using iHS, $XPEHH$ or Tajima's

D. The genome region containing *PDE6G* was found to show significant signals of selection, however the region features a cluster of many genes and the signals reside primarily upstream of *PDE6G*. Convincing evidence of recent adaptive change in *RGS9* fits well with the predictions of the present study, while further investigation of the recent evolution of *RHO* and *GNAT1* is needed.

6.4.2 Non-additive interactions are pervasive in phototransduction

When considering the evolution of proteins that interact in a system, it is important to know whether any epistatic interactions exist between them. Epistasis will cause the functional effect of a mutation to be dependent upon the genetic background in which it occurs. Typically, this should manifest as non-additive mutational effects, which are greater or smaller than what is expected [196], and it would implicate co-evolution between some of the proteins [197]. Perhaps most importantly, the identification and characterization of epistasis is an important challenge in understanding the nature of the genotype-to-phenotype map [198]. Here we have proposed a novel approach that employs an accurate, detailed model to predict non-additive functional effects. It proved to be a promising means to quickly assay for the potential for epistatic interactions in a given biological system. We found non-additive interactions to be pervasive in the system, potentially involving all of the genes in the study. This indicates a high probability of finding true epistatic interactions between the genes of the phototransduction pathway and the potential for detecting co-evolution between them.

6.4.3 Limitations

Some limitations were imposed by the model on this study. The first is that it is possible that the parameter values used in the model are, in fact, not similar to the physiological values. Many of the parameters in the model were taken directly from published data, however others were un-

known. Unknown parameters were estimated according to biochemical knowledge or using parameter optimization techniques in order to fit *in vivo* electrophysiological data (Chapter 5). The parameter sensitivity values at other points in parameter space may differ significantly from those that we measured. Such problems may be resolved over time as more physiological parameters are measured.

Second, the model was tuned to fit murine electrophysiological data and known parameter values were taken from biochemical research using proteins derived from the mouse or the cow. It is assumed that, while each species should have the same reaction network for this system, they would occupy different points in parameter space due to molecular evolution. Unfortunately, we lack sufficient data to build individual models for each mammalian species. Therefore, we can only take the model as an approximation of phototransduction in a generalized mammal and we assume, given the observed rates of molecular evolution, that the true points in parameter space that specific species occupy are not greatly separated from that of the model.

Furthermore, several potentially interesting genes were omitted from the analysis due to the mathematical nature of their associated model parameters. For example, the cGMP-gated ion channels and the $Na^+/Ca^{2+}K^+$ ion exchanger, which were previously found to be under the most relaxed evolutionary constraint in the system [16], were removed from the analysis. The ion channels are not directly represented in the model, aside from a Hill equation-like influence of cGMP channel-gating on Ca^{2+} influx [84]. The associated parameters carry very different meanings from the binding and dissociation rates given by the law of mass action and thus they could not be easily compared. The rate of Ca^{2+} efflux via the exchanger, on the other hand, follows the law of mass action like the majority of the rate kinetics in the model, but it is set strictly according to a steady-state with Ca^{2+} influx in the dark. The dark influx rate is in turn determined by the cytoplasmic volume of the rod outer segment and the fraction of the current across the membrane that is carried by Ca^{2+} [55, 84]. Interestingly, the gene encoding the rod $Na^+/Ca^{2+}K^+$ exchanger was previously found to show evidence of adaptive selection during the

divergence of rodents [16]. It is possible that evolution of the rodent rod photoreceptor morphology may have necessitated adaptation in the ion exchanger in order to maintain proper Ca^{2+} homeostasis.

Finally, it is expected that the ability of the rod photoreceptor to respond to a single photon would be evolutionarily significant. This scenario cannot be accurately reproduced with the present model because properly simulating signal amplification from a single receptor would require an implementation of the stochastic nature of protein interactions at the scale of a singly activated receptor. Nevertheless, the model quite accurately reproduces photoresponses to stimuli ranging several orders of magnitude, capturing a significant portion of the important dynamics of the system, and the results presented herein demonstrate its utility in making evolutionary predictions despite these limitations.

6.4.4 Conclusions

This investigation has offered an intriguing insight into molecular evolution in the context of biochemical systems. Whether reduced evolutionary constraint is a common feature of proteins with higher influence on system dynamics remains to be seen. This investigation depended on a high quality mathematical model of the phototransduction system dynamics. The model gives focus to the proteins, rather than second messengers and it consists of low-level descriptions of the reactions rather than mathematically convenient, albeit more abstract, empirical formulas. Its existence was made possible by the fact that phototransduction is perhaps one of the best-studied G-protein signaling pathways, with a rich history of biochemical research that spans decades. Future studies using models of a similar scale will help to elucidate any general trends in the influence of system dynamics on molecular evolution.

Furthermore, it is hoped that the insights gained in the present study will help to guide future investigations into the evolution of phototransduction proteins and, in general, into the evolution of biological systems. For example, biochemical assaying of the dynamically sensitive proteins from diverse mammalian species may reveal functional differences. Al-

ternatively, computational methods may be used to make quantitative predictions about functional differences in the proteins based on observed genetic variation [189]. Additionally, given the significantly more rapid signal dynamics that have developed in mammals relative to other vertebrates [55], it would be informative to broaden the evolutionary scope and analyze the molecular divergence across a deeper phylogenetic tree. Finally, our predictions of pervasive epistasis between phototransduction genes merit further investigation *in vivo*, as no such interactions have been previously described.

Acknowledgments

We would like to thank Alexander V. Kolesnikov for kindly providing the electrophysiological data used in Figure 6.1. This research was funded by grant BFU2010-19443 (subprogram BMC) awarded by the Ministerio de Ciencia y Tecnología (Spain) and by the Direccío General de Recerca, Generalitat de Catalunya (Grup de Recerca Consolidat 2009SGR 1101). BMI is supported by FI-DGR and BE-DGR grants from AGAUR, Generalitat de Catalunya (2011 F1 B1 00275). LM acknowledges funding from the Juan de la Cierva Program of the Spanish Ministry of Science and Innovation (MICINN).

Part III

Discussion

Open your eyes now. I will. One moment. Has all vanished since? If I open and am for ever in the black adiaphane. *Basta!* I will see if I can see.

Ulysses
JAMES JOYCE

Chapter 7

DISCUSSION

As outlined in the Objectives (Chapter 2), this thesis has two primary aims. The first is to give a clearer picture of the molecular evolutionary histories of the proteins of the mammalian visual phototransduction pathway, especially in considering the influence of the structure and dynamics of the system. This was accomplished through an analysis of their molecular evolutionary rates and the integration of those results with both a network representation of the system and a novel technique employing a dynamic model. The second aim was to develop robust models of phototransduction for hypothesis-formation and experimental prediction. These models are to be of use not only for the purposes of the research presented in this thesis but also for other phototransduction researchers.

7.1 System-level evolutionary analysis of phototransduction

7.1.1 Molecular evolutionary rates

An analysis of the molecular evolutionary histories of the proteins of the phototransduction pathway was provided in Chapters 3 and 6. In Chapter 3, the evolutionary rates d_N and d_S were computed for the proteins di-

rectly involved in phototransduction signaling, as well as their d_N/d_S ratios. The analysis also included the proteins of the closely related retinoid cycle, which is essential in the recovery of the photoreceptor cell after a light stimulus; and the transcription factors that determine photoreceptor cell fate. d_N/d_S ratios for all genes were below one, indicating that purifying selection has been the dominant selective force acting on the genes.

7.1.2 System-level analyses

When considering the proteins as a system, patterns in the evolutionary rates emerged. First, by classifying the genes according to protein function, it was found that certain classes have been more strongly conserved than others. In particular, the G proteins and the transcription factors have shown very low d_N/d_S ratios, indicating strong overall selective constraint. The ion channels and the enzymes of the retinoid cycle, on the other hand, have experienced relatively relaxed purifying selection. The results could not, however, support the hypothesis that rod- and cone-specific proteins have evolved under different selective pressures in mammals, nor that the proteins of the signaling pathway were significantly more or less constrained than those of the retinoid cycle or of the photoreceptor development pathway.

It is likely that, as mammalian species transitioned from nocturnal to diurnal lifestyles, more efficient recycling of the visual pigment was required, leading to evolution in the enzymes that recycle it. On the other hand, the ion channels and exchangers are crucial for the maintenance of proper Ca^{2+} homeostasis (Chapter 4 and Chapter 5); it is probable that, as the cytoplasmic volume of the photoreceptor varied during divergence [55], the ion channels and exchangers evolved to maintain functionality.

Next, the phototransduction pathway was encoded as a network (Figure 3.1, page 43). Using this network, we considered whether the topology of the interactions of the system might have placed any constraint on the evolution of the proteins. Indeed, we found that the proteins that are most central in the network have shown the strongest constraint.

These proteins' high centrality scores indicate that they are essential to the proper communication of the signal through the network; this essentiality is reflected in their low d_N/d_S values.

Interestingly, by incorporating a kinetic model of phototransduction into the analysis as presented in Chapter 6, we found that these highly constrained, central proteins, in fact, do not necessarily have strong, individual impacts on the overall system dynamics. That is, if a mutation were to affect the rates of interactions of one of these proteins, the overall photoresponse would not be strongly affected. The strong selective constraint exhibited by these genes would lead one to expect otherwise, though. The genes that encode proteins that do have a significant influence on the dynamics, on the other hand, have experienced relatively relaxed selective constraint.

The results of Chapter 3 and Chapter 6 may be resolved by considering that some proteins are simply essential for the process to proceed, regardless of their overall influence on the shape of the photoresponse, while others may not be as essential but strongly influence system dynamics. For example, the system is largely robust against changes to rates of phosphodiesterase (PDE) interactions but if PDE is removed from the system, no photoresponse is generated. On the other hand the protein recoverin (Rec) showed among the highest sensitivity scores but when it is knocked out, a photoresponse may still be generated, albeit with a faster signal recovery (see Figure 5.4, page 116).

These results make an excellent contribution to the growing field of evolutionary systems biology. The network of the phototransduction pathway has a significantly different topology compared to previously published evolutionary network analyses, particularly in its lack of upstream and downstream regions. Additionally, it represents, to my knowledge, the first system-level analysis in which the central proteins are more constrained in their evolution, a feature that appears also in recent interactome-level analyses [22, 24, 26]. It is important that individual systems continue to be characterized in this manner in order to further understand how selection on the system is translated into genetic evolution.

7.1.3 Biochemical models as tools in evolutionary research

The approach presented in Chapter 6 is a novel method to determine system-level selective pressures. To perform similar hypothesis-testing *in vivo* or *in vitro*, involving the mutagenesis and phenotypic characterization of many proteins, would be extremely expensive and time-consuming. By employing an accurate model of the system, such behavior can be first simulated in order to investigate general trends. Because many models of biochemical systems are publicly available, these methods should be used to explore the influence of system dynamics on molecular evolution in other systems. It will prove interesting to learn if decreased constraint is a common feature of dynamically sensitive proteins or if, as found in network-based analyses, the trends vary from system to system.

It is important, however, that models be not only accurate but also of a simplified mathematical form in order for this analysis to be applicable. The model of phototransduction presented herein is largely constructed of fundamental reactions occurring at rates according to the law of mass action. Thus, most of the parameters not only carry the same mathematical value (that is, they are combined linearly in the rate equations) but also they carry basic biological meanings (binding or dissociation rates, rate of phosphorylation, etc.). Many models are built using rate kinetics, such as the Hill equation, that are constructed to fit a known, empirical behavior. While these are useful in reproducing system dynamics, they can introduce sensitive exponential parameters. Furthermore, these carry more abstract biological meanings, such as binding cooperativity, or they have strictly empirical meanings, such as the ligand concentration of half-maximal activity. Indeed, reactions in the phototransduction model related to cGMP and Ca^{2+} regulation were omitted from our analyses for precisely these reasons. Thus, future analyses of other systems will require further development of models following the same "bottom-up" strategy employed in Chapter 4 and Chapter 5.

7.1.4 Non-additive interactions

It was also found that the system dynamics indicate a strong tendency towards non-additive interactions (Section 6.4.2). Thus, the phenotypic effect of a mutation that perturbs one of these non-additive interactions will depend on the genetic background. In other words, the mutational effect will be more or less than what would be expected, depending on other gene sequences. In order to maintain a successful phenotype, natural selection would have to coordinate the sequences of all proteins involved in the non-additive interaction; thus, such epistatic interactions often result in co-evolution [197]. While we did not specifically test for evidence of co-evolution between the genes of the phototransduction pathway, our results suggest that it merits further investigation and that co-evolution would be likely to be found.

7.1.5 Adaptive selection

We found evidence for adaptive selection in two proteins of the phototransduction pathway: *OPN1SW*, encoding the SWS1 (blue/short-wave) cone opsin, in hominids; and *SLC24A1*, encoding the Na^+/Ca^{2+} K^+ ion exchanger, in rodents. Many events of adaptive evolution have been described for the opsins, however the specific event and putatively selected sites that we presented have not been previously described. Unfortunately, the posterior allele-identification analysis lacked the power to strongly identify the allele or alleles that have undergone adaptive selection. Nevertheless, it appears likely that the selected allele had an effect on the spectral tuning of the receptor. Functional analyses would be required in order to verify this.

Given the lack of structural information on the ion exchanger, we could not definitively know the functionality of the sites that we found to have been under adaptive selection in rodents. The sites' locations in the extracellular region, however, indicate that they could be involved in ion exchange. Because the ion exchangers play an important role in the maintenance of Ca^{2+} homeostasis, it is reasonable to expect these proteins to evolve in response to electrochemical pressures imposed by, for exam-

ple, changes in cell morphology. The evidence of elevated d_N/d_S rates, adaptive selection in rodents, and possible recent evolution in humans [106] lend support to this hypothesis. Thus, this gene merits closer investigation, particularly in the form of a reanalysis of its evolution between human populations (see Section 6.4.1 for a discussion).

Unfortunately, existing tests lack power to robustly detect adaptive selection without having an orthologous sequence alignment of many species. While several mammalian species have genome sequences available, the majority were found not to be of high enough quality to perform analyses on a full suite of system proteins. Thus, the desire to analyze all phototransduction proteins resulted in a strong limitation on the number of species analyzed. With the predictions produced in this thesis, targeted research with many more species can be performed on specific genes of interest. In particular, it is predicted that the genes encoding proteins to which the system is more sensitive (e.g. *RGS9* or *RCVRN*) have undergone functional tuning. Deep investigations into the evolution of these particular proteins in mammals would be a promising future direction.

7.2 Modeling of the phototransduction system

In the course of this research, two robust models of phototransduction were produced: an amphibian model (Chapter 4) and a mammalian model (Chapter 5). Both models were produced in an iterative manner, building upon past efforts. This was made possible by the inherently modular nature of the model from which they were developed [84]. Both models accurately reproduced a variety of photoresponses to stimuli ranging several orders of magnitude and under several different mutant conditions. The mammalian model, in particular, is notable as being the first comprehensive model of light-adaptation in mammals. Because a large portion of modern vision research is performed using mammals, a quantitatively accurate model that encompasses a wide range of the underlying biochemical mechanisms will be an important tool.

7.2.1 Bottom-up kinetic modeling

It was stressed repeatedly that the "bottom-up" strategy employed in the development of this model was an important feature. By this, it is meant that attention is given to modeling the fundamental reactions of the system in a detailed manner and allowing complex system behaviors to emerge from these reactions. This is in contrast to more complex mathematical representations that inherently capture the desired dynamics. Several advantages are imparted by the bottom-up strategy. First, the resulting model becomes effectively modular, allowing new reactions to be added easily without disrupting the rest of the reaction network [84, 152, 153]. Second, the simple parameters used in reaction rates defined according to the law of mass action are intuitive and easy to manipulate in a biologically meaningful way. Finally, by reducing the steps of the process to the fundamental reactions, discrepancies between the model behavior and experimental data more clearly point to gaps in the biochemical knowledge of the system.

7.2.2 Insights into the phototransduction system

Using the two models of phototransduction, several inferences about the system were made. A primary conclusion of Chapter 4 was that Arr homo-oligomerization serves to delay the inactivation of the receptor R^*, in addition to its previously supposed function of maintaining an ideal concentration of the Arr monomer (Section 4.2.7). Arr oligomerization also serves to buffer the effect of increased RK activity, a scenario which the model of Dell'Orco et al. [84] failed to accurately predict. Despite the partial resolution of this discrepancy offered by this homo-oligomerization mechanism, both the present amphibian model and the mammalian model continue to show an unexpected shortening of saturation times when RK activity is increased. Furthermore, the models were found to be very sensitive to the precise nature of the relationship between RK's affinity for R^* and the number of phosphates attached to R^*. Finally, overly rapid inactivation of the receptor may be disrupting the light-adaptation mechanisms present in the model (Section 5.3.2). These results point to a potentially

unknown mechanism that regulates RK's activity.

It was also demonstrated that the cGMP regulatory dynamics in the model are insufficient (Section 5.3.2). In the photoreceptor cell, there are two distinct guanylate cyclases and two GCAPs that act in concert as a Calcium-relay mechanism [75]. Several reactions are involved, including the association and dissociation of Ca^{2+} to the GCAPs and the independent binding of the two GCAPs with each GC. Yet, in the model, this is reduced to a single reaction with a Hill-based rate equation. Based on our simulations, it is clear that important nuances of cGMP regulation are missing from the model, as evidenced by a partial disruption to the light-adaptation mechanisms induced by cGMP regulation (Figure 5.2) and a subtle imbalance in the recovery between dim-light and bright-light photoresponses (Section 5.3.2). Unfortunately, we presently lack mechanistic information to build a detailed model of this sub-system.

7.3 Conclusions

In this thesis, a broad analysis of the structure, function and evolution of the phototransduction system has been presented. A combination of molecular evolutionary techniques and systems biology methods was used to uncover fascinating trends in the constraints imposed on proteins by the systems in which they function. Meanwhile, the development and use of comprehensive kinetic models of the system provided novel views of its underlying dynamics and insight into shortcomings in our current knowledge. In addition, a novel method of integrating a mathematical model of a biochemical system into an evolutionary analysis was presented. This technique offers new insight into the relationship between the dynamic influence of proteins and the selective pressures acting on them and it will be interesting to see it applied to a variety of systems in the future.

The results presented herein provide evidence for the importance of protein interactions and system-level properties in evolution. In particular, it appears that selection on high-level, empirical properties of the photoresponse has induced differential evolutionary rates in the under-

lying proteins, such that those with the greatest influence on system dynamics have accrued more non-synonymous substitutions over time while essential, topologically central proteins have been strongly constrained in their evolution. Notably, the proteins with the greatest dynamic influence are largely related to the signal recovery mechanisms of the phototransduction pathway, which have been shown to consist of complex, interwoven reactions and feedback loops that proceed with subtle, finely tuned timing. Furthermore, much of this tangled network of interactions produces non-additive effects, raising the likelihood of epistatic interactions between the genes. Taken together, these results point to broad patterns of concerted evolution in the proteins of the phototransduction pathway.

Part IV

Appendix

LIST OF PUBLICATIONS

Colombo M, Laayouni H, **Invergo BM**, Bertranpetit J, Montanucci L. Metabolic flux is a determinant of the evolutionary rates of enzyme-encoding genes. *Evolution*, 2013. doi:10.1111/evo.12262.

Invergo BM, Montanucci L, Koch KW, Bertranpetit J, Dell'Orco D. Exploring the rate-limiting steps in visual phototransduction recovery by bottom-up kinetic modeling. *Cell Communication and Signaling*, 11(1):36, 2013. ISSN 1478-811X. doi:10.1186/ 1478-811X-11-36.

Invergo BM, Montanucci L, Laayouni H, Bertranpetit J. A system-level, molecular evolutionary analysis of mammalian phototransduction. *BMC Evolutionary Biology*, 13:52, 2013.

Talevich E, **Invergo BM**, Cock PJ, Chapman BA. Bio.Phylo: A unified toolkit for processing, analyzing and visualizing phylogenetic trees in Biopython. *BMC Bioinformatics*, 13:209, 2012. ISSN 1471-2105. doi:10.1186/1471-2105-13-209.

Dall'Olio GM, Marino J, Schubert M, Keys KL, Stefan MI, Gillespie CS, Poulain P, Shameer K, Sugar R, **Invergo BM**, Jensen LJ, Bertranpetit J, Laayouni H. Ten simple rules for getting help from online scientific communities. *PLoS Computational Biology*, 7(9):e1002202, 2011. ISSN 1553-7358. doi:10.1371/journal.pcbi. 1002202.

Oostra V, de Jong MA, **Invergo BM**, Kesbeke F, Wende F, Brakefield PM, Zwaan BJ. Translating environmental gradients into discontinuous

reaction norms via hormone signalling in a polyphenic butterfly. *Proceedings of the Royal Society B: Biological Sciences*, 2010. ISSN 1471-2954. doi:10.1098/rspb.2010.1560.

McCall MA, Maddox DM, Vessey KA, Yarbrough GL, **Invergo BM**, Cantrell DR, Inayat S, Balannik V, Hicks WL, Hawes NL, Byers S, Smith RS, Hurd R, Howell D, Gregg RG, Chang B, Troy JB, Pinto LH, Nishina PM. Allelic variance between GRM6 mutants, Grm6nob3 and Grm6nob4 results in differences in retinal ganglion cell visual responses. *The Journal of Physiology*, 586(18):4409– 4424, 2008. doi:10.1113/jphysiol.2008.157289.

Pinto LH, Vitaterna MH, Shimomura K, Siepka SM, Balannik V, Mcdearmon EL, Omura C, Lumayag S, **Invergo BM**, Glawe B, Cantrell DR, Inayat S, Olvera MA, Vessey KA, Maddox D, Morgans CW, Young B, Pletcher MT, Mullins RF, Troy JB, Takahashi JS. Generation, identification and functional characterization of the nob4 mutation of Grm6 in the mouse. *Visual Neuroscience*, 24(1):111–123, 2007.

Pinto LH, **Invergo B**, Troy JB, Shimomura K, Takahashi JS. Interpretation of the mouse electroretinogram. *Documenta Ophthalmologica*, 115(3):127–136, 2007. ISSN 0012-4486. doi:10.1007/ s10633-007-9064-y.

Pinto LH, Vitaterna MH, Shimomura K, Siepka SM, McDearmon EL, Fenner D, Lumayag SL, Omura C, Andrews AW, Baker M, **Invergo BM**, Olvera MA, Heffron E, Mullins RF, Sheffield VC, Stone EM, Takahashi JS. Generation, characterization, and molecular cloning of the Noerg-1 mutation of rhodopsin in the mouse. *Visual Neuroscience*, 22(5):619–629, 2005. ISSN 0952-5238. doi: 10.1017/S0952523805225117.

WORD CLOUDS

Figure S1: Chapter 3: A system-level, molecular evolutionary analysis of mammalian phototransduction

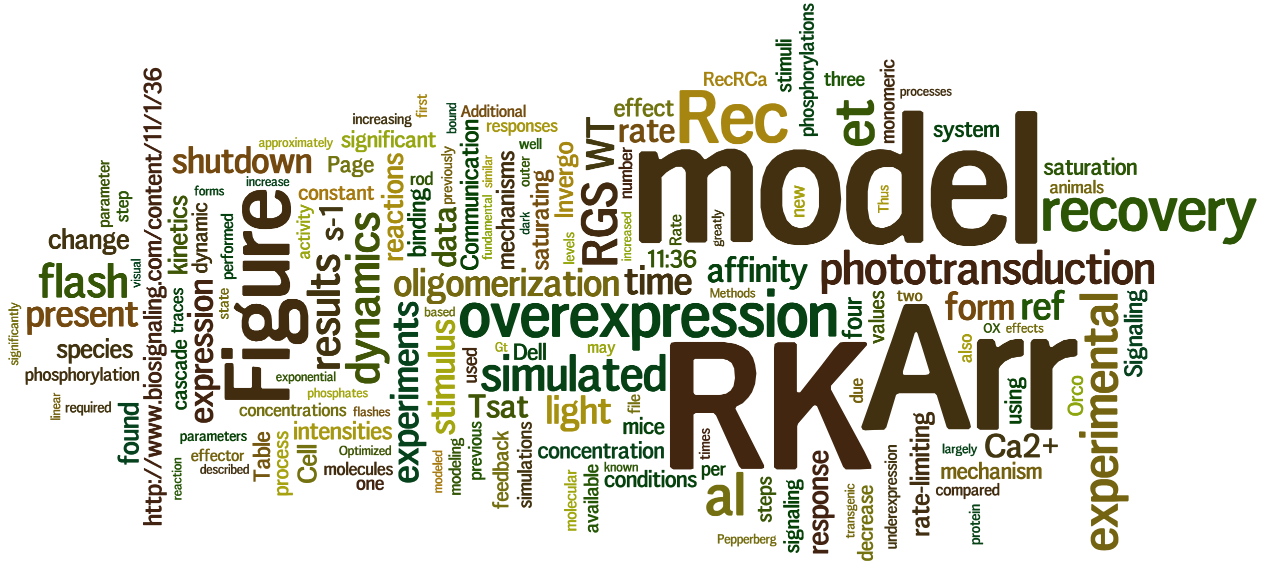

Figure S2: Chapter 4: Exploring the rate-limiting steps in visual phototransduction recovery by bottom-up kinetic modeling

Figure S3: Chapter 5: A comprehensive model of light adaptation in mammalian rod cells

Figure S4: Chapter 6: A dynamic model of mammalian phototransduction reveals insights into the molecular evolution of systems

SUPPLEMENTARY MATERIALS

A system-level, molecular-evolutionary analysis of mammalian phototransduction

Table S1: Classification of the genes. Genes were assigned classifications according to their photoreceptor cell-type specificity, the process in which the encoded protein is primarily active, and the general function of the encoded protein. (Note: here "enzyme" specifically refers to enzymes involved in retinoid recycling.)

Gene	Cell Type	Process	Function
ABCA4	shared	retinoid cycle	enzyme
AIPL1	shared	phototransduction	other
ARR3	cone	phototransduction	signal regulator
ASCL1	rod	development	transcription regulation
CNGA1	rod	phototransduction	ion channel
CNGA3	cone	phototransduction	ion channel
CNGB1	rod	phototransduction	ion channel
CNGB3	cone	phototransduction	ion channel
CRX	shared	development	transcription regulation
GNAT1	rod	phototransduction	G protein
GNAT2	cone	phototransduction	G protein
GNB1	rod	phototransduction	G protein

Table S1 – *Continued from previous page*

Gene	Cell Type	Process	Function
GNB3	cone	phototransduction	G protein
GNB5	shared	phototransduction	G protein
GNGT1	rod	phototransduction	G protein
GNGT2	cone	phototransduction	G protein
GPSM2	shared	phototransduction	other
GRK1	shared	phototransduction	signal regulator
GUCA1A	shared	phototransduction	signal regulator
GUCA1B	shared	phototransduction	signal regulator
GUCY2D	shared	phototransduction	other
GUCY2F	shared	phototransduction	other
LRAT	shared	retinoid cycle	enzyme
NEUROD1	shared	development	transcription regulation
NR2E3	rod	development	transcription regulation
NR2F1	cone	development	transcription regulation
NRL	rod	development	transcription regulation
OPN1SW	cone	phototransduction	other
OTX2	shared	development	transcription regulation
PDC	shared	phototransduction	signal regulator
PDE6A	rod	phototransduction	phosphodiesterase
PDE6B	rod	phototransduction	phosphodiesterase
PDE6C	cone	phototransduction	phosphodiesterase
PDE6G	rod	phototransduction	phosphodiesterase
PDE6H	cone	phototransduction	phosphodiesterase
PIAS3	rod	development	transcription regulation
PRPH2	shared	development	other
RBP1	shared	retinoid cycle	chaperon
RBP3	shared	retinoid cycle	chaperon
RCVRN	shared	phototransduction	signal regulator
RDH12	shared	retinoid cycle	enzyme
RDH5	shared	retinoid cycle	enzyme
RDH8	shared	retinoid cycle	enzyme
RGR	shared	retinoid cycle	enzyme

Table S1 – *Continued from previous page*

Gene	Cell Type	Process	Function
RGS9	shared	phototransduction	signal regulator
RGS9BP	shared	phototransduction	other
RHO	rod	phototransduction	other
RLBP1	shared	retinoid cycle	chaperon
ROM1	shared	development	other
RORA	cone	development	transcription regulation
RORB	shared	development	transcription regulation
RPE65	shared	retinoid cycle	enzyme
RXRG	cone	development	transcription regulation
SAG	rod	phototransduction	signal regulator
SLC24A1	rod	phototransduction	ion channel
SLC24A2	cone	phototransduction	ion channel
THRB	cone	development	transcription regulation

Table S2: Protein interactions in the phototransduction signaling pathway. The status of each interaction is defined as "confirmed", or generally considered to be true by multiple sources such as reviews; "suggested", or proposed by a primary research source but not replicated; or "inferred", or inferred from a primary research source, such as indirect interactions across a molecular complex where no direct interaction is described or interactions of a paralogous protein to that described in the research.

Gene 1	Gene 2	Status	Primary Source
SAG	*SAG*	confirmed	[71]
GRK1	*RCVRN*	confirmed	[143]
SLC24A2	*CNGA3*	confirmed	[199]
SLC24A2	*CNGB3*	confirmed	[199]
SLC24A1	*CNGA1*	confirmed	[199]
SLC24A1	*CNGB1*	confirmed	[199]
CNGB1	*PRPH2*	confirmed	[200]
CNGB3	*CNGA3*	confirmed	[201]
CNGA3	*CNGA3*	confirmed	[201]

Table S2 – *Continued from previous page*

Gene 1	Gene 2	Status	Primary Source
CNGB3	*CNGB3*	confirmed	[201]
CNGA1	*CNGB1*	confirmed	[202]
CNGA1	*CNGA1*	confirmed	[203]
CNGB3	*PDE6C*	inferred	[204]
CNGB3	*PDE6H*	inferred	[204]
CNGB1	*PDE6A*	suggested	[204]
CNGB1	*PDE6B*	suggested	[204]
CNGB1	*PDE6G*	suggested	[204]
GPSM2	*GNAT2*	suggested	[205]
GPSM2	*GNAT1*	suggested	[205]
PDE6C	*GNAT2*	inferred	[206]
PDE6H	*GNAT2*	inferred	[207]
GNAT1	*PDE6A*	inferred	[206]
GNAT1	*PDE6G*	confirmed	[207]
GNAT1	*PDE6B*	inferred	[206]
ARR3	*OPN1SW*	confirmed	[208]
GRK1	*OPN1SW*	confirmed	[208]
OPN1SW	*GNAT2*	inferred	[209, 210]
OPN1SW	*GNB3*	inferred	[211]
OPN1SW	*GNGT2*	inferred	[212]
SAG	*RHO*	confirmed	[213]
GRK1	*RHO*	confirmed	[214]
RHO	*GNAT1*	confirmed	[215]
RHO	*GNB1*	confirmed	[215]
RHO	*GNGT1*	confirmed	[215]
PRPH2	*PRPH2*	confirmed	[216]
PRPH2	*ROM1*	confirmed	[216]
PDC	*GNB3*	confirmed	[217]
PDC	*GNGT2*	confirmed	[217]
PDC	*GNB1*	confirmed	[218]
PDC	*GNGT1*	confirmed	[218]
PDE6C	*PDE6H*	confirmed	[219, 220]

Table S2 – *Continued from previous page*

Gene 1	Gene 2	Status	Primary Source
PDE6C	*PDE6C*	inferred	[220]
PDE6H	*PDE6H*	inferred	[221]
PDE6A	*PDE6G*	confirmed	[222]
PDE6A	*PDE6B*	confirmed	[222]
PDE6B	*PDE6G*	confirmed	[222]
PDE6G	*PDE6G*	inferred	[221]
GUCY2D	*GUCY2F*	inferred	[223]
GUCY2D	*GUCY2D*	confirmed	[223]
GUCY2F	*GUCY2F*	inferred	[223]
GNAT2	*GUCY2D*	confirmed	[224]
GNAT2	*GUCY2F*	confirmed	[224]
GNAT1	*GUCY2D*	confirmed	[224]
GNAT1	*GUCY2F*	confirmed	[224]
GUCA1A	*GUCY2F*	confirmed	[225]
GUCA1B	*GUCY2F*	confirmed	[225]
GUCA1A	*GUCY2D*	confirmed	[225]
GUCA1B	*GUCY2D*	confirmed	[225]
RGS9	*GUCY2F*	confirmed	[226, 227]
RGS9	*GUCY2D*	confirmed	[226, 227]
RGS9	*RGS9BP*	confirmed	[228]
GNB5	*RGS9*	confirmed	[229]
GNB5	*GNAT1*	inferred	[230]
RGS9	*PDE6G*	confirmed	[230, 231]
RGS9	*GNAT1*	confirmed	[230]
GNAT2	*RGS9*	inferred	[230]
GNB5	*GNAT2*	inferred	[230]
PDE6H	*RGS9*	inferred	[230, 231]
ROM1	*ROM1*	confirmed	[216]
GNAT2	*GNB3*	inferred	[210, 211, 215]
GNAT2	*GNGT2*	inferred	[210, 212, 215]
GNB3	*GNGT2*	inferred	[211, 212, 215]
GNAT1	*GNB1*	confirmed	[215]

Table S2 – *Continued from previous page*

Gene 1	Gene 2	Status	Primary Source
GNAT1	*GNGT1*	confirmed	[215]
GNB1	*GNGT1*	confirmed	[215]

Table S3: The molecular evolutionary results calculated for each gene are listed: the human protein length in amino acids, the non-synonymous substitution rate (d_N), the synonymous substitution rate (d_S), and the ratio d_N/d_S (ω).

Gene	Length	$\mathbf{d_N}$	$\mathbf{d_S}$	ω
ABCA4	2273	0.13	0.94	0.139
AIPL1	384	0.095	2.329	0.041
ARR3	388	0.178	0.802	0.222
ASCL1	236	0.012	1.534	0.008
CNGA1	759	0.096	1.043	0.092
CNGA3	698	0.156	1.452	0.107
CNGB1	1251	0.173	1.423	0.121
CNGB3	809	0.253	0.81	0.312
CRX	299	0.052	1.322	0.039
GNAT1	350	0.004	1.894	0.002
GNAT2	354	0.041	0.882	0.047
GNB1	340	0.003	1.047	0.003
GNB3	340	0.042	1.094	0.039
GNB5	395	0.011	1.011	0.01
GNGT1	74	0.037	1.01	0.037
GNGT2	69	0.119	1.056	0.113
GPSM2	684	0.076	0.994	0.077
GRK1	563	0.157	2.422	0.065
GUCA1A	205	0.052	2.569	0.02
GUCA1B	200	0.056	1.542	0.036
GUCY2D	1103	0.158	1.533	0.103
GUCY2F	1108	0.122	0.621	0.196
LRAT	230	0.215	1.367	0.157

Table S3 – *Continued from previous page*

Gene	**Length**	$\mathbf{d_N}$	$\mathbf{d_S}$	ω
NEUROD1	356	0.037	1.407	0.026
NR2E3	410	0.079	1.386	0.057
NR2F1	423	0.004	0.927	0.004
NRL	237	0.191	1.165	0.164
OPN1SW	348	0.157	0.972	0.162
OTX2	297	0.023	0.377	0.06
PDC	270	0.099	0.918	0.108
PDE6A	860	0.055	1.187	0.046
PDE6B	854	0.1	1.884	0.053
PDE6C	858	0.142	1.051	0.135
PDE6G	137	0.022	0.817	0.027
PDE6H	83	0.091	0.953	0.096
PIAS3	628	0.042	0.771	0.054
PRPH2	346	0.08	1.579	0.051
RBP1	197	0.023	1.141	0.021
RBP3	1274	0.161	2.025	0.08
RCVRN	200	0.121	1.293	0.094
RDH12	316	0.125	1.104	0.113
RDH5	318	0.129	0.883	0.146
RDH8	311	0.149	1.183	0.126
RGR	297	0.219	1.556	0.141
RGS9	674	0.117	1.275	0.092
RGS9BP	235	0.179	2.468	0.073
RHO	348	0.052	1.905	0.027
RLBP1	347	0.091	1.461	0.063
ROM1	198	0.209	0.794	0.263
RORA	556	0.012	0.697	0.017
RORB	470	0.025	0.574	0.043
RPE65	533	0.061	0.98	0.062
RXRG	463	0.027	1.035	0.027
SAG	405	0.137	1.09	0.126
SLC24A1	1099	0.4	0.91	0.44

Table S3 – *Continued from previous page*

Gene	Length	d_N	d_S	ω
SLC24A2	661	0.107	0.696	0.153
THRB	476	0.041	0.668	0.062

Table S4: GenBank Accession Numbers for resequenced exons. Several exons were resequenced to account for their absence or poor sequence quality in the public genome databases. All exon sequences are available on GenBank.

Gene	Species	Exon	Accession Number
CNGB1	*P. pygmaeus*	1	KC484731
CNGB1	*P. pygmaeus*	24	KC484732
CNGB1	*P. troglodytes*	5	KC484733
CNGB1	*P. troglodytes*	6	KC484734
CNGB1	*P. troglodytes*	24	KC484735
CNGB1	*G. gorilla*	28	KC484736
GRK1	*P. troglodytes*	3	KC484737
PDE6B	*P. troglodytes*	2	KC484738
PDE6B	*P. troglodytes*	4	KC484739
PDE6B	*P. troglodytes*	9	KC484740
PDE6B	*P. troglodytes*	10	KC484741
PDE6B	*P. troglodytes*	13	KC484742
PDE6B	*P. troglodytes*	14	KC484743
PDE6B	*P. troglodytes*	21	KC484744
PDE6B	*P. pygmaeus*	5	KC484745
PDE6B	*P. pygmaeus*	10	KC484746
RGS9	*R. norvegicus*	1	KC484747
RGS9	*R. norvegicus*	6	KC484748
SLC24A1	*P. pygmaeus*	7	KC484749
SLC24A1	*G. gorilla*	7	KC484750

Exploring the rate-limiting steps in visual phototransduction recovery by bottom-up kinetic modeling

Supplementary figures

In the following two figures, we reproduce simulations performed by Dell’Orco et al. [84]. We compare the results using the model of Dell’Orco and Koch [151] (black traces) and the present model (red traces).

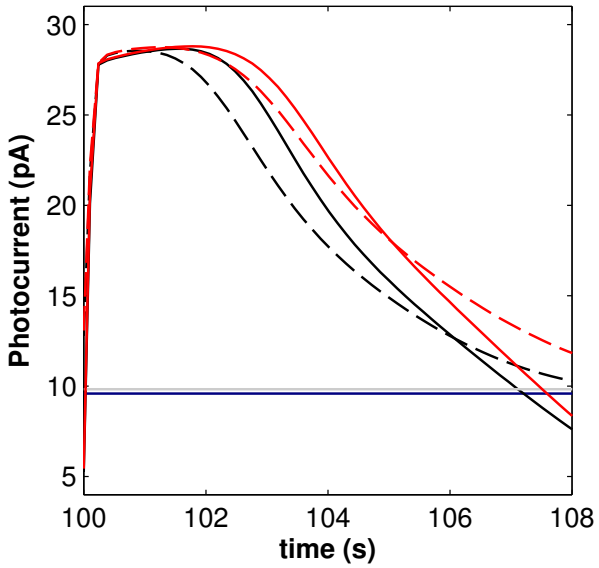

Figure S5: Simulated manifestations of light adaptation in WT rods illuminated by a saturating bright flash in the presence (dashed lines) or in the absence (solid lines) of a previous, non- saturating steady illumination. Both models accurately reproduce the reduction in T_{sat} when exposed to a previous, steady illumination.

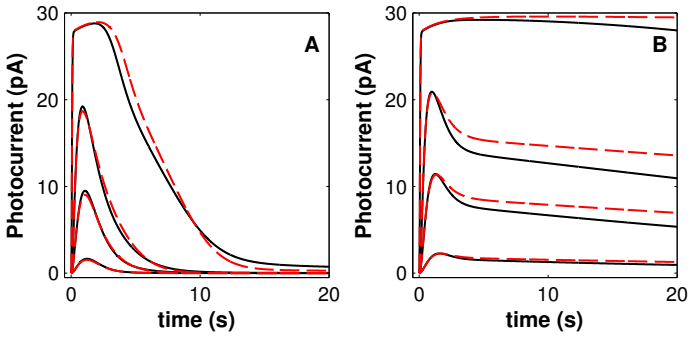

Figure S6: Simulated families of photoresponses from rods stimulated by flashes of increasing strength. While WT rods (A) recover normally, rods lacking RGS (B) show severely prolonged recovery. Note that the experimental and simulated time scales differ due to species differences, and that the experimental photocurrents are normalized to the maximum experimental photocurrent. Both models perform similarly. The present model features slower innate E^* shutoff than previous models, thus they show slower recovery in RGS knockout experiments.

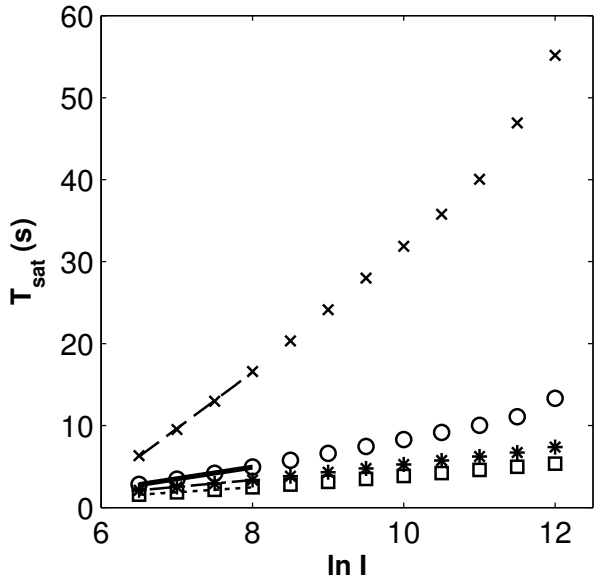

Figure S7: Simulations of RGS expression experiments of Burns and Pugh [107]. τ_D, the rate of change in saturation time for increasing log stimulus intensities, is strongly dependent on RGS expression level (0.2x underexpression: X's; 2x overexpression: stars; 4x overexpression: squares; WT: circles).

A comprehensive model of light adaptation in mammalian rod cells

Table S5: Reactions and kinetics of the phototransduction model

Reaction Equation	Reaction kinetics	Comments
$\mathrm{R} \xrightarrow{stimulus} \mathrm{R}_0$	$v_f = \text{stimulus}\frac{R}{R_{tot}}$	Photoactivation of unphosphorylated R
$\mathrm{R}\cdot\mathrm{G_t} \xrightarrow{stimulus} \mathrm{R}_0\cdot\mathrm{G_t}$	$v_f = \text{stimulus}\frac{R\cdot G_t}{R_{tot}}$	Photoactivation of pre-coupled $\mathrm{R}\cdot\mathrm{G_t}$
$\mathrm{R_n} + \mathrm{RK} \underset{kRK2}{\overset{kRK1_n}{\rightleftharpoons}} \mathrm{R_n}\cdot\mathrm{RK_{pre}} \,\vert_{n=0,1,\ldots,6}$	$v_f = kRK1_n \times R_n \times RK$ $v_r = kRK2 \times R_n \times RK_{pre}$	Binding of $\mathrm{R_n}$ and RK. The association rate constant is assumed to decrease exponentially with increasing phosphorylations: $kRK1_n = kRK1_0\, e^{-\omega n}$
$\mathrm{R_n}\cdot\mathrm{RK_{pre}} \xrightarrow{kRK3_{ATP}} \mathrm{R_{n+1}}\cdot\mathrm{RK_{post}} \,\vert_{n=0,1,\ldots,5}$	$v_f = kRK3_{ATP} \times R_n \cdot RK_{pre}$	Phosphorylation of $\mathrm{R_n}$ to give $\mathrm{R_{n+1}}$
$\mathrm{R_n}\cdot\mathrm{RK_{post}} \xrightarrow{kRK4} \mathrm{R_n} + \mathrm{RK} \,\vert_{n=1,2,\ldots,6}$	$v_f = kRK4 \times R_n \cdot RK_{post}$	Dissociation of the $\mathrm{R_n}\cdot\mathrm{RK}$ complex
$\mathrm{R_n} + \mathrm{Arr} \underset{kA2}{\overset{kA1_n}{\rightleftharpoons}} \mathrm{R_n}\cdot\mathrm{Arr} \,\vert_{n=1,2,\ldots,6}$	$v_f = kA1_n \times R_n \times Arr$ $v_r = kA2 \times R_n \cdot Arr$	Binding of $\mathrm{R_n}$ and Arr. The association rate constant increases linearly with the first four phosphorylations: $kA1_n = \begin{cases} kArr + (n-1)m_{Arr} & n \le 4 \\ kArr + 3m_{Arr} & n > 4 \end{cases}$
$\mathrm{R_n}\cdot\mathrm{Arr} \xrightarrow{kA3} \mathrm{Ops} + \mathrm{Arr} \,\vert_{n=1,2,\ldots,6}$	$v_f = kA3 \times R_n \cdot Arr$	Arr-mediated inactivation of $\mathrm{R_n}$. Ops indicates the ligand-free receptor

Table S5 – *Continued from previous page*

Reaction Equation	Reaction kinetics	Comments
$\text{Arr} + \text{Arr} \underset{kA5}{\overset{kA4}{\rightleftharpoons}} \text{Arr}_{\text{di}}$	$v_f = kA4 \times Arr^2$ $v_r = kA5 \times Arr_{di}$	Arr homo-dimerization
$\text{Arr}_{\text{di}} + \text{Arr}_{\text{di}} \underset{kA5}{\overset{kA4}{\rightleftharpoons}} \text{Arr}_{\text{tetra}}$	$v_f = kA4 \times Arr_{di}^2$ $v_r = kA5 \times Arr_{tetra}$	Arr homo-tetramerization
$\text{R}_\text{n} \xrightarrow{ktherm} \text{Ops} \mid_{n=0,1,...,6}$	$v_f = ktherm \times R_n$	Thermal decay of catalytic active form of R_n to give Ops
$\text{Ops} + \text{G}_\text{t} \underset{kG2}{\overset{kOps}{\rightleftharpoons}} \text{Ops} \cdot \text{G}_\text{t}$	$v_f = kOps \times Ops \times G_t$ $v_r = kG2 \times Ops.G_t$	Spontaneous Ops activity
$\text{Ops} \cdot \text{G}_\text{t} \underset{kG4_{GDP}}{\overset{kG3}{\rightleftharpoons}} \text{Ops} \cdot \text{G}$	$v_f = kG3 \times Ops \cdot G_t$ $v_r = kG4_{GDP} \times Ops \cdot G$	GDP dissociation from the $\text{Ops} \cdot \text{G}_\text{t}$ complex
$\text{Ops} \cdot \text{G} \xrightarrow{kG5_{GTP}} \text{Ops} \cdot \text{G}_{\text{GTP}}$	$v_f = kG5_{GTP} \times Ops.G$	GTP binding to the $\text{Ops} \cdot \text{G}_\text{t}$ complex
$\text{Ops} \cdot \text{G}_{\text{GTP}} \xrightarrow{kG6} \text{Ops} + \text{G}_{\text{GTP}}$	$v_f = kG6 \times Ops \cdot G_{GTP}$	Dissociation of the $\text{Ops} \cdot \text{G}_{\text{GTP}}$ complex
$\text{Ops} \xrightarrow{kR_{recyc}} \text{R}$	$v_f = kR_{recyc} \times Ops$	Chromophore regeneration by 11-cis retinal binding to Ops
$\text{R} + \text{G}_\text{t} \underset{kG_{pre2}}{\overset{kG_{pre1}}{\rightleftharpoons}} \text{R} \cdot \text{G}_\text{t}$	$v_f = kG_{pre1} \times G_t \times R$ $v_r = kG_{pre2} \times R \cdot G_t$	Pre-coupling of inactive R to G_t, where $kG_{pre1} = 1.6\ kG1_0$ and $kG_{pre2} = 315\ kG2$

Table S5 – *Continued from previous page*

Reaction Equation	Reaction kinetics	Comments
$R_n + G_t \underset{kG2}{\overset{kG1_n}{\rightleftharpoons}} R_n \cdot G_t \mid_{n=0,1,...,6}$	$v_f = kG1_n \times R \times G_t$ $v_r = kG2 \times R \cdot G_t$	Binding of R_n and G_t. The association rate constant is assumed to decrease exponentially with increasing phosphorylations: $kG1_n = kG1_0\, e^{-\omega_G n}$
$R_n \cdot G_t \underset{kG4_{GDP}}{\overset{kG3}{\rightleftharpoons}} R_n \cdot G \mid_{n=0,1,...,6}$	$v_f = kG3 \times R_n \cdot G_t$ $v_r = kG4_{GDP} \times R_n \cdot G$	GDP dissociation from the $R_n \cdot G_t$ complex
$R_n \cdot G \xrightarrow{kG5_{GTP}} R_n \cdot G_{GTP} \mid_{n=0,1,...,6}$	$v_f = kG5_{GTP} \times R_n \cdot G$	GTP binding to the $R_n \cdot G_t$ complex
$R_n \cdot G_{GTP} \xrightarrow{kG6} R_n + G_{GTP} \mid_{n=0,1,...,6}$	$v_f = kG6 \times R_n \cdot G_{GTP}$	Dissociation of the $R_n \cdot G_{GTP}$ complex
$G_{GTP} \xrightarrow{kG7} G_{\alpha GTP} + G_{\beta\gamma}$	$v_f = kG7 \times G_{GTP}$	Dissociation of trimeric G_t into α and $\beta\gamma$ subunits
$PDE + G_{\alpha GTP} \underset{kP1_{rev}}{\overset{kP1}{\rightleftharpoons}} PDE \cdot G_{\alpha GTP}$	$v_f = kP1 \times PDE \times G_{\alpha GTP}$ $v_r = kP1_{rev} \times PDE \cdot G_{\alpha GTP}$	Binding of $G_{\alpha GTP}$ to one PDE inactive subunit
$PDE \cdot G_{\alpha GTP} \xrightarrow{kP2} PDE^* \cdot G_{\alpha GTP}$	$v_f = kP2 \times PDE \cdot G_{\alpha GTP}$	Activation of the $PDE \cdot G_{\alpha GTP}$ complex
$PDE^* \cdot G_{\alpha GTP} + G_{\alpha GTP} \xrightarrow{kP3} G_{\alpha GTP} \cdot PDE^* \cdot G_{\alpha GTP}$	$v_f = kP3 \times PDE^* \cdot G_{\alpha GTP} \times G_{\alpha GTP}$	Binding of $G_{\alpha GTP}$ to singly active PDE
$G_{\alpha GTP} \cdot PDE^* \cdot G_{\alpha GTP} \xrightarrow{kP4} G_{\alpha GTP} \cdot {}^*PDE^* \cdot G_{\alpha GTP}$	$v_f = kP4 \times G_{\alpha GTP} \cdot PDE^* \cdot G_{\alpha GTP}$	Activation of the second $G_{\alpha GTP}$-bound PDE subunit

Table S5 – *Continued from previous page*

Reaction Equation	**Reaction kinetics**	**Comments**
$\text{RGS}+\text{PDE}^* \cdot \text{G}_{\alpha\text{GTP}} \xrightarrow{kRGS1} \text{RGS} \cdot \text{PDE}^* \cdot \text{G}_{\alpha\text{GTP}}$	$v_f = kRGS1 \times RGS \times PDE^* \cdot G_{\alpha GTP}$	Binding of RGS9-1 complex to a singly-active PDE tetramer
$\text{RGS} \cdot \text{G}_{\alpha\text{GTP}} \cdot {}^*\text{PDE}^* \cdot \text{G}_{\alpha\text{GTP}} \xrightarrow{kRGS2} \text{PDE}^* \cdot \text{G}_{\alpha\text{GTP}} + \text{RGS} + \text{G}_{\alpha\text{GDP}}$	$v_f = kRGS2 \times RGS \cdot G_{\alpha GTP} \cdot {}^*PDE^* \cdot G_{\alpha GTP}$	RGS9-1-mediated deactivation of one of two PDE active subunits
$\text{RGS}+\text{PDE}^* \cdot \text{G}_{\alpha\text{GTP}} \xrightarrow{kRGS1} \text{RGS} \cdot \text{PDE}^* \cdot \text{G}_{\alpha\text{GTP}}$	$v_f = kRGS1 \times RGS \times PDE^* \cdot G_{\alpha GTP}$	Binding of RGS9-1 complex to a singly active PDE
$\text{RGS} \cdot \text{PDE}^* \cdot \text{G}_{\alpha\text{GTP}} \xrightarrow{kRGS2} \text{PDE} + \text{RGS} + \text{G}_{\alpha\text{GDP}}$	$v_f = kRGS2 \times RGS \cdot PDE^* \cdot G_{\alpha GTP}$	RGS9-1-mediated deactivation of the singly active PDE
$\text{PDE}^* \cdot \text{G}_{\alpha\text{GTP}} \xrightarrow{kPDE_{shutoff}} \text{PDE} + \text{G}_{\alpha\text{GDP}}$	$v_f = kPDE_{shutoff} \times PDE^* \cdot G_{\alpha GTP}$	Inactivation of the $\text{PDE}^* \cdot \text{G}_{\alpha\text{GTP}}$ complex by $\text{G}_{\alpha\text{GTP}}$'s GTPase activity
$\text{G}_{\alpha\text{GTP}} \cdot {}^*\text{PDE}^* \cdot \text{G}_{\alpha\text{GTP}} \xrightarrow{kPDE_{shutoff}} \text{PDE}^* \cdot \text{G}_{\alpha\text{GTP}} + \text{G}_{\alpha\text{GDP}}$	$v_f = kPDE_{shutoff} \times G_{\alpha GTP} \cdot {}^*PDE^* \cdot G_{\alpha GTP}$	Inactivation of one of the two active PDE subunits by $\text{G}_{\alpha\text{GTP}}$'s GTPase activity
$\text{G}_{\alpha\text{GTP}} \xrightarrow{kG_{shutoff}} \text{G}_{\alpha\text{GDP}}$	$v_f = kG_{shutoff} \times G_{\alpha GTP}$	$\text{G}_{\alpha\text{GTP}}$ auto-catalytic GTPase activity
$\text{G}_{\alpha\text{GDP}} + \text{G}_{\beta\gamma} \xrightarrow{kG_{recyc}} \text{G}_\text{t}$	$v_f = kGrecyc \times G_{\alpha GDP} \times G_{\beta\gamma}$	Reconstitution of G_t heterotrimer from inactive subunits
$\text{Rec}_\text{T} + \text{Ca}^{2+}_\text{free} \underset{kRec2}{\overset{kRec1}{\rightleftharpoons}} \text{Rec}_\text{R} \cdot \text{Ca}^{2+}$	$v_f = kRec1 \times Rec_T \times Ca^{2+}_{free}$ $v_r = kRec2 \times Rec_R \cdot Ca^{2+}$	Ca^{2+}-induced Rec conformation change

Table S5 – *Continued from previous page*

Reaction Equation	**Reaction kinetics**	**Comments**
$\text{Rec}_\text{R} \cdot \text{Ca}^{2+} + \text{RK} \underset{kRec4}{\overset{kRec3}{\rightleftharpoons}} \text{Rec}_\text{R} \cdot \text{Ca}^{2+} \cdot \text{RK}$	$v_f = kRec3 \times Rec_R \cdot Ca^{2+} \times RK$ $v_r = kRec4 \times Rec_R \cdot Ca^{2+} \cdot RK$	Binding of RK to Rec
$\text{Ca}^{2+}_\text{free} \underset{k2}{\overset{k1}{\rightleftharpoons}} \text{Ca}^{2+}_\text{buff}$	$v_f = k1 \times (eT - Ca^{2+}_{buff}) \times Ca^{2+}_{free}$ $v_r = k2 \times Ca^{2+}_{buff}$	Ca^{2+} association and dissociation from intracellular buffers with total concentration eT
$\text{Ca}^{2+}_\text{free} \xrightarrow{\gamma_{Ca}}$	$v_f = \gamma_{Ca} \times (Ca^{2+}_{free} - Ca^{2+}_0)$	Intracellular Ca^{2+}-efflux via the Na^+/Ca^{2+} K^+ exchanger
$\longrightarrow \text{Ca}^{2+}_\text{free}$	$v_f = \frac{10^6 \ fCa \times J_{dark}}{(2+fCa) \times F \times V_{cyto}} \times \left(\frac{cGMP}{cGMP_{dark}}\right)^{n_{cg}}$	Extracellular Ca^{2+}-influx via the cGMP-gated cation channels
$\longrightarrow \text{cGMP}$	$v_f = \frac{\alpha_{max}}{1+\left(\frac{Ca^{2+}_{free}}{Kc_1}\right)^{m_1}} + \frac{\alpha_{max}}{1+\left(\frac{Ca^{2+}_{free}}{Kc_2}\right)^{m_2}}$	cGMP synthesis by guanylate cyclase
$\text{cGMP} \longrightarrow$	$v_f = (\beta_{dark} + \beta_{sub} \times E) \times cGMP$	cGMP hydrolysis by PDE

Table S6: Amplification-related model parameter values and sources

Parameter	Description	Value	Source
ω_G	Exponential rate of decay of G_t affinity for R^* with increasing phosphorylations	0.6	ref. [68]
$kG1_0$	Binding rate of G_t to unphosphorylated R^*	$1 \times 10^{-3}\,s^{-1}$	manually tuned
$kG2$	Dissociation rate of the $R^* \cdot G_t$ complex	$2200\,s^{-1}$	manually tuned
$kG3$	Dissociation rate of GDP from the $R^* \cdot G_t$ complex	$8500\,s^{-1}$	manually tuned
$kG4_{GDP}$	Association rate of GDP to the $R^* \cdot G_t$ complex	$400\,s^{-1}$	manually tuned
$kG5_{GTP}$	Association rate of GTP to the $R^* \cdot G_t$ complex	$3500\,s^{-1}$	manually tuned
$kG6$	Dissociation rate of the $R^* \cdot G_{GTP}$ complex	$8500\,s^{-1}$	manually tuned
$kG7$	Dissociation rate of G_{GTP} into $G_{\beta\gamma}$ and $G_{\alpha GTP}$	$200\,s^{-1}$	ref. [84]
$kOps$	Association rate of Ops (ligand-free R) and G_t due to basal activity	$6.1172 \times 10^{-13}\,s^{-1}$	ref. [232]
$kP1$	Binding rate of PDE to $G_{\alpha GTP}$	$0.054\,97\,s^{-1}$	ref. [84]
$kP1_{rev}$	Dissociation rate of PDE $\cdot$ $G_{\alpha GTP}$, without PDE activation	$0\,s^{-1}$	ref. [84]

Table S6 – *Continued from previous page*

Parameter	Description	Value	Source
$kP2$	Rate of activation of the first PDE_{γ} subunit of $PDE \cdot G_{\alpha GTP}$	$940.7\,s^{-1}$	ref. [84]
$kP3$	Binding rate of $G_{\alpha GTP}$ to an active $PDE \cdot G_{\alpha GTP}$ complex	$1.4983 \times 10^{-9}\,s^{-1}$	ref. [84]
$kP4$	Rate of activation of the second PDE_{γ} subunit of $G_{\alpha GTP} \cdot PDE \cdot G_{\alpha GTP}$	$21.088\,s^{-1}$	ref. [84]

Table S7: Recovery-related model parameter values and sources

Parameter	Description	Value	Source
$kRK1_0$	Binding rate of RK to unphosphorylated R^*	$0.1724\,s^{-1}$	manually tuned
ω	Exponential rate of decay of RK affinity for R^* with increasing phosphorylations	2.5	manually tuned
$kRK2$	Dissociation rate of R^* from RK prior to phosphorylation	$250\,s^{-1}$	ref. [84]
$kRK3_{ATP}$	Binding rate of ATP to $R^* \cdot RK$	$4000\,s^{-1}$	estimated
$kRK4$	Dissociation rate of R^* from the $R^* \cdot RK$ complex following phosphorylation	$250\,s^{-1}$	manually tuned
$kArr$	Binding rate of Arr to singly-phosphorylated R^*	$9.9147 \times 10^{-6}\,s^{-1}$	manually tuned
$kA2$	Dissociation rate of R^* from the $Arr \cdot R^*$ complex prior to R^* inactivation	$0.026\,s^{-1}$	manually tuned *c.f.* ref. [68]
m_{Arr}	Linear rate of increase of Arr affinity for R^* with increasing phosphorylations	9.5475×10^{-6}	manually tuned *c.f.* ref. [68]
$kA3$	Dissociation rate of R^* from the $Arr \cdot R^*$ complex following R^* inactivation	$1.1651\,s^{-1}$	estimated
$kA4$	Binding rate of Arr to form homo-oligomers	$2.9965 \times 10^{-7}\,s^{-1}$	estimated
$kA5$	Dissociation rate of Arr from homo-oligomers	$0.424\,s^{-1}$	manually tuned *c.f.* ref. [72]

Table S7 – *Continued from previous page*

Parameter	Description	Value	Source
$kRrecyc$	Rate constant for R regeneration from Ops.	$0.0007\,\mathrm{s}^{-1}$	ref. [233]
k_{therm}	Thermal decay of R^*	$0.0238\,\mathrm{s}^{-1}$	ref. [234]
$kGrecyc$	Binding rate for $G_{\alpha GDP}$ to $G_{\beta\gamma}$	$2\,\mathrm{s}^{-1}$	ref. [80]
$kGshutoff$	Rate of $G_{\alpha GTP}$ auto-catalytic GTPase activity	$0.05\,\mathrm{s}^{-1}$	ref. [80]
$kPDEshutoff$	Rate of PDE-induced spontaneous $PDE \cdot G_{\alpha GTP}$ shutoff	$0.1\,\mathrm{s}^{-1}$	manually tuned
$kRGS1$	Binding rate of $RGS_9{-}1$ to $PDE \cdot G_{\alpha GTP}$ (one or both active subunits)	$4.8182 \times 10^{-5}\,\mathrm{s}^{-1}$	estimated
$kRGS2$	Rate of hydrolysis and dissociation of one PDE subunit from $G_{\alpha GTP}$	$98\,\mathrm{s}^{-1}$	ref. [181]
$kRec1$	Rate of Ca^{2+}-triggered Rec conformational change (tense to relaxed)	$0.011\,\mu\mathrm{M}^{-1}\,\mathrm{s}^{-1}$	ref. [62]
$kRec2$	Rate of Rec conformational change (relaxed to tense)	$0.05\,\mathrm{s}^{-1}$	ref. [62]
$kRec3$	Binding rate of $Rec \cdot Ca^{2+}$ to RK	$4.1081 \times 10^{-4}\,\mathrm{s}^{-1}$	ref. [84]
$kRec4$	Dissociation rate of RK from $Rec{-}Ca^{2+}$	$0.610\,084\,\mathrm{s}^{-1}$	ref. [84]

Table S8: Ca^{2+} and cGMP regulation-related model parameter values and sources

Parameter	Description	Value	Source
V_{cyto}	Outer segment cytoplasmic volume	0.039 16 pL	ref. [178]
Kc_1	EC_{50} for $GCAP_1$-mediated Ca^{2+} feedback on GC activity	139 nM	ref. [176]
Kc_2	EC_{50} for $GCAP_2$-mediated Ca^{2+} feedback on GC activity	59 nM	ref. [176]
m_1	Hill coefficient for $GCAP_1$-mediated Ca^{2+} feedback on GC activity	1.7	ref. [176]
m_2	Hill coefficient for $GCAP_2$-mediated Ca^{2+} feedback on GC activity	1.7	ref. [176]
α_{max}	Maximal rate of cGMP synthesis	60 μM s^{-1}	ref. [182]
β_{dark}	Dark rate of cGMP hydrolysis	4.1 s^{-1}	ref. [108]
β_{sub}	Rate constant for one catalytic PDE subunit	2.1826×10^{-3} s^{-1}	calculated *c.f.* ref. [78] ($k_{cat} = 3500s^{-1}$, $K_m = 17\mu M$, $B_{cG} = 2$)
fCa	Fraction of the circulating current carried by Ca^{2+}	0.12	ref. [108]
J_{dark}	Dark circulating current	14.87 pA	manually tuned
$cGMP_{dark}$	Dark cGMP concentration	5.1 μM	steady-state analysis
n_{cg}	Hill coefficient for opening cGMP-gated ion channels	3.8	manually tuned

Table S8 – *Continued from previous page*

Parameter	Description	Value	Source
γ_{Ca}	Rate of Ca^{2+} extrusion by Na^+/Ca^{2+} K^+ ion exchanger	$981.3558\,s^{-1}$	steady-state analysis
Ca^{2+}_{dark}	Dark Ca^{2+} concentration	$0.25\,\mu M$	ref. [183]
Ca^{2+}_{0}	Minimum intracellular Ca^{2+} concentration	$0.023\,\mu M$	ref. [183]
k_1	Binding rate of Ca^{2+} to cytoplasmic buffers	$9.370\,59\,\mu M^{-1}\,s^{-1}$	estimated
k_2	Dissociation rate of Ca^{2+} from cytoplasmic buffers	$46.412\,s^{-1}$	steady-state analysis
eT	Total Ca^{2+} buffer molecules concentration	$400\,\mu M$	[84]

A dynamic model of mammalian phototransduction reveals insights into the molecular evolution of systems

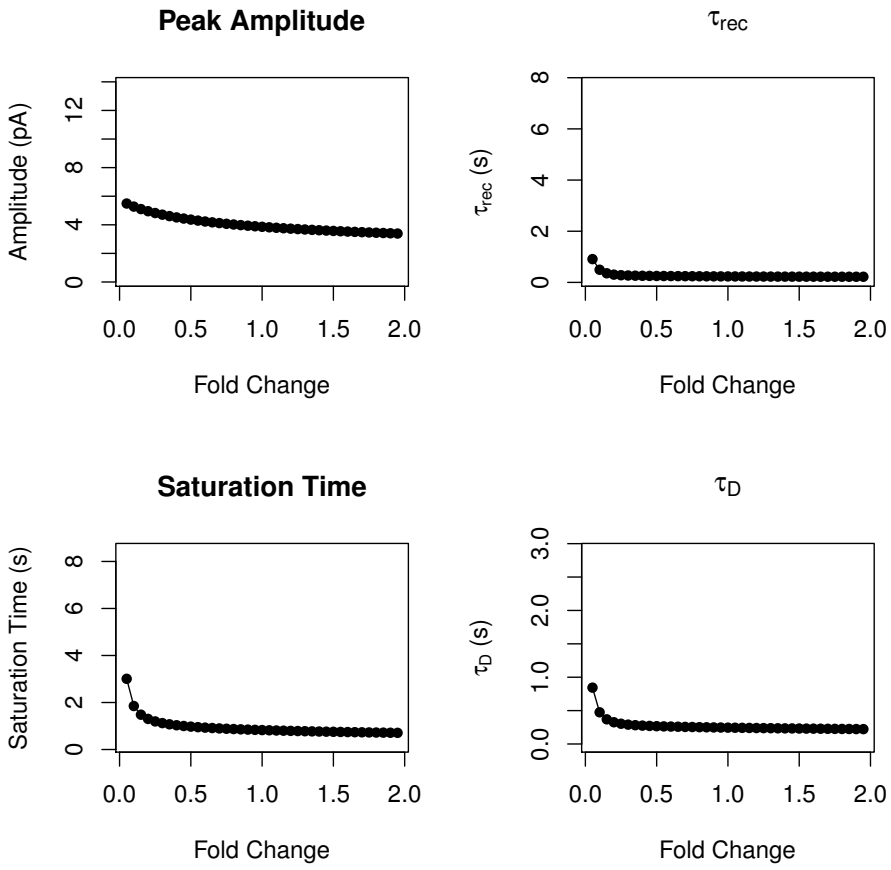

Figure S8: Electrophysiological measurements as functions of the parameter $kRK1_0$.

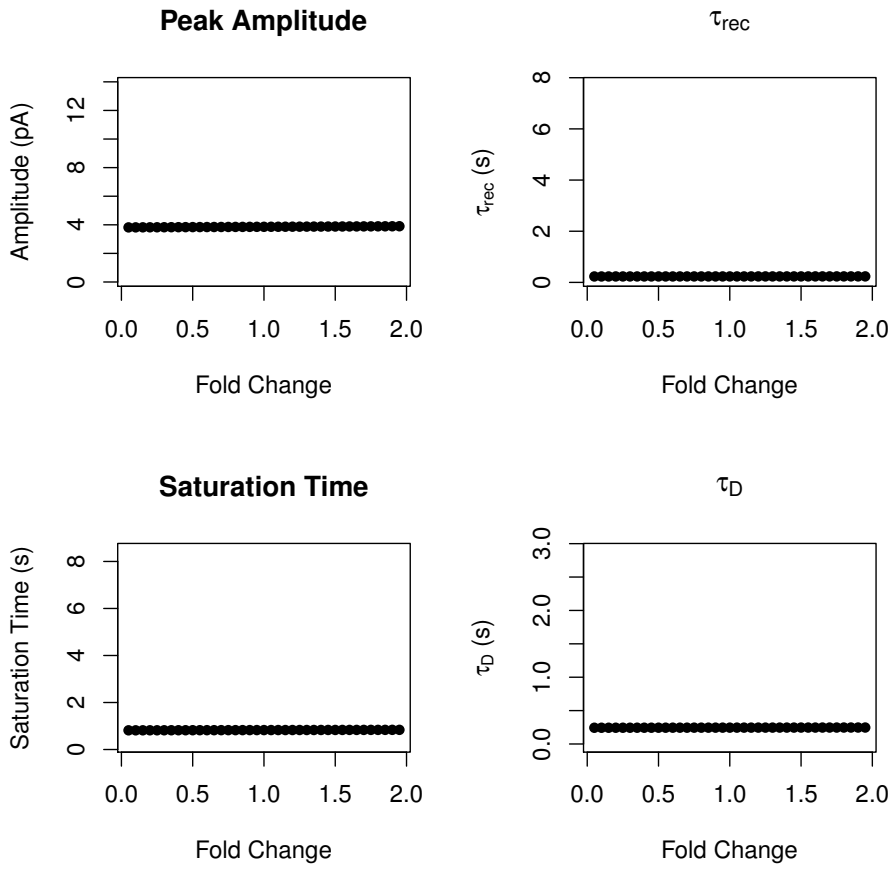

Figure S9: Electrophysiological measurements as functions of the parameter $kRK2$.

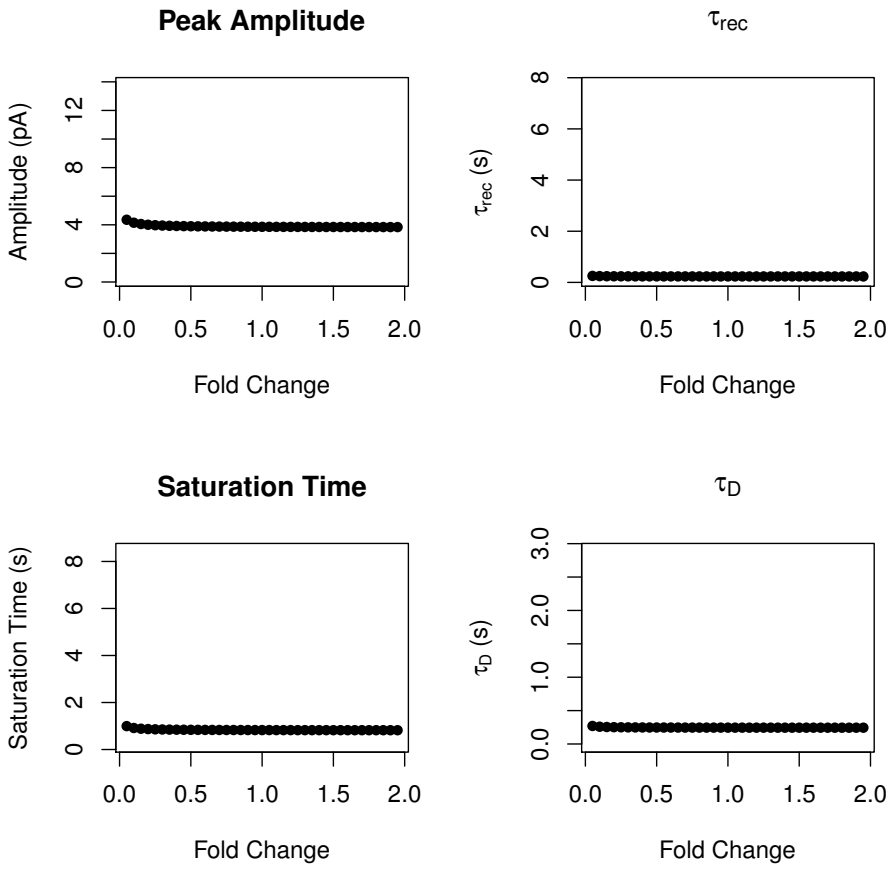

Figure S10: Electrophysiological measurements as functions of the parameter $kRK3_{ATP}$.

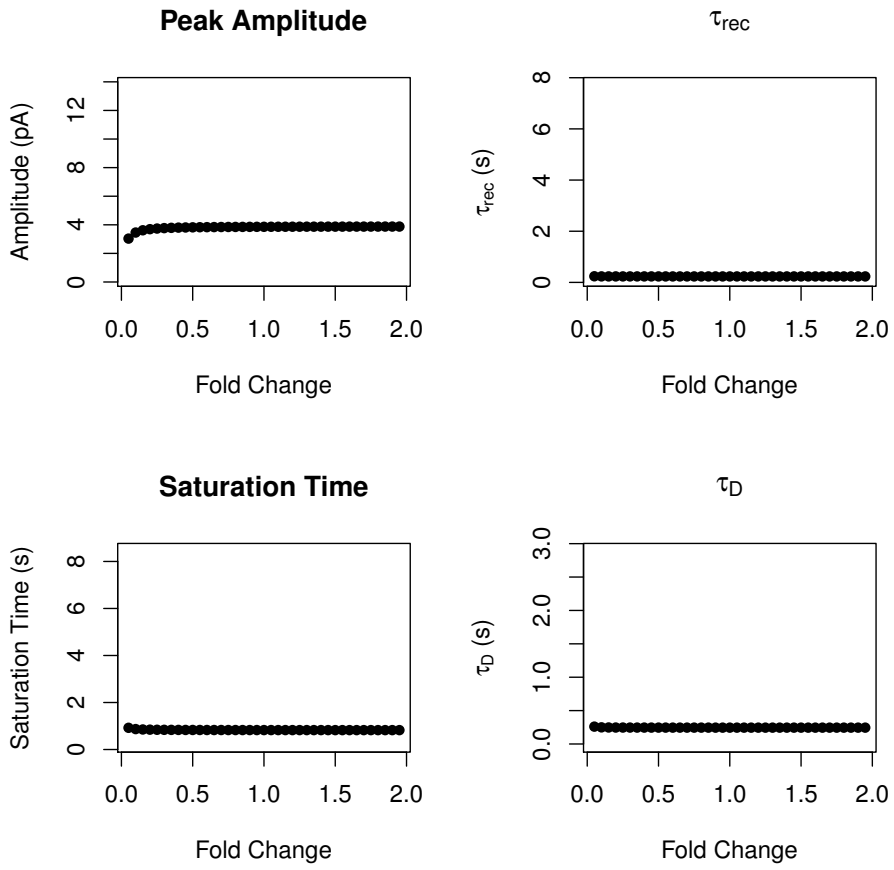

Figure S11: Electrophysiological measurements as functions of the parameter $kRK4$.

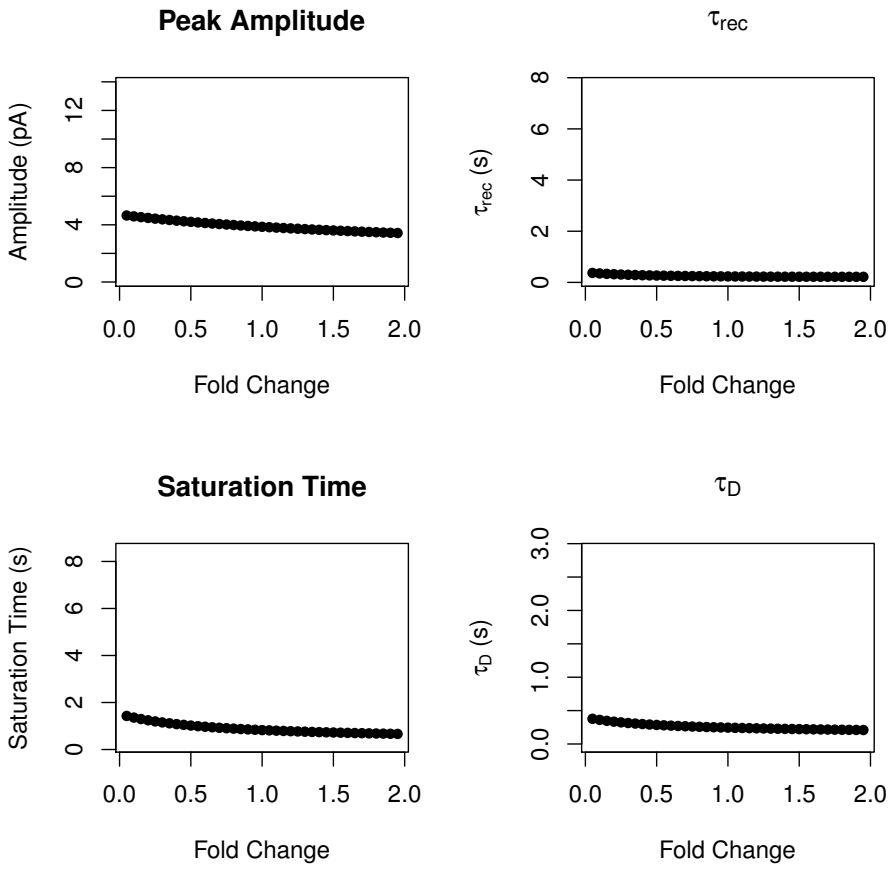

Figure S12: Electrophysiological measurements as functions of the parameter $kArr$.

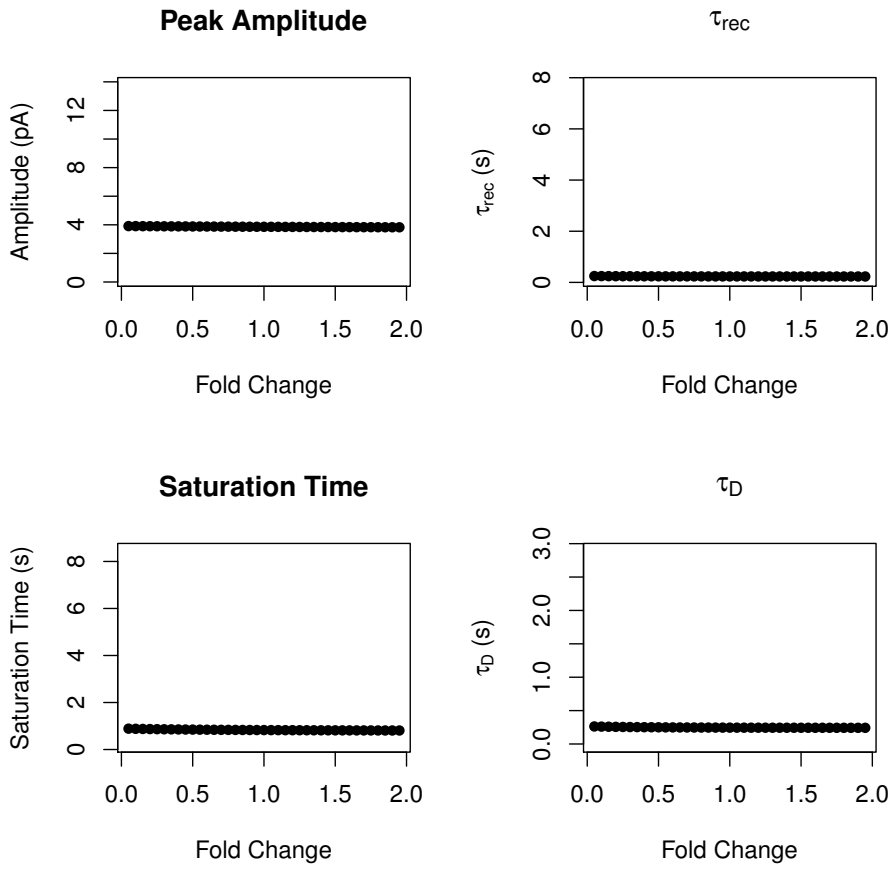

Figure S13: Electrophysiological measurements as functions of the parameter m_{Arr}.

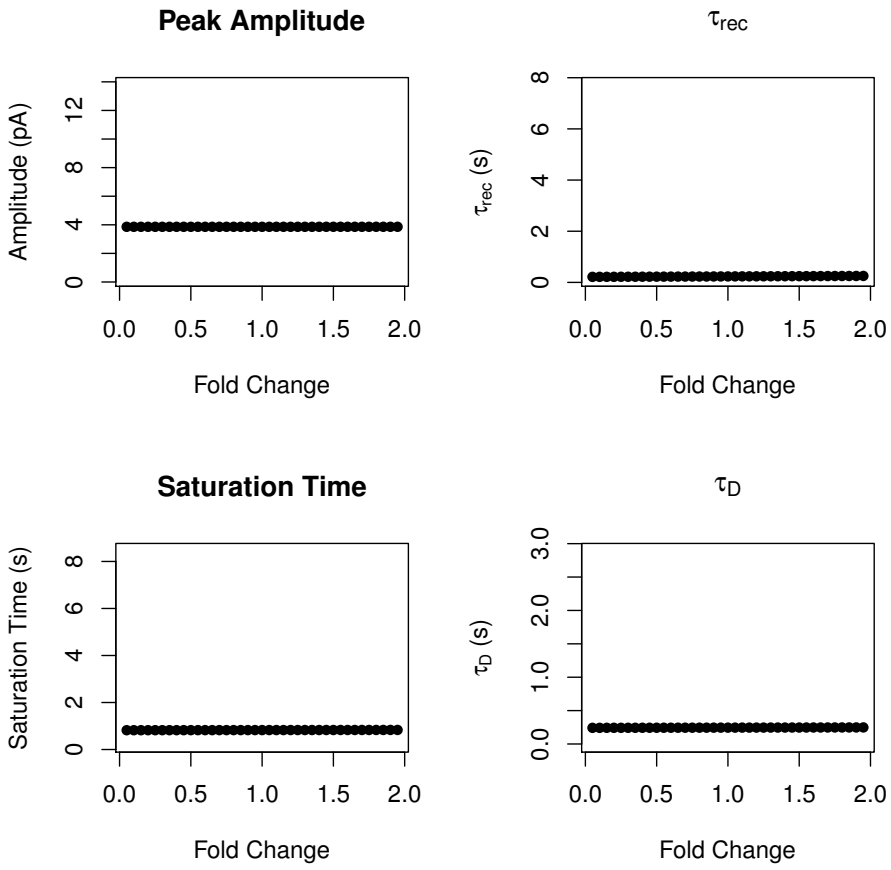

Figure S14: Electrophysiological measurements as functions of the parameter $kA2$.

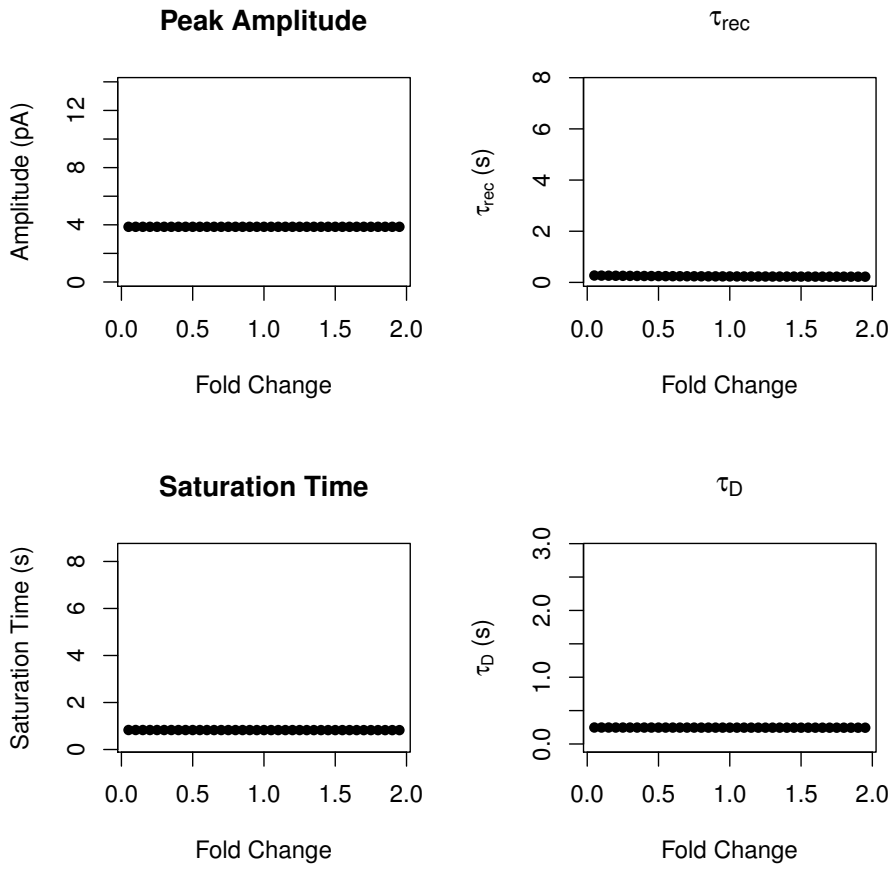

Figure S15: Electrophysiological measurements as functions of the parameter $kA3$.

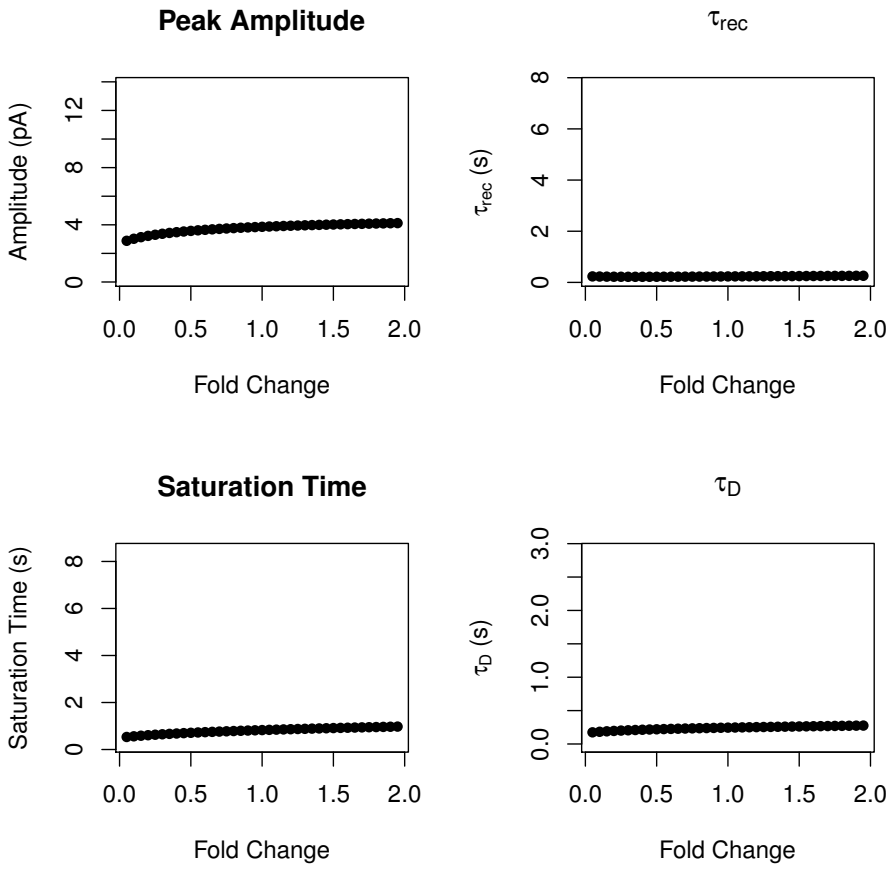

Figure S16: Electrophysiological measurements as functions of the parameter $kA4$.

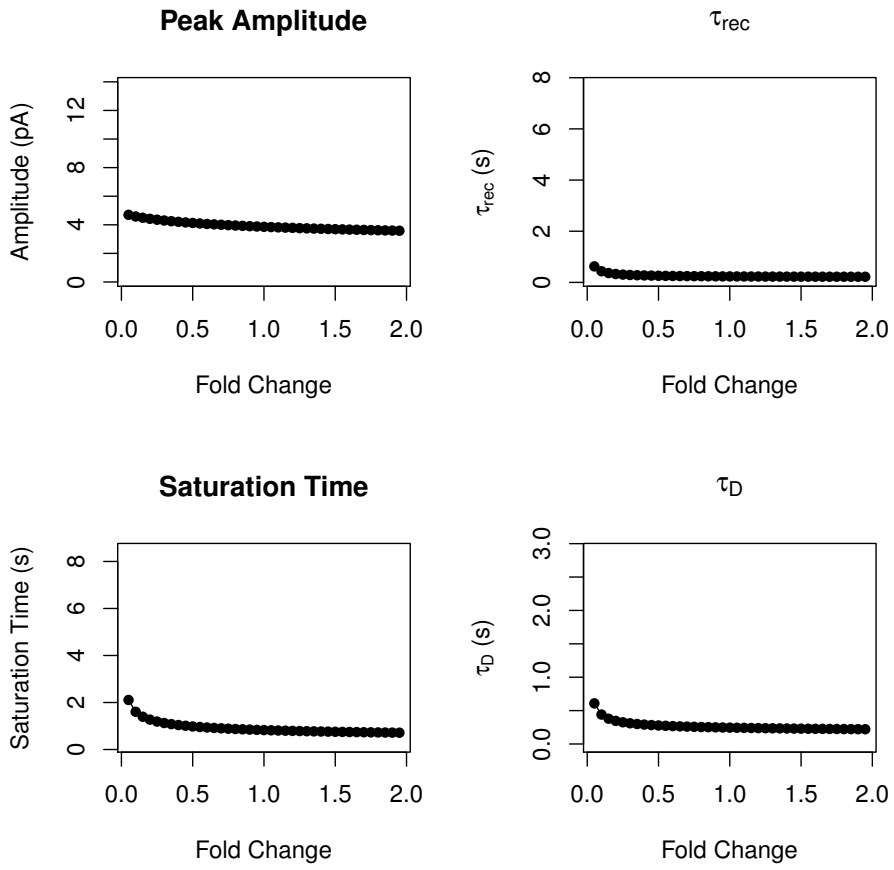

Figure S17: Electrophysiological measurements as functions of the parameter $kA2$.

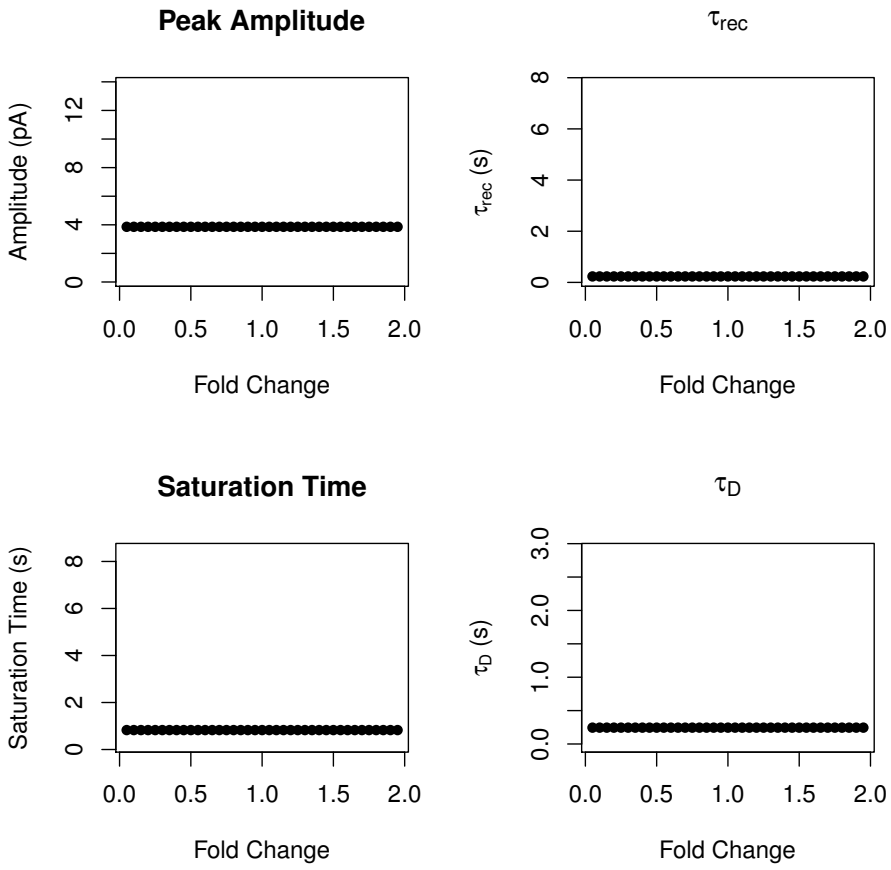

Figure S18: Electrophysiological measurements as functions of the parameter $kOps$.

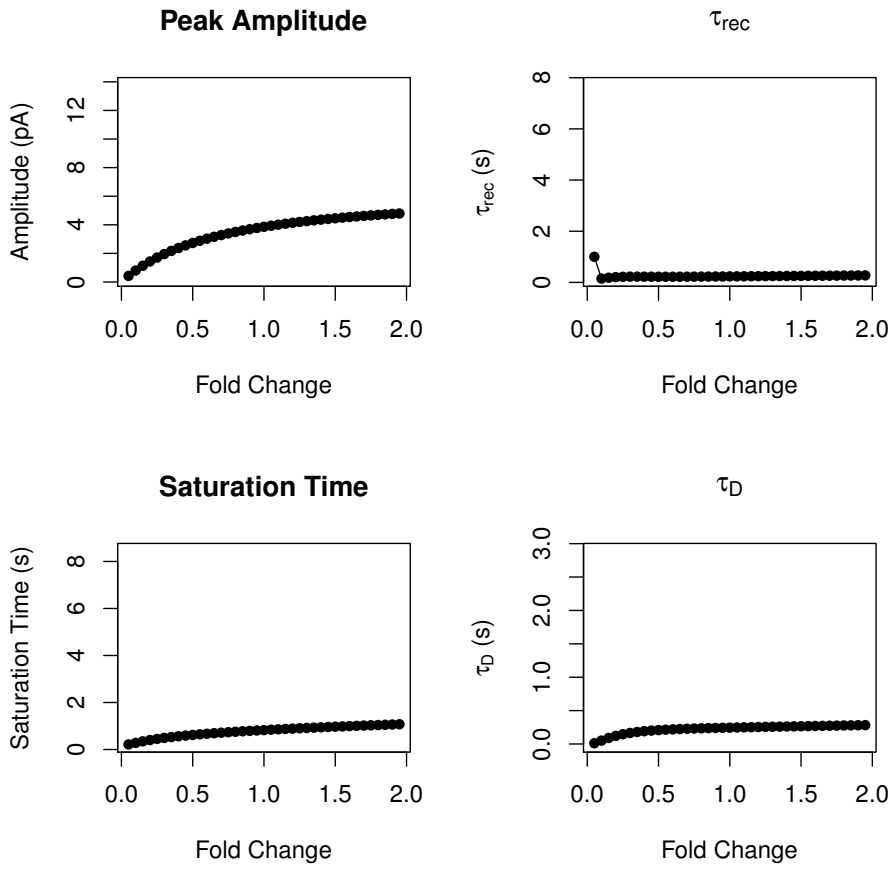

Figure S19: Electrophysiological measurements as functions of the parameter $kG1_0$.

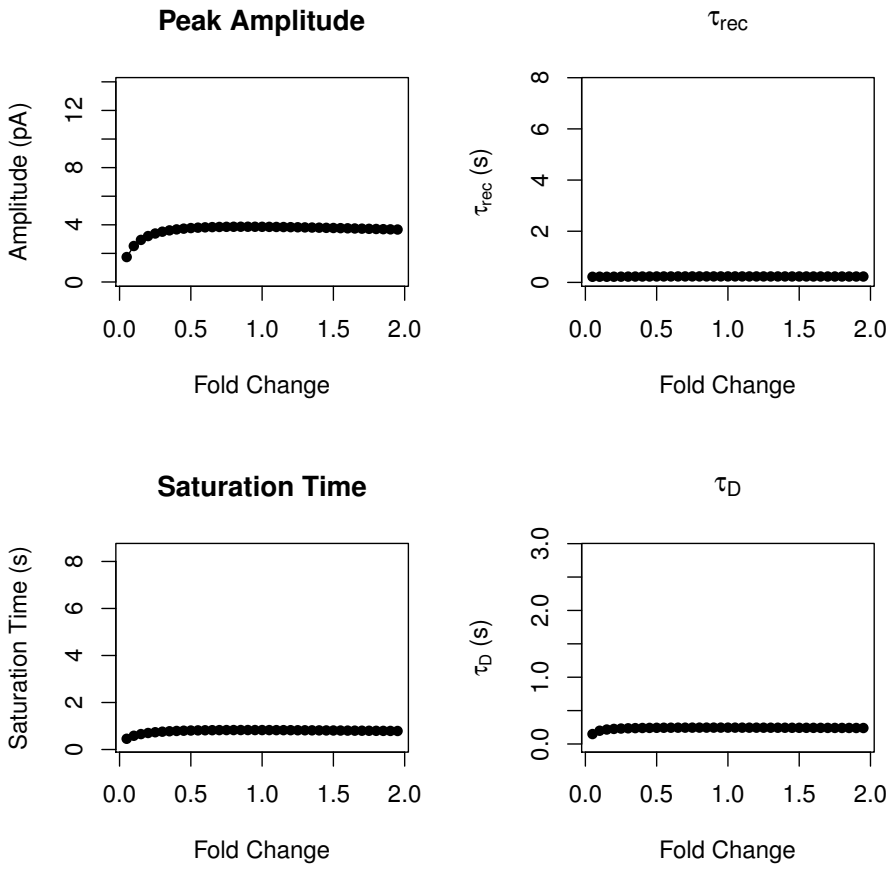

Figure S20: Electrophysiological measurements as functions of the parameter $kG2$.

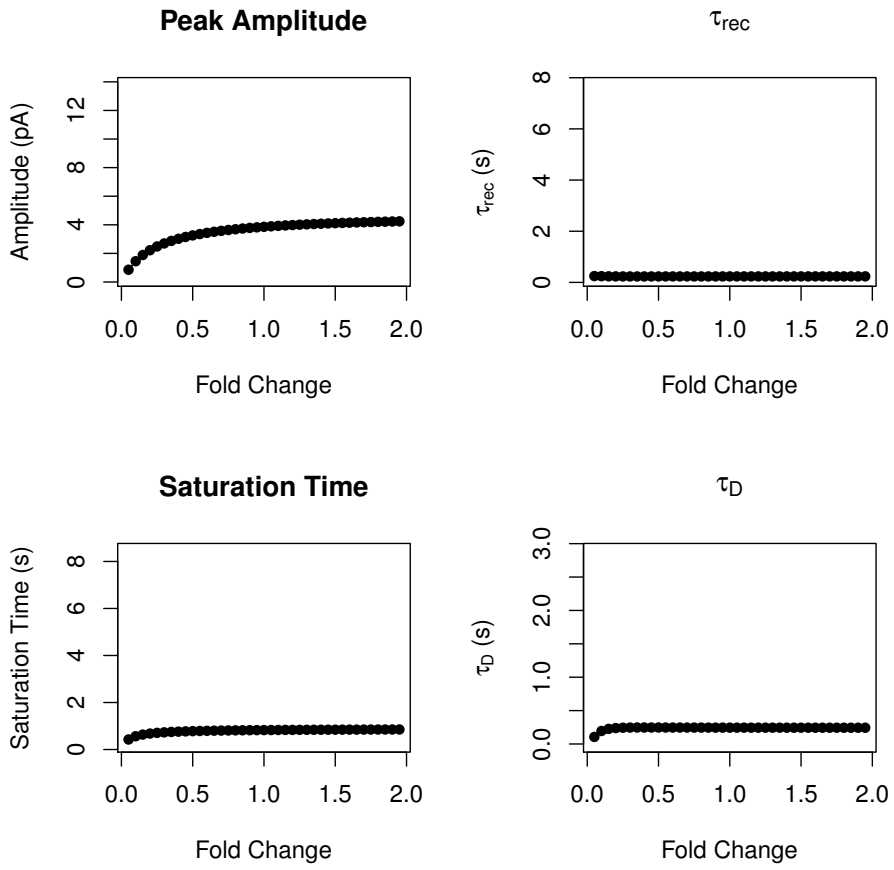

Figure S21: Electrophysiological measurements as functions of the parameter $kG3$.

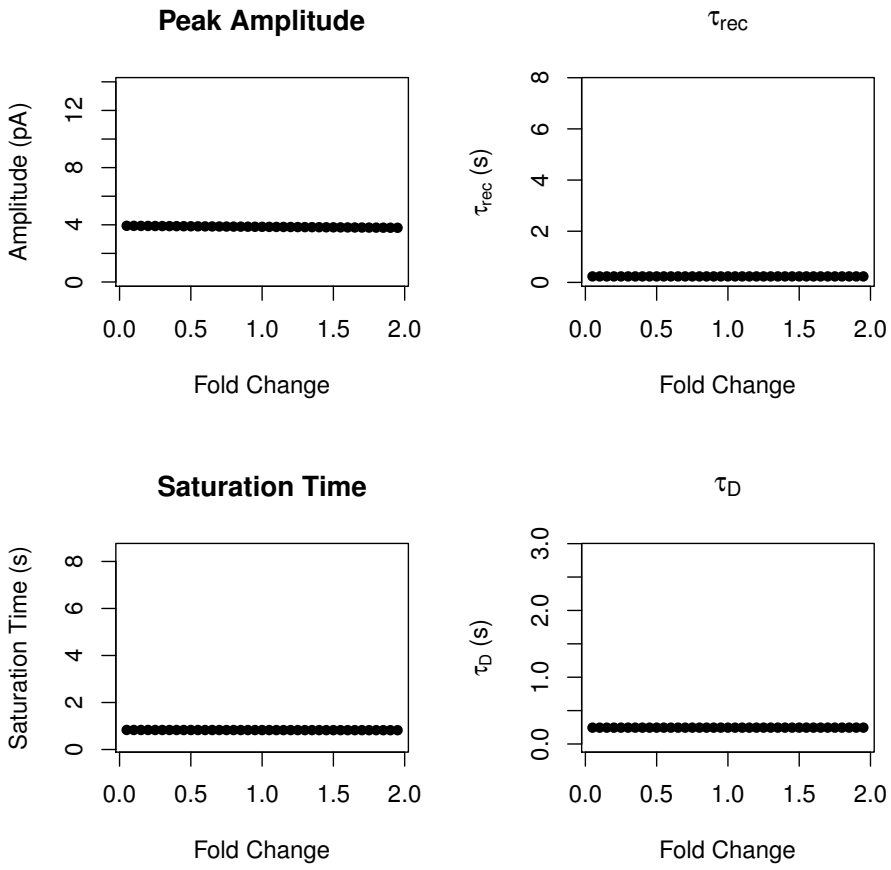

Figure S22: Electrophysiological measurements as functions of the parameter $kG4_{GDP}$.

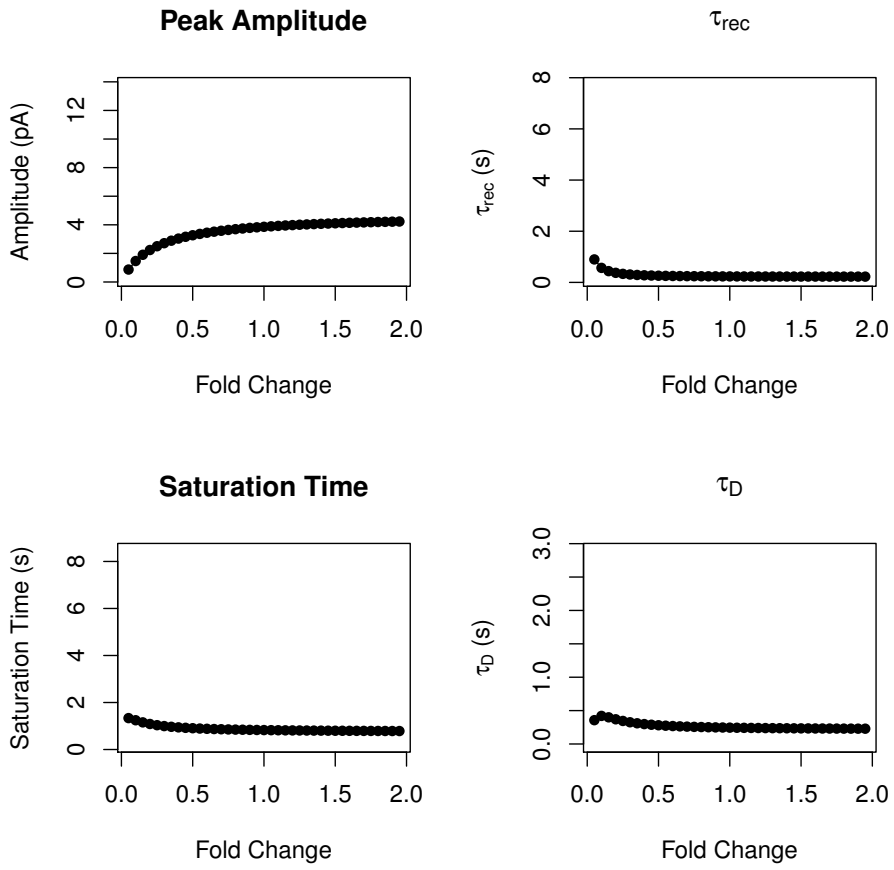

Figure S23: Electrophysiological measurements as functions of the parameter $kG5_{GTP}$.

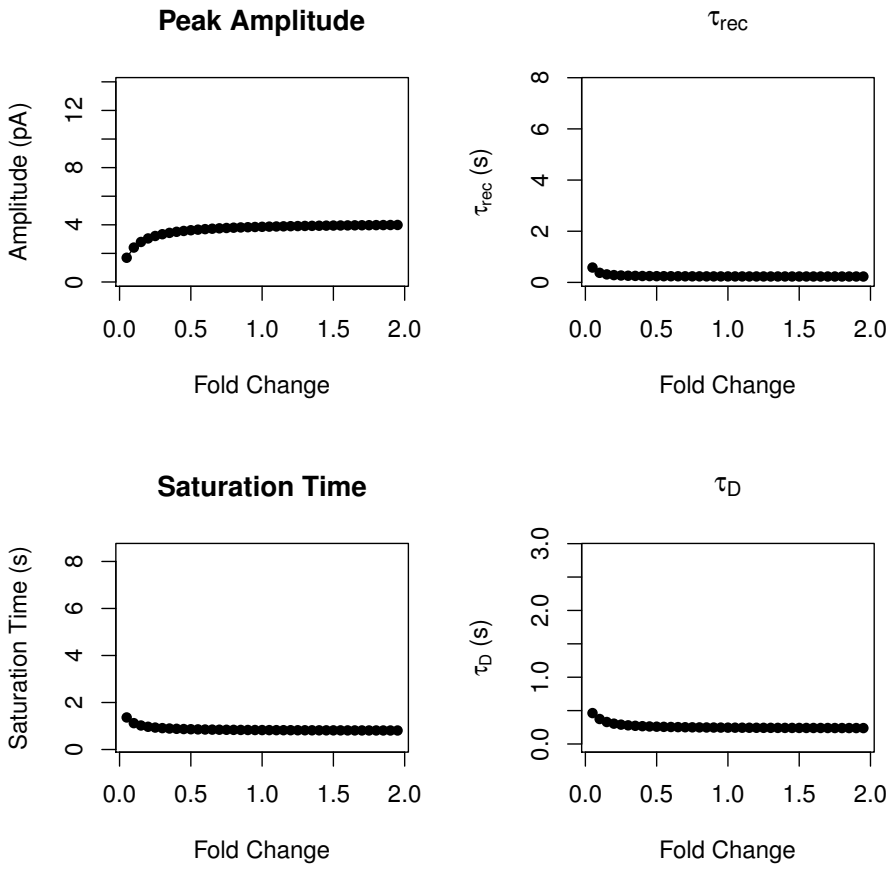

Figure S24: Electrophysiological measurements as functions of the parameter $kG6$.

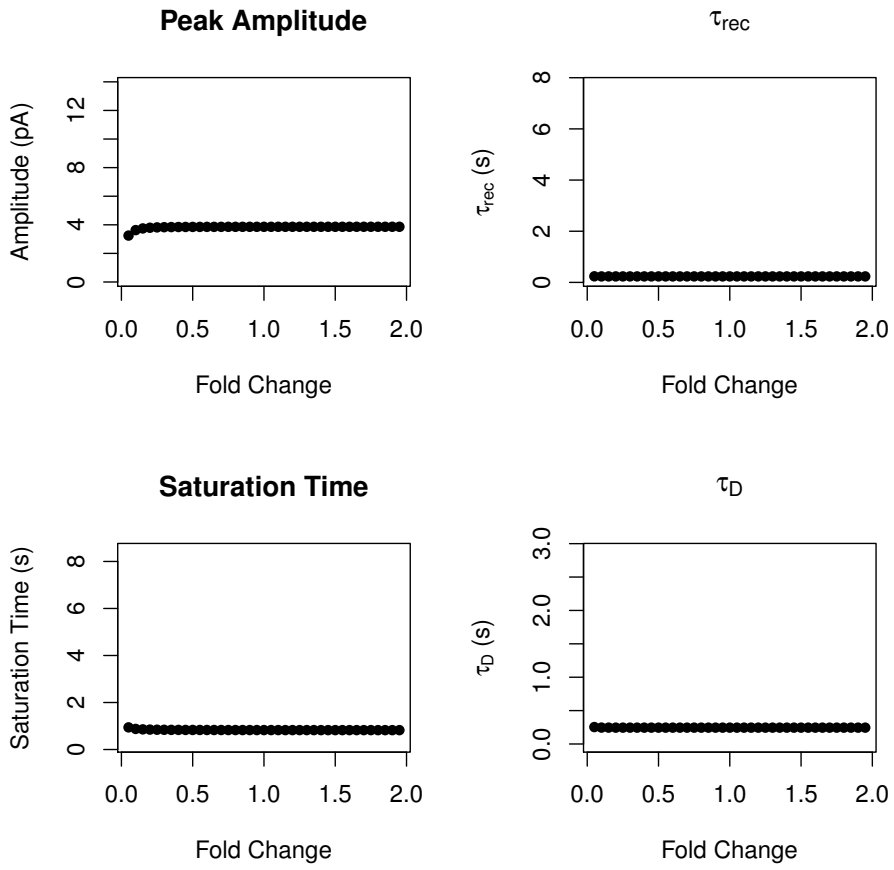

Figure S25: Electrophysiological measurements as functions of the parameter $kG7$.

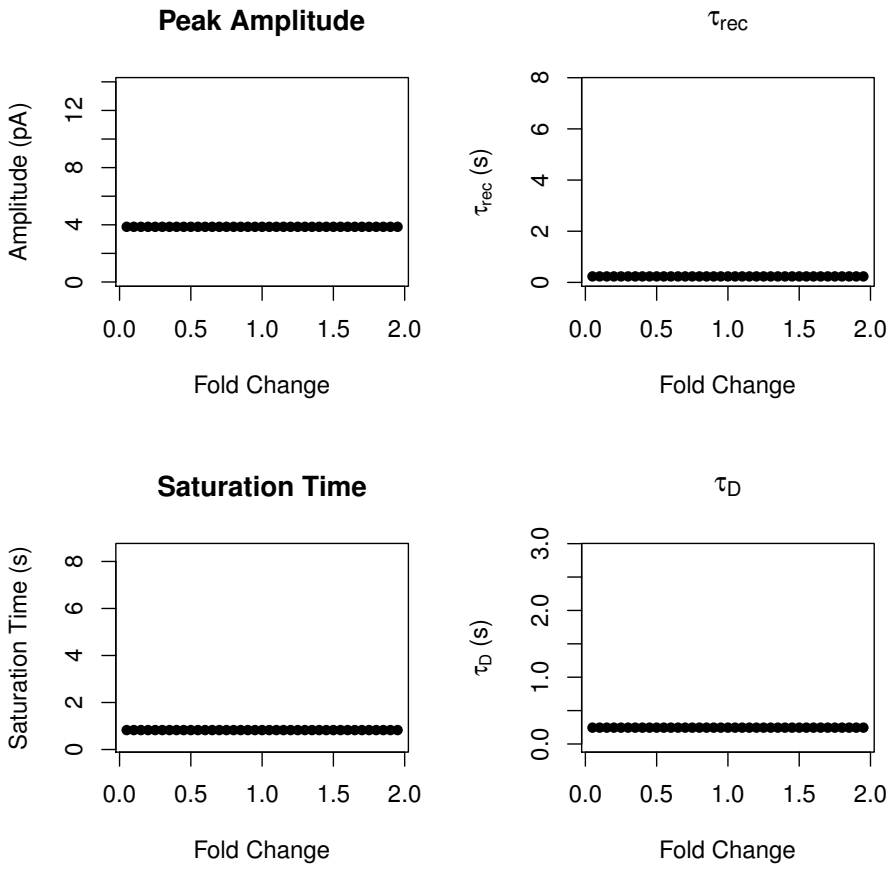

Figure S26: Electrophysiological measurements as functions of the parameter $kG_{shutoff}$.

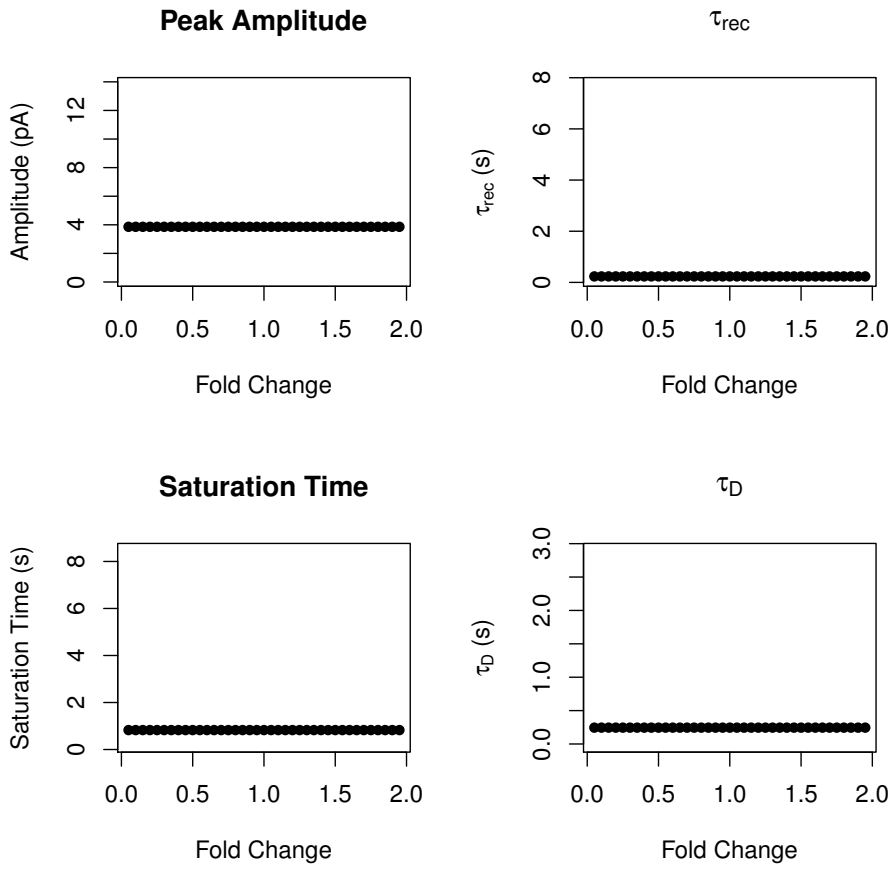

Figure S27: Electrophysiological measurements as functions of the parameter $kP1$.

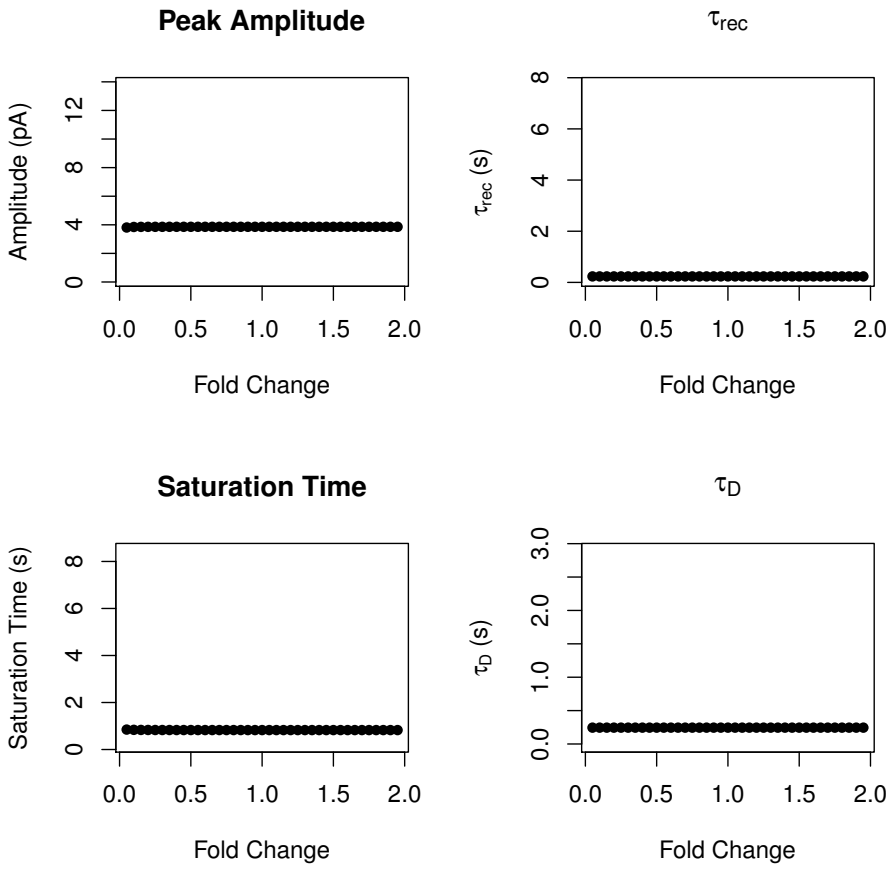

Figure S28: Electrophysiological measurements as functions of the parameter $kP2$.

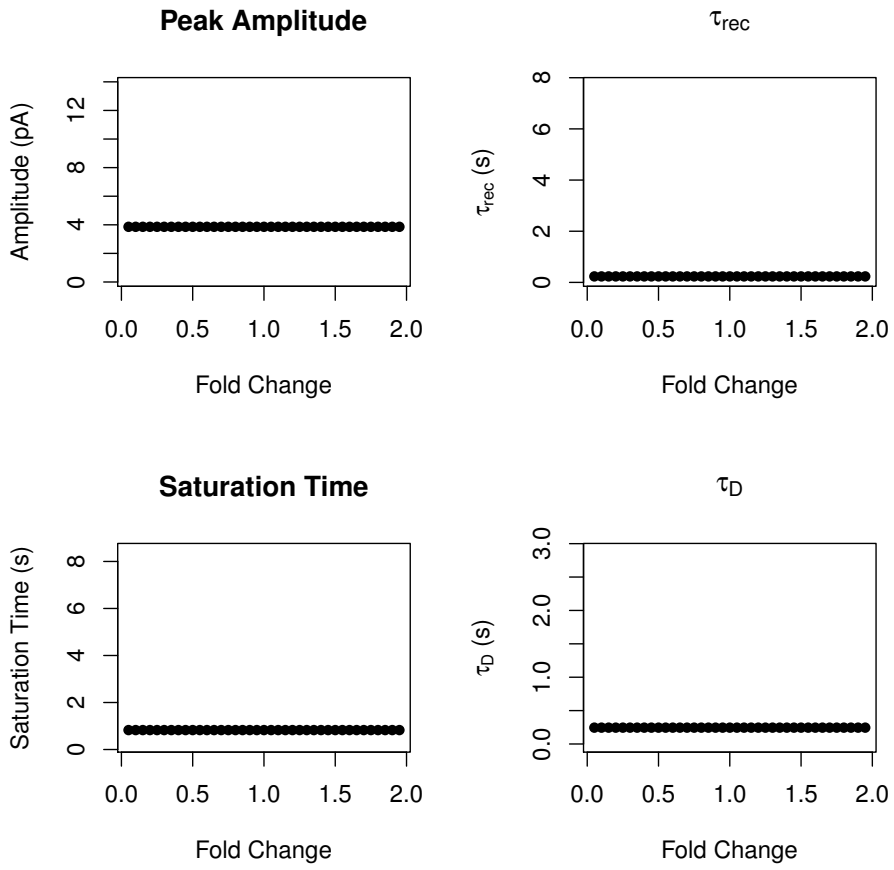

Figure S29: Electrophysiological measurements as functions of the parameter $kP3$.

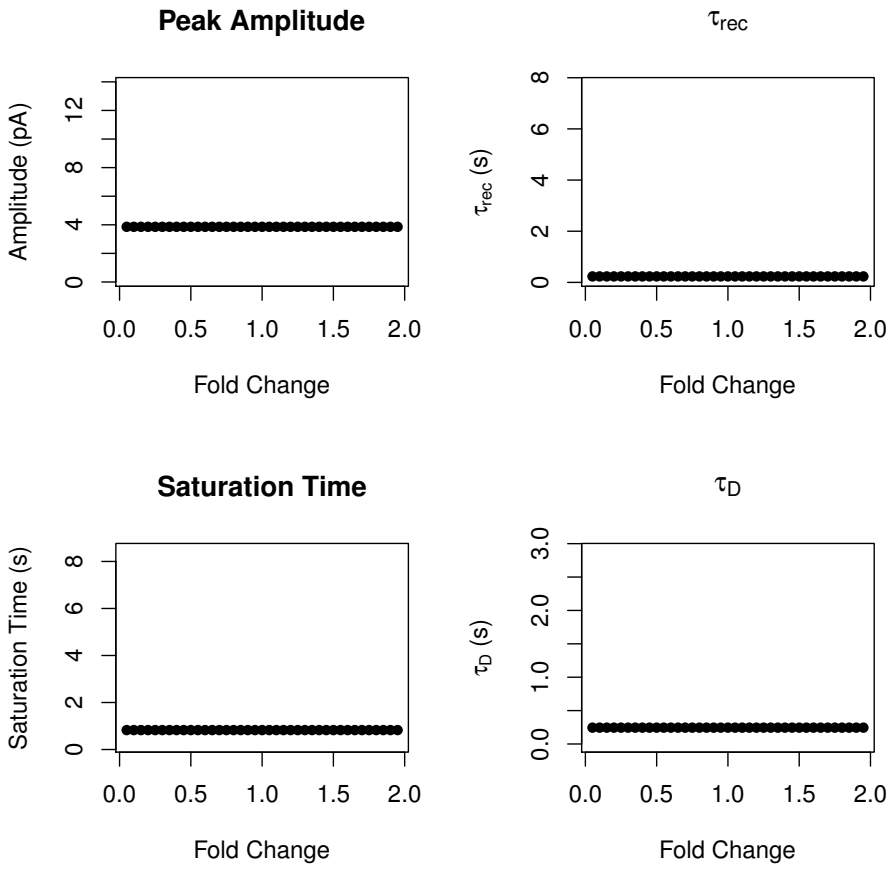

Figure S30: Electrophysiological measurements as functions of the parameter $kP4$.

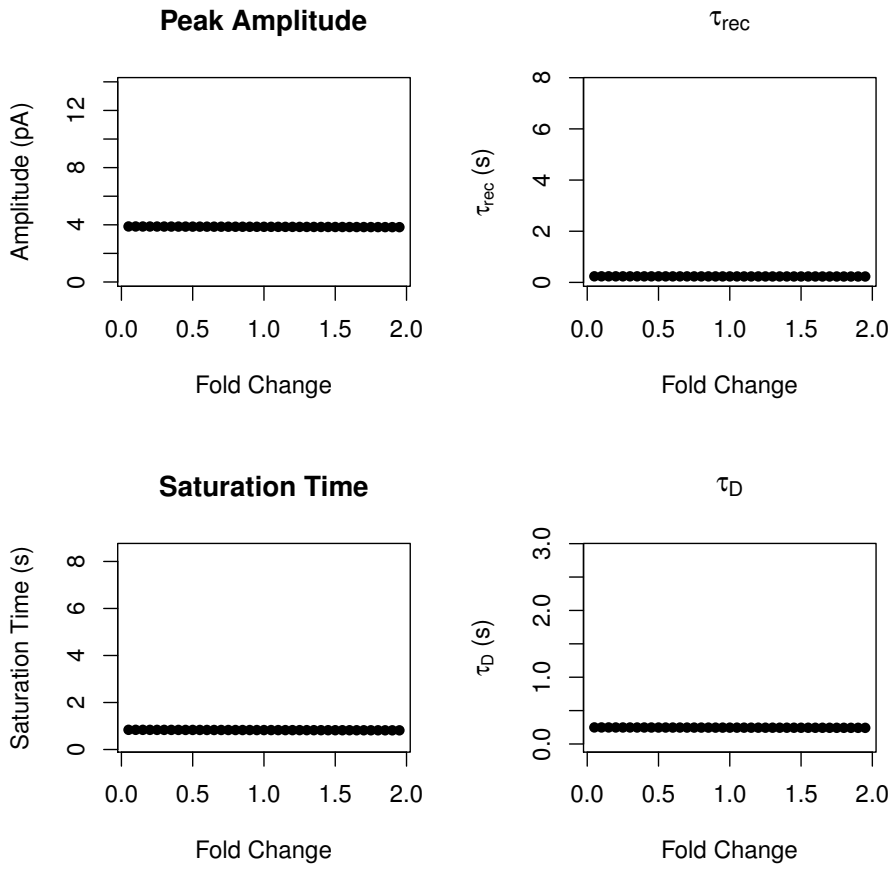

Figure S31: Electrophysiological measurements as functions of the parameter $kPDEshutoff$.

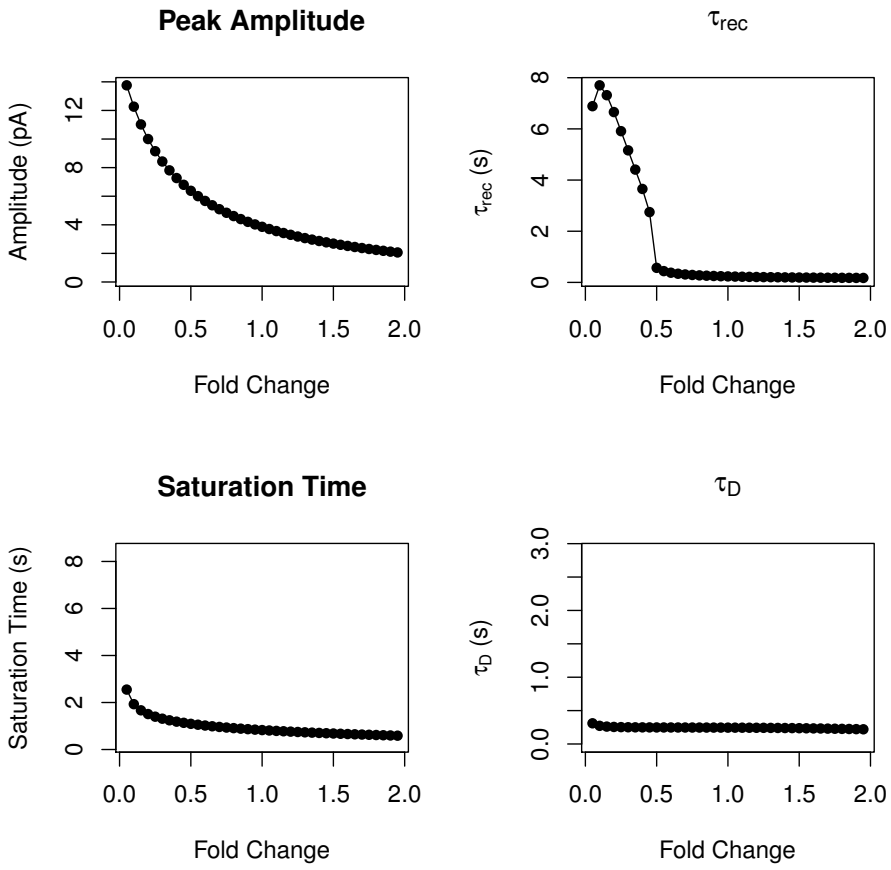

Figure S32: Electrophysiological measurements as functions of the parameter β_{dark}.

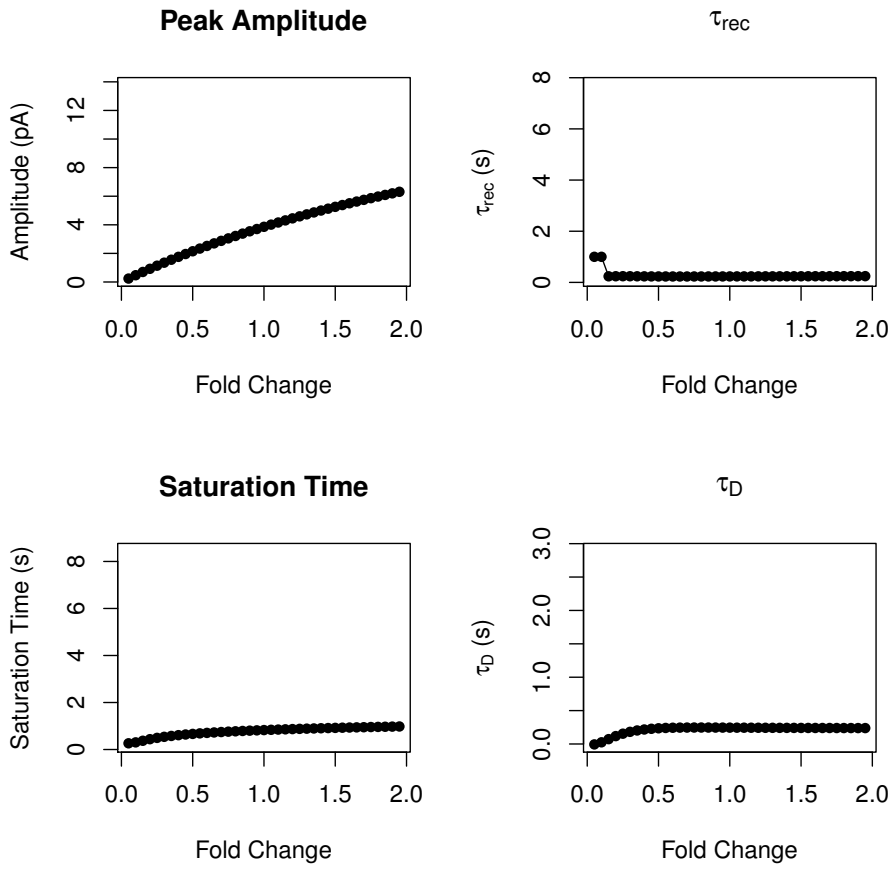

Figure S33: Electrophysiological measurements as functions of the parameter β_{sub}.

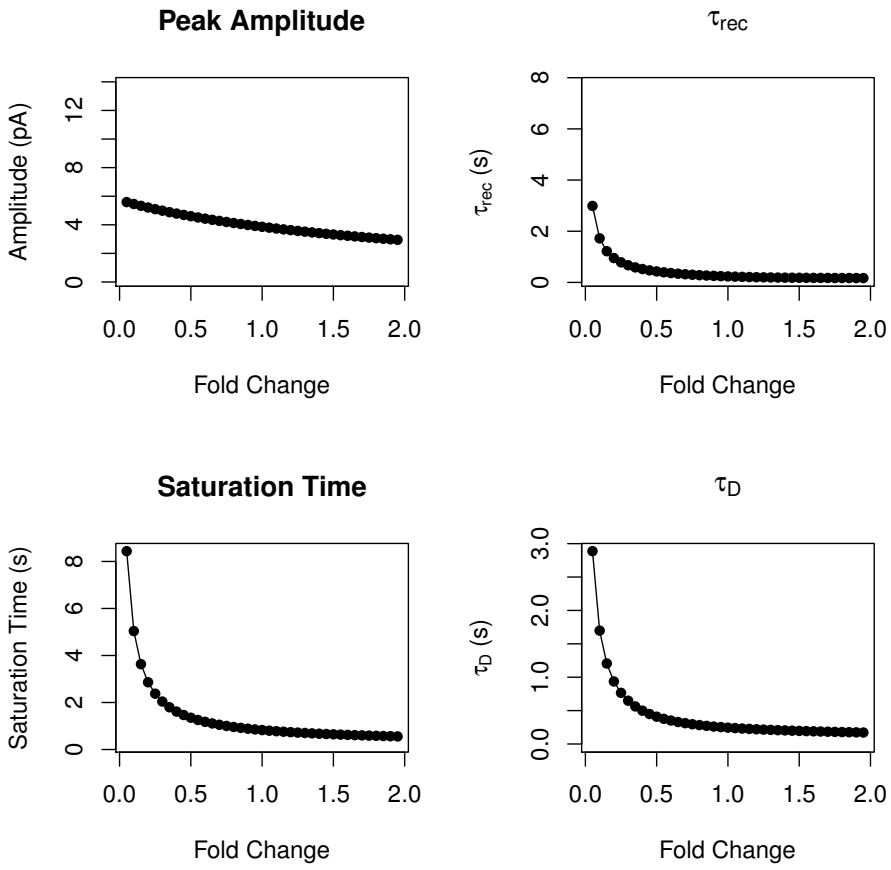

Figure S34: Electrophysiological measurements as functions of the parameter $kRGS1$.

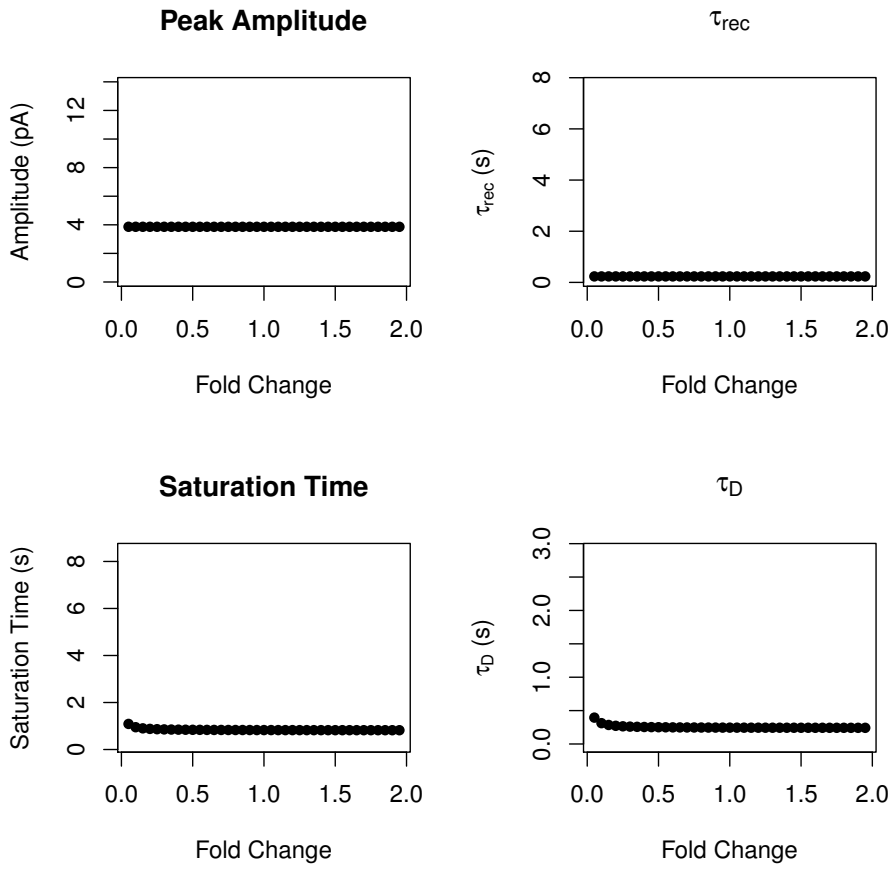

Figure S35: Electrophysiological measurements as functions of the parameter $kRGS2$.

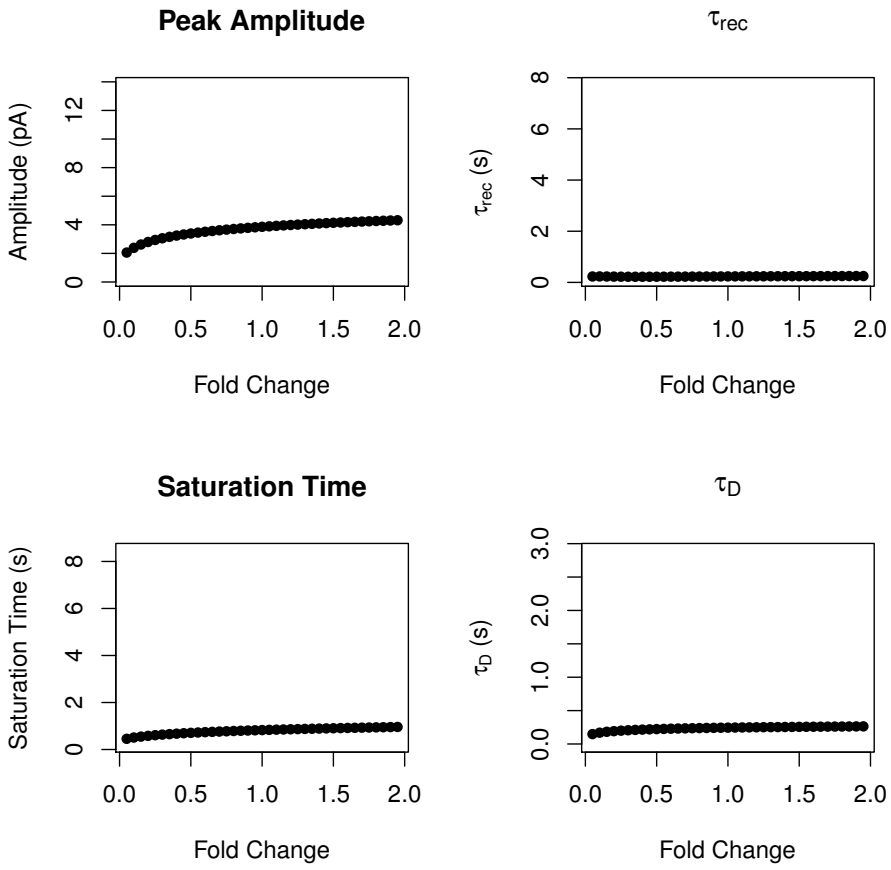

Figure S36: Electrophysiological measurements as functions of the parameter $kRec1$.

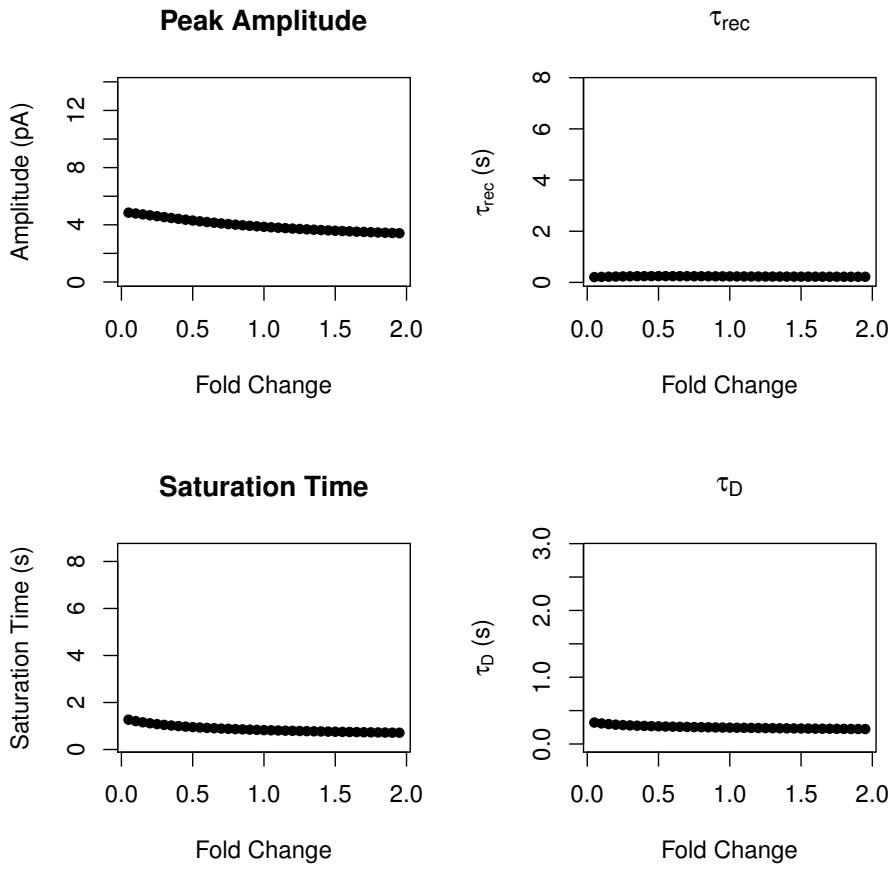

Figure S37: Electrophysiological measurements as functions of the parameter $kRec2$.

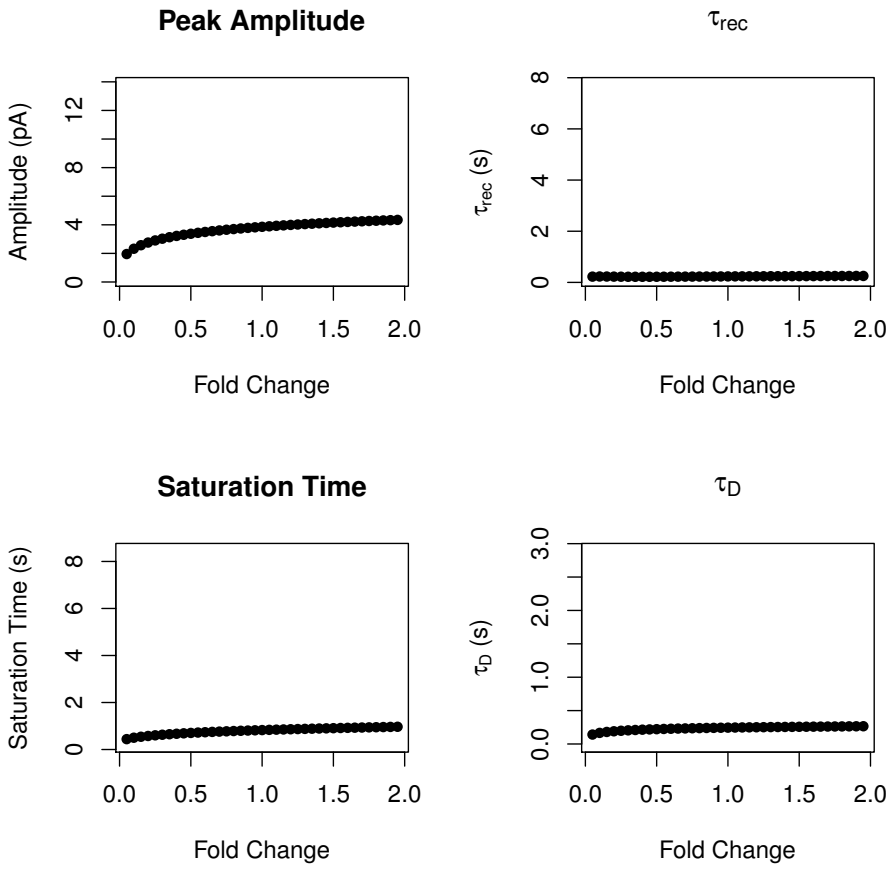

Figure S38: Electrophysiological measurements as functions of the parameter $kRec3$.

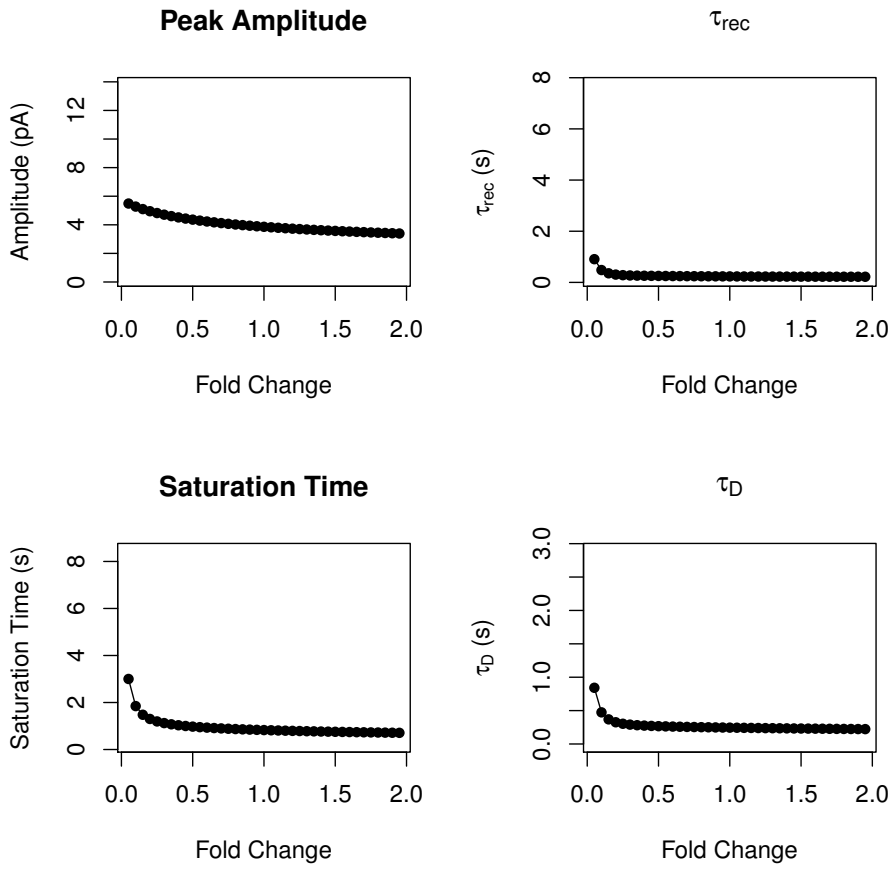

Figure S39: Electrophysiological measurements as functions of the parameter $kRec4$.

Bibliography

[1] Dawkins R. *The Selfish Gene*. Oxford University Press, 1976. ISBN 0192860925.

[2] Breen MS, Kemena C, Vlasov PK, Notredame C, Kondrashov FA. Epistasis as the primary factor in molecular evolution. *Nature*, 490(7421):535–538, 2012.

[3] Rausher MD, Miller RE, Tiffin P. Patterns of evolutionary rate variation among genes of the anthocyanin biosynthetic pathway. *Molecular Biology and Evolution*, 16(2):266–274, 1999. ISSN 0737-4038.

[4] Lu Y, Rausher MD. Evolutionary rate variation in anthocyanin pathway genes. *Molecular Biology and Evolution*, 20(11):1844–1853, 2003. ISSN 0737-4038. doi:10.1093/molbev/msg197.

[5] Riley RM, Jin W, Gibson G. Contrasting selection pressures on components of the Ras-mediated signal transduction pathway in Drosophila. *Molecular Ecology*, 12(5):1315–1323, 2003. ISSN 0962-1083.

[6] Flowers JM, Sezgin E, Kumagai S, Duvernell DD, Matzkin LM, Schmidt PS, Eanes WF. Adaptive evolution of metabolic pathways in Drosophila. *Molecular Biology and Evolution*, 24(6):1347–1354, 2007. ISSN 0737-4038. doi:10.1093/molbev/msm057.

[7] Rausher MD, Lu Y, Meyer K. Variation in constraint versus positive selection as an explanation for evolutionary rate variation among anthocyanin genes. *Journal of Molecular Evolution*, 67(2):137–144, 2008. ISSN 0022-2844. doi:10.1007/s00239-008-9105-5.

[8] Livingstone K, Anderson S. Patterns of variation in the evolution of carotenoid biosynthetic pathway enzymes of higher plants. *The Journal of Heredity*, 100(6):754–761, 2009. ISSN 1465-7333. doi:10.1093/jhered/esp026.

[9] Yang Yh, Zhang Fm, Ge S. Evolutionary rate patterns of the Gibberellin pathway genes. *BMC Evolutionary Biology*, 9:206, 2009. ISSN 1471-2148. doi:10.1186/1471-2148-9-206.

[10] Ramsay H, Rieseberg LH, Ritland K. The correlation of evolutionary rate with pathway position in plant terpenoid biosynthesis. *Molecular Biology and Evolution*, 26(5):1045–1053, 2009. ISSN 1537-1719. doi:10.1093/molbev/msp021.

[11] Alvarez-Ponce D, Aguadé M, Rozas J. Network-level molecular evolutionary analysis of the insulin/TOR signal transduction pathway across 12 Drosophila genomes. *Genome Research*, 19(2):234–242, 2009. ISSN 1088-9051. doi:10.1101/gr.084038.108.

[12] Montanucci L, Laayouni H, Dall'Olio GM, Bertranpetit J. Molecular evolution and network-level analysis of the N-glycosylation metabolic pathway across primates. *Molecular Biology and Evolution*, 28(1):813–823, 2011. ISSN 1537-1719. doi:10.1093/molbev/msq259.

[13] Alvarez-Ponce D, Aguadé M, Rozas J. Comparative genomics of the vertebrate insulin/TOR signal transduction pathway: a network-level analysis of selective pressures. *Genome Biology and Evolution*, 3:87–101, 2011. ISSN 1759-6653. doi:10.1093/gbe/evq084.

[14] Luisi P, Alvarez-Ponce D, Dall'Olio GM, Sikora M, Bertranpetit J, Laayouni H. Network-level and population genetics analysis of the insulin/TOR signal transduction pathway across human populations. *Molecular Biology and Evolution*, 29(5):1379–1392, 2012. ISSN 1537-1719. doi:10.1093/molbev/msr298.

[15] Dall'Olio GM, Laayouni H, Luisi P, Sikora M, Montanucci L, Bertranpetit J. Distribution of events of positive selection and population differentiation in a metabolic pathway: the case of asparagine N-glycosylation. *BMC Evolutionary Biology*, 12(1):98, 2012. ISSN 1471-2148. doi:10.1186/1471-2148-12-98.

[16] Invergo BM, Montanucci L, Laayouni H, Bertranpetit J. A system-level, molecular evolutionary analysis of mammalian phototransduction. *BMC Evolutionary Biology*, 13:52, 2013.

[17] Fraser HB, Hirsh AE, Steinmetz LM, Scharfe C, Feldman MW. Evolutionary rate in the protein interaction network. *Science*, 296(5568):750–752, 2002. ISSN 1095-9203. doi:10.1126/science.1068696.

[18] Jordan IK, Wolf Y, Koonin E. No simple dependence between protein evolution rate and the number of protein-protein interactions: only the most prolific interactors tend to evolve slowly. *BMC Evolutionary Biology*, 3(1):1, 2003. ISSN 1471-2148. doi:10.1186/1471-2148-3-1.

[19] Fraser H, Wall D, Hirsh A. A simple dependence between protein evolution rate and the number of protein-protein interactions. *BMC Evolutionary Biology*, 3(1):11, 2003. ISSN 1471-2148. doi:10.1186/1471-2148-3-11.

[20] Fraser H, Hirsh A. Evolutionary rate depends on number of protein-protein interactions independently of gene expression level. *BMC Evolutionary Biology*, 4(1):13, 2004. ISSN 1471-2148. doi:10.1186/1471-2148-4-13.

[21] Bloom J, Adami C. Apparent dependence of protein evolutionary rate on number of interactions is linked to biases in protein-protein interactions data sets. *BMC Evolutionary Biology*, 3(1):21, 2003. ISSN 1471-2148. doi:10.1186/1471-2148-3-21.

[22] Hahn M, Kern AD. Comparative Genomics of Centrality and Essentiality in Three Eukaryotic Protein-Interaction Networks. *Molecular Biology and Evolution*, 22(4):803–806, 2005. doi: 10.1093/molbev/msi072.

[23] Kim PM, Korbel JO, Gerstein MB. Positive selection at the protein network periphery: evaluation in terms of structural constraints and cellular context. *Proceedings of the National Academy of Sciences*, 104(51):20274–20279, 2007. ISSN 1091-6490. doi:10.1073/pnas.0710183104.

[24] Vitkup D, Kharchenko P, Wagner A. Influence of metabolic network structure and function on enzyme evolution. *Genome Biology*, 7(5):R39, 2006. ISSN 1465-6906. doi:10.1186/gb-2006-7-5-r39.

[25] Greenberg AJ, Stockwell SR, Clark AG. Evolutionary Constraint and Adaptation in the Metabolic Network of Drosophila. *Molecular Biology and Evolution*, 25(12):2537–2546, 2008. doi: 10.1093/molbev/msn205.

[26] Alvarez-Ponce D, Fares MA. Evolutionary Rate and Duplicability in the Arabidopsis thaliana Protein-Protein Interaction Network. *Genome Biology and Evolution*, 4(12):1263–1274, 2012. doi:10.1093/gbe/evs101.

[27] Alvarez-Ponce D. The relationship between the hierarchical position of proteins in the human signal transduction network and their rate of evolution. *BMC Evolutionary Biology*, 12(1):192, 2012. ISSN 1471-2148. doi:10.1186/1471-2148-12-192.

[28] Cui Q, Purisima E, Wang E. Protein evolution on a human signaling network. *BMC Systems Biology*, 3(1):21, 2009. ISSN 1752-0509. doi:10.1186/1752-0509-3-21.

[29] Masel J. Genetic drift. *Current Biology*, 21(20):R837–R838, 2011. ISSN 1879-0445. doi:10.1016/j.cub.2011.08.007.

[30] Kimura M. *The Neutral Theory of Molecular Evolution*. Cambridge University Press, 1985. ISBN 9780521317931.

[31] Nathans J, Thomas D, Hogness DDS. Molecular genetics of human color vision: the genes encoding blue, green, and red pigments. *Science*, 232(4747):193–202, 1986.

[32] Nei M. Selectionism and neutralism in molecular evolution. *Molecular Biology and Evolution*, 22(12):2318–2342, 2005. ISSN 0737-4038. doi:10.1093/molbev/msi242.

[33] Nei M, Gojobori T. Simple methods for estimating the numbers of synonymous and nonsynonymous nucleotide substitutions. *Molecular Biology and Evolution*, 3(5):418–426, 1986. ISSN 0737-4038.

[34] Jukes TH, Cantor CR. Evolution of protein molecules. In Munro HN, editor, *Mammalian Protein Metabolism*, volume III, pages 21–132. Academic Press, New York, 1969.

[35] Goldman N, Yang Z. A codon-based model of nucleotide substitution for protein-coding DNA sequences. *Molecular Biology and Evolution*, 11(5):725–736, 1994. ISSN 0737-4038.

[36] Seo TK, Kishino H, Thorne JL. Estimating absolute rates of synonymous and nonsynonymous nucleotide substitution in order to characterize natural selection and date species divergences. *Molecular Biology and Evolution*, 21(7):1201–1213, 2004. ISSN 0737-4038. doi:10.1093/molbev/msh088.

[37] Suzuki Y, Gojobori T. A method for detecting positive selection at single amino acid sites. *Molecular Biology and Evolution*, 16(10):1315–1328, 1999. ISSN 0737-4038.

[38] Suzuki Y. New methods for detecting positive selection at single amino acid sites. *Journal of Molecular Evolution*, 59(1):11–19, 2004. ISSN 0022-2844. doi:10.1007/s00239-004-2599-6.

[39] Massingham T, Goldman N. Detecting amino acid sites under positive selection and purifying selection. *Genetics*, 169(3):1753–1762, 2005. ISSN 0016-6731. doi:10.1534/genetics.104.032144.

[40] Kosakovsky Pond SL, Frost SDW. Not so different after all: a comparison of methods for detecting amino acid sites under selection. *Molecular Biology and Evolution*, 22(5):1208–1222, 2005. ISSN 0737-4038. doi:10.1093/molbev/msi105.

[41] Nielsen R, Yang Z. Likelihood models for detecting positively selected amino acid sites and applications to the HIV-1 envelope gene. *Genetics*, 148(3):929–936, 1998. ISSN 0016-6731.

[42] Yang Z, Nielsen R, Goldman N, Krabbe Pedersen AM. Codon-substitution models for heterogeneous selection pressure at amino acid sites. *Genetics*, 155:431–449, 2000.

[43] Yang Z, Wong WSW, Nielsen R. Bayes empirical Bayes inference of amino acid sites under positive selection. *Molecular Biology and Evolution*, 22(4):1107–1118, 2005. doi:10.1093/molbev/msi097.

[44] Anisimova M, Bielawski JP, Yang Z. Accuracy and power of the likelihood ratio test in detecting adaptive molecular evolution. *Molecular Biology and Evolution*, 18(6):1585–1592, 2002.

[45] Yang Z, Nielsen R. Codon-substitution models for detecting molecular adaptation at individual sites along specific lineages. *Molecular Biology and Evolution*, 19(6):908—-917, 2002. ISSN 0737-4038.

[46] Zhang J, Nielsen R, Yang Z. Evaluation of an improved branch-site likelihood method for detecting positive selection at the molecular level. *Molecular Biology and Evolution*, 22(12):2472–2479, 2005. ISSN 0737-4038. doi:10.1093/molbev/msi237.

[47] Murrell B, Wertheim JO, Moola S, Weighill T, Scheffler K, Kosakovsky Pond SL. Detecting individual sites subject to episodic diversifying selection. *PLoS Genetics*, 8(7):e1002764, 2012. ISSN 1553-7404. doi:10.1371/journal.pgen.1002764.

[48] Yang Z, dos Reis M. Statistical properties of the branch-site test of positive selection. *Molecular Biology and Evolution*, 28(3):1217–28, 2011. ISSN 1537-1719. doi:10.1093/molbev/msq303.

[49] Freeman LC. Centrality in social networks conceptual clarification. *Social Networks*, 1:215–239, 1979.

[50] Conrad ED, Tyson JJ. Modeling molecular interaction networks with nonlinear ordinary differential equations. In Szallasi Z, Stelling J, Periwal V, editors, *System Modeling in Cellular Biology: From Concepts to Nuts and Bolts*, pages 97–123. MIT Press, Cambridge, MA, 2006. ISBN 9780262195485.

[51] Alvarez-Ponce D, Guirao-Rico S, Orengo DJ, Segarra C, Rozas J, Aguadé M. Molecular population genetics of the insulin/TOR signal transduction pathway: a network-level analysis in Drosophila melanogaster. *Molecular Biology and Evolution*, 29(1):123–132, 2012. ISSN 1537-1719. doi:10.1093/molbev/msr160.

[52] Ebrey T, Koutalos Y. Vertebrate photoreceptors. *Progress in Retinal and Eye Research*, 20(1):49–94, 2001. ISSN 1350-9462.

[53] Luo DG, Xue T, Yau KW. How vision begins: an odyssey. *Proceedings of the National Academy of Sciences*, 105(29):9855–9862, 2008.

[54] Fadool JM, Dowling JE. Zebrafish: a model system for the study of eye genetics. *Progress in Retinal and Eye Research*, 27(1):89–110, 2008. ISSN 1350-9462. doi:10.1016/j.preteyeres.2007.08.002.

[55] Pugh Jr EN, Lamb TD. Phototransduction in vertebrate rods and cones: molecular mechanisms of amplification, recovery and light adaptation. In Stavenga D, DeGrip W, Pugh E, editors, *Handbook of Biological Physics (Volume 3)*, volume 3, pages 183–255. Elsevier, North Holland, 2000. doi:10.1016/S1383-8121(00)80008-1.

[56] Yau KW, Hardie RC. Phototransduction motifs and variations. *Cell*, 139(2):246–264, 2009. ISSN 1097-4172. doi:10.1016/j.cell.2009.09.029.

[57] Shichida Y, Morizumi T. Mechanism of G-protein activation by rhodopsin. *Photochemistry and Photobiology*, 83(1):70–75, 2007. ISSN 0031-8655. doi:10.1562/2006-03-22-IR-854.

[58] Bennett N, Clerc A. Activation of cGMP phosphodiesterase in retinal rods: mechanism of interaction with the GTP-binding protein (transducin). *Biochemistry*, 28(18):7418–7424, 1989.

[59] Clerc A, Bennett N. Activated cGMP phosphodiesterase of retinal rods. A complex with transducin alpha subunit. *The Journal of Biological Chemistry*, 267(10):6620–6627, 1992. ISSN 0021-9258.

[60] Schnetkamp P. Sodium-calcium exchange in the outer segments of bovine rod photoreceptors. *The Journal of Physiology*, 373(1):25–45, 1986.

[61] Schnetkamp PPM, Basu DK, Szerencsei RT. Na^{+}-Ca^{2+} exchange in bovine rod outer segments requires and transports K^{+}. *American Journal of Physiology*, 257(1 Pt 1):C153–C157, 1989.

[62] Dell'Orco D, Müller M, Koch KW. Quantitative detection of conformational transitions in a calcium sensor protein by surface plasmon resonance. *Chemical Communications*, 46(39):7316–7318, 2010. ISSN 1364-548X. doi:10.1039/c0cc02086a.

[63] Gorodovikova EN, Senin II, Philippov PP. Calcium-sensitive control of rhodopsin phosphorylation in the reconstituted system consisting of photoreceptor membranes, rhodopsin kinase and recoverin. *FEBS Letters*, 353(2):171–172, 1994.

[64] Klenchin VA, Calvert PD, Bownds MD. Inhibition of rhodopsin kinase by recoverin. *The Journal of Biological Chemistry*, 270(27):16147–16152, 1995.

[65] Kennedy MJ, Lee KA, Niemi GA, Craven KB, Garwin GG, Saari JC, Hurley JB. Multiple phosphorylation of rhodopsin and the in vivo chemistry underlying rod photoreceptor dark adaptation. *Neuron*, 31(1):87–101, 2001. ISSN 0896-6273.

[66] Maeda T, Imanishi Y, Palczewski K. Rhodopsin phosphorylation: 30 years later. *Progress in Retinal and Eye Research*, 22(4):417–434, 2003. ISSN 13509462. doi:10.1016/S1350-9462(03)00017-X.

[67] Doan T, Mendez A, Detwiler PB, Chen J, Rieke F. Multiple phosphorylation sites confer reproducibility of the rod's single-photon responses. *Science*, 313:530–533, 2006. doi:10.1126/science.1126612.

[68] Gibson SK, Parkes JH, Liebman PA. Phosphorylation modulates the affinity of light-activated rhodopsin for G protein and arrestin. *Biochemistry*, 39(19):5738–5749, 2000. ISSN 0006-2960.

[69] Pulvermüller A, Palczewski K, Hofmann KP. Interaction between photoactivated rhodopsin and its kinase: stability and kinetics of complex formation. *Biochemistry*, 32(51):14082–14088, 1993. ISSN 0006-2960.

[70] Vishnivetskiy SA, Raman D, Wei J, Kennedy MJ, Hurley JB, Gurevich VV. Regulation of arrestin binding by rhodopsin phosphorylation level. *The Journal of Biological Chemistry*, 282(44):32075–32083, 2007. doi:10.1074/jbc.M706057200.Regulation.

[71] Hanson SM, Van Eps N, Francis DJ, Altenbach C, Vishnivetskiy SA, Arshavsky VY, Klug CS, Hubbell WL, Gurevich VV. Structure and function of the visual arrestin oligomer. *The EMBO Journal*, 26(6):1726–1736, 2007. ISSN 0261-4189. doi:10.1038/sj.emboj.7601614.

[72] Kim M, Hanson SM, Vishnivetskiy SA, Song X, Cleghorn WM, Hubbell WL, Gurevich VV. Robust self-association is a common feature of mammalian visual arrestin-1. *Biochemistry*, 50(12):2235–2242, 2011. doi:10.1021/bi1018607.Robust.

[73] Gurevich VV, Hanson SM, Song X, Vishnivetskiy SA, Gurevich EV. The functional cycle of visual arrestins in photoreceptor cells. *Progress in Retinal and Eye Research*, 30(6):405–430, 2011. ISSN 1873-1635. doi:10.1016/j.preteyeres.2011.07.002.

[74] Natochin M, Granovsky AE, Artemyev NO. Regulation of transducin GTPase activity by human retinal RGS. *Journal of Biological Chemistry*, 272:17444–17449, 1997. ISSN 00219258. doi:10.1074/jbc.272.28.17444.

[75] Koch KW, Dell'Orco D. A calcium-relay mechanism in vertebrate phototransduction. *ACS Chemical Neuroscience*, 4:909–917, 2013. ISSN 1948-7193. doi:10.1021/cn400027z.

[76] Forti S, Menini A, Rispoli G, Torre V. Kinetics of phototransduction in retinal rods of the newt Triturus cristatus. *The Journal of Physiology*, 419:265–295, 1989.

[77] Pugh Jr EN, Lamb TD. Cyclic GMP and calcium: the internal messengers of excitation and adaptation in vertebrate photoreceptors. *Vision Research*, 30(12):1923–1948, 1990.

[78] Lamb TD, Pugh Jr EN. A quantitative account of the activation steps involved in phototransduction in amphibian photoreceptors. *The Journal of Physiology*, 449:719–758, 1992.

[79] Lamb TD. Stochastic simulation of activation in the G-protein cascade of phototransduction. *Biophysical Journal*, 67(4):1439–1454, 1994. ISSN 0006-3495. doi:10.1016/S0006-3495(94)80617-4.

[80] Felber S, Breuer HP, Petruccione F, Honerkamp J, Hofmann KP. Stochastic simulation of the transducin GTPase cycle. *Biophysical Journal*, 71(6):3051–3063, 1996. ISSN 0006-3495. doi:10.1016/S0006-3495(96)79499-7.

[81] Lamb TD. Gain and kinetics of activation in the G-protein cascade of phototransduction. *Proceedings of the National Academy of Sciences of the United States of America*, 93(2):566–70, 1996. ISSN 0027-8424.

[82] Hamer RD, Nicholas SC, Tranchina D, Liebman PA, Lamb TD. Multiple steps of phosphorylation of activated rhodopsin can account for the reproducibility of vertebrate rod single-photon responses. *The Journal of General Physiology*, 122(4):419–444, 2003. ISSN 0022-1295. doi:10.1085/jgp.200308832.

[83] Hamer RD, Nicholas SC, Tranchina D, Lamb TD, Jarvinen JLP. Toward a unified model of vertebrate rod phototransduction. *Visual Neuroscience*, 22(4):417–436, 2005. ISSN 1090-2139. doi:10.1016/j.bbi.2008.05.010.

[84] Dell'Orco D, Schmidt H, Mariani S, Fanelli F. Network-level analysis of light adaptation in rod cells under normal and altered conditions. *Molecular BioSystems*, 5(10):1232–1246, 2009. ISSN 1742-2051. doi:10.1039/b908123b.

[85] Andreucci D, Bisegna P, Caruso G, Hamm HE, DiBenedetto E. Mathematical model of the spatio-temporal dynamics of second messengers in visual transduction. *Biophysical Journal*, 85(3):1358–1376, 2003. ISSN 0006-3495. doi:10.1016/S0006-3495(03)74570-6.

[86] Caruso G, Khanal H, Alexiades V, Rieke F. Mathematical and computational modeling of spatiotemporal signaling in rod phototransduction. *IEEE Proc Syst Biol*, 152(3):119–137, 2005. doi: 10.1049/ip-syb.

[87] Bisegna P, Caruso G, Andreucci D, Shen L, Gurevich VV, Hamm HE, DiBenedetto E. Diffusion of the second messengers in the cytoplasm acts as a variability suppressor of the single photon response in vertebrate phototransduction. *Biophysical Journal*, 94(9):3363–3383, 2008. ISSN 1542-0086. doi:10.1529/biophysj.107.114058.

[88] Caruso G, Bisegna P, Shen L, Andreucci D, Hamm HE, DiBenedetto E. Modeling the role of incisures in vertebrate phototransduction. *Biophysical Journal*, 91(4):1192–1212, 2006. ISSN 0006-3495. doi:10.1529/biophysj.106.083618.

[89] Shichida Y, Matsuyama T. Evolution of opsins and phototransduction. *Philosophical Transactions of the Royal Society B: Biological Sciences*, 364(1531):2881–2895, 2009. ISSN 1471-2970. doi:10.1098/rstb.2009.0051.

[90] Jacobs GH. Evolution of colour vision in mammals. *Philosophical Transactions of the Royal Society B: Biological Sciences*, 364(1531):2957–2967, 2009. ISSN 1471-2970. doi:10.1098/rstb.2009.0039.

[91] Bowmaker JK. Evolution of vertebrate visual pigments. *Vision Research*, 48(20):2022–2041, 2008. ISSN 1878-5646. doi: 10.1016/j.visres.2008.03.025.

[92] Porter ML, Blasic JR, Bok MJ, Cameron EG, Pringle T, Cronin TW, Robinson PR. Shedding new light on opsin evolution. *Proceedings of the Royal Society B: Biological Sciences*, 279(1726):3–14, 2012. ISSN 1471-2954. doi:10.1098/rspb.2011.1819.

[93] Hunt DM, Carvalho LS, Cowing JA, Davies WL. Evolution and spectral tuning of visual pigments in birds and mammals. *Philosophical Transactions of the Royal Society B: Biological Sciences*, 364:2941–2955, 2009. doi:10.1098/rstb.2009.0044.

[94] Zhao H, Ru B, Teeling E, Faulkes C, Zhang S, Rossiter S. Rhodopsin molecular evolution in mammals inhabiting low light environments. *PLoS One*, 4(12):e8326, 2009.

[95] Zhao H, Rossiter S, Teeling E, Li C, Cotton J, Zhang S. The evolution of color vision in nocturnal mammals. *Proceedings of the National Acadamy of Sciences*, 106(22):8980–8985, 2009.

[96] Verrelli BC, Lewis CM, Stone AC, Perry GH. Different selective pressures shape the molecular evolution of color vision in chimpanzee and human populations. *Molecular Biology and Evolution*, 25(12):2735–2743, 2008. ISSN 1537-1719. doi:10.1093/molbev/msn220.

[97] Wang D, Oakley T, Mower J, Shimmin L, Yim S, Honeycutt R, Tsao H, Li W. Molecular evolution of bat color vision genes. *Molecular Biology and Evolution*, 21(2):295–302, 2004.

[98] Shyue S, Hewett-Emmett D, Sperling H, Hunt D, Bowmaker J, Mollon J, Li W. Adaptive evolution of color vision genes in higher primates. *Science*, 269(5228):1265–1267, 1995.

[99] Hunt DM, Cowing JA, Patel R, Appukuttan B, Bowmaker JK, Mollon JD. Sequence and evolution of the blue cone pigment gene in Old and New World primates. *Genomics*, 27(3):535–538, 1995.

[100] Deeb SS, Jorgensen AL, Battisti L, Iwasaki L, Motulsky AG. Sequence divergence of the red and green visual pigments in great apes and humans. *Proceedings of the National Academy of Sciences*, 91(15):7262–7266, 1994. ISSN 0027-8424.

[101] Dulai K, Bowmaker J, Mollon J, Hunt D. Sequence divergence, polymorphism and evolution of the middle-wave and long-wave visual pigment genes of great apes and Old World monkeys. *Vision Research*, 34(19):2483–2491, 1994.

[102] Hunt D, Williams A, Bowmaker J, Mollon J. Structure and evolution of the polymorphic photopigment gene of the marmoset. *Vision Research*, 33(2):147–154, 1993.

[103] Yokoyama S, Yokoyama R. Molecular evolution of human visual pigment genes. *Molecular Biology and Evolution*, 6(2):186–197, 1989.

[104] Hisatomi O, Tokunaga F. Molecular evolution of proteins involved in vertebrate phototransduction• 1. *Comparative Biochemistry and Physiology - Part B: Biochemistry & Molecular Biology*, 133(4):509–522, 2002. ISSN 1096-4959.

[105] Larhammar D, Nordström K, Larsson Ta. Evolution of vertebrate rod and cone phototransduction genes. *Philosophical Transactions of the Royal Society B: Biological Sciences*, 364(1531):2867–80, 2009. ISSN 1471-2970. doi:10.1098/rstb.2009.0077.

[106] Christopher M, Scheetz TE, Mullins RF, Abràmoff MD. Selection of phototransduction genes in *Homo sapiens*. *Investigative Ophthalmology and Visual Science*, 54(8):5489–5496, 2013. doi: 10.1167/iovs.12-11454.

[107] Burns ME, Pugh EN. RGS9 concentration matters in rod phototransduction. *Biophysical Journal*, 97(6):1538–1547, 2009. ISSN 1542-0086. doi:10.1016/j.bpj.2009.06.037.

[108] Gross OP, Pugh EN, Burns ME. Spatiotemporal cGMP dynamics in living mouse rods. *Biophysical Journal*, 102(8):1775–1784, 2012. ISSN 1542-0086. doi:10.1016/j.bpj.2012.03.035.

[109] Swaroop A, Kim D, Forrest D. Transcriptional regulation of photoreceptor development and homeostasis in the mammalian retina. *Nature Reviews Neuroscience*, 11(8):563–576, 2010. ISSN 1471-0048. doi:10.1038/nrn2880.

[110] Yang Z. User Guide PAML : Phylogenetic Analysis by Maximum Likelihood. 2009.

[111] Yang Z. PAML 4: phylogenetic analysis by maximum likelihood. *Molecular Biology and Evolution*, 24(8):1586–1591, 2007. ISSN 0737-4038. doi:10.1093/molbev/msm088.

[112] Plachetzki DC, Degnan BM, Oakley TH. The origins of novel protein interactions during animal opsin evolution. *PLoS One*, 2(10):e1054, 2007. ISSN 1932-6203. doi:10.1371/journal.pone.0001054.

[113] Dall'Olio GM, Bertranpetit J, Laayouni H. The annotation and the usage of scientific databases could be improved with public issue tracker software. *Database*, 2010:baq035, 2010. ISSN 1758-0463. doi:10.1093/database/baq035.

[114] Dall'Olio GM, Marino J, Schubert M, Keys KL, Stefan MI, Gillespie CS, Poulain P, Shameer K, Sugar R, Invergo BM, Jensen LJ, Bertranpetit J, Laayouni H. Ten simple rules for getting help from online scientific communities. *PLoS Computational Biology*, 7(9):e1002202, 2011. ISSN 1553-7358. doi:10.1371/journal.pcbi.1002202.

[115] Comeron JM, Kreitman M, Aguadé M. Natural selection on synonymous sites is correlated with gene length and recombination in Drosophila. *Genetics*, 151(1):239–249, 1999. ISSN 0016-6731.

[116] Locke DP, Hillier LW, Warren WC, Worley KC, Nazareth LV, Muzny DM, Yang SP, Wang Z, Chinwalla AT, Minx P, Mitreva M, Cook L, Delehaunty KD, Fronick C, Schmidt H, Fulton LA,

Fulton RS, Nelson JO, Magrini V, Pohl C, Graves TA, Markovic C, Cree A, Dinh HH, Hume J, Kovar CL, Fowler GR, Lunter G, Meader S, Heger A, Ponting CP, Marques-Bonet T, Alkan C, Chen L, Cheng Z, Kidd JM, Eichler EE, White S, Searle S, Vilella AJ, Chen Y, Flicek P, Ma J, Raney B, Suh B, Burhans R, Herrero J, Haussler D, Faria R, Fernando O, Darré F, Farré D, Gazave E, Oliva M, Navarro A, Roberto R, Capozzi O, Archidiacono N, Della Valle G, Purgato S, Rocchi M, Konkel MK, Walker JA, Ullmer B, Batzer MA, Smit AFA, Hubley R, Casola C, Schrider DR, Hahn MW, Quesada V, Puente XS, Ordoñez GR, López-Otín C, Vinar TT, Brejova B, Ratan A, Harris RS, Miller W, Kosiol C, Lawson HA, Taliwal V, Martins AL, Siepel A, Roychoudhury A, Ma X, Degenhardt J, Bustamante CD, Gutenkunst RN, Mailund T, Dutheil JY, Hobolth A, Schierup MH, Ryder Oa, Yoshinaga Y, de Jong PJ, Weinstock GM, Rogers J, Mardis ER, Gibbs Ra, Wilson RK, Valle GD. Comparative and demographic analysis of orang-utan genomes. *Nature*, 469(7331):529–533, 2011. ISSN 1476-4687. doi:10.1038/nature09687.

[117] Gibbs Ra, Rogers J, Katze MG, Bumgarner R, Weinstock GM, Mardis ER, Remington Ka, Strausberg RL, Venter JC, Wilson RK, Batzer Ma, Bustamante CD, Eichler EE, Hahn MW, Hardison RC, Makova KD, Miller W, Milosavljevic A, Palermo RE, Siepel A, Sikela JM, Attaway T, Bell S, Bernard KE, Buhay CJ, Chandrabose MN, Dao M, Davis C, Delehaunty KD, Ding Y, Dinh HH, Dugan-Rocha S, Fulton La, Gabisi RA, Garner TT, Godfrey J, Hawes AC, Hernandez J, Hines S, Holder M, Hume J, Jhangiani SN, Joshi V, Khan ZM, Kirkness EF, Cree A, Fowler RG, Lee S, Lewis LR, Li Z, Liu YS, Moore SM, Muzny D, Nazareth LV, Ngo DN, Okwuonu GO, Pai G, Parker D, Paul Ha, Pfannkoch C, Pohl CS, Rogers YH, Ruiz SJ, Sabo A, Santibanez J, Schneider BW, Smith SM, Sodergren E, Svatek AF, Utterback TR, Vattathil S, Warren W, White CS, Chinwalla AT, Feng Y, Halpern AL, Hillier LW, Huang X, Minx P, Nelson JO, Pepin KH, Qin X, Sutton GG, Venter E, Walenz BP,

Wallis JW, Worley KC, Yang SP, Jones SM, Marra Ma, Rocchi M, Schein JE, Baertsch R, Clarke L, Csürös M, Glasscock J, Harris RA, Havlak P, Jackson AR, Jiang H, Liu Y, Messina DN, Shen Y, Song HXZ, Wylie T, Zhang L, Birney E, Han K, Konkel MK, Lee J, Smit AFa, Ullmer B, Wang H, Xing J, Burhans R, Cheng Z, Karro JE, Ma J, Raney B, She X, Cox MJ, Demuth JP, Dumas LJ, Han SG, Hopkins J, Karimpour-Fard A, Kim YH, Pollack JR, Vinar T, Addo-Quaye C, Degenhardt J, Denby A, Hubisz MJ, Indap A, Kosiol C, Lahn BT, Lawson Ha, Marklein A, Nielsen R, Vallender EJ, Clark AG, Ferguson B, Hernandez RD, Hirani K, Kehrer-Sawatzki H, Kolb J, Patil S, Pu LL, Ren Y, Smith DG, Wheeler Da, Schenck I, Ball EV, Chen R, Cooper DN, Giardine B, Hsu F, Kent WJ, Lesk A, Nelson DL, O'brien WE, Prüfer K, Stenson PD, Wallace JC, Ke H, Liu XM, Wang P, Xiang AP, Yang F, Barber GP, Haussler D, Karolchik D, Kern AD, Kuhn RM, Smith KE, Zwieg AS. Evolutionary and biomedical insights from the rhesus macaque genome. *Science*, 316(5822):222–234, 2007. ISSN 1095-9203. doi:10.1126/science.1139247.

[118] Rocha EPC, Danchin A. An analysis of determinants of amino acids substitution rates in bacterial proteins. *Molecular Biology and Evolution*, 21(1):108–116, 2004. ISSN 0737-4038. doi:10.1093/molbev/msh004.

[119] Fasick JI, Robinson PR. Mechanism of spectral tuning in the dolphin visual pigments. *Biochemistry*, 37(2):433–438, 1998.

[120] Lin SW, Kochendoerfer GG, Carroll KS, Wang D, Mathies RA, Sakmar TP. Mechanisms of spectral tuning in blue cone visual pigments. Visible and raman spectroscopy of blue-shifted rhodopsin mutants. *The Journal of Biological Chemistry*, 273(38):24583–24591, 1998. ISSN 0021-9258.

[121] Janz JM, Farrens DL. Engineering a functional blue-wavelength-shifted rhodopsin mutant. *Biochemistry*, 40(24):7219–7227, 2001. ISSN 0006-2960.

[122] Takahashi Y, Ebrey TG. Molecular basis of spectral tuning in the newt short wavelength sensitive visual pigment. *Biochemistry*, 42(20):6025–6034, 2003. ISSN 0006-2960. doi:10.1021/bi020629+.

[123] Yokoyama S, Zhang H, Radlwimmer FB, Blow NS. Adaptive evolution of color vision of the Comoran coelacanth (Latimeria chalumnae). *Proceedings of the National Academy of Sciences*, 96(11):6279–6284, 1999. ISSN 0027-8424.

[124] Sun H, Macke JP, Nathans J. Mechanisms of spectral tuning in the mouse green cone pigment. *Proceedings of the National Academy of Sciences*, 94(16):8860–8865, 1997. ISSN 0027-8424.

[125] Fasick JI, Lee N, Oprian DD. Spectral tuning in the human blue cone pigment. *Biochemistry*, 38(36):11593–11596, 1999. ISSN 0006-2960.

[126] Zhang L, Sports CD, Osawa S, Weiss ER. Rhodopsin phosphorylation sites and their role in arrestin binding. *The Journal of Biological Chemistry*, 272(23):14762–14768, 1997. ISSN 0021-9258.

[127] Reiländer H, Achilles A, Friedel U, Maul G, Lottspeich F, Cook NJ. Primary structure and functional expression of the Na/Ca,K-exchanger from bovine rod photoreceptors. *The EMBO Journal*, 11(5):1689–1695, 1992. ISSN 0261-4189.

[128] Murray F, MacLean MR, Pyne NJ. An assessment of the role of the inhibitory gamma subunit of the retinal cyclic GMP phosphodiesterase and its effect on the p42/p44 mitogen-activated protein kinase pathway in animal and cellular models of pulmonary hypertension. *British Journal of Pharmacology*, 138(7):1313–1319, 2003. ISSN 0007-1188. doi:10.1038/sj.bjp.0705190.

[129] Vilella AJ, Severin J, Ureta-Vidal A, Heng L, Durbin R, Birney E. EnsemblCompara GeneTrees: complete, duplication-aware phy-

logenetic trees in vertebrates. *Genome Research*, 19(2):327–335, 2009. ISSN 1088-9051. doi:10.1101/gr.073585.107.

[130] Notredame C, Higgins DG, Heringa J. T-Coffee: a novel method for fast and accurate multiple sequence alignment. *Journal of Molecular Biology*, 302(1):205–217, 2000. ISSN 0022-2836. doi: 10.1006/jmbi.2000.4042.

[131] Talavera G, Castresana J. Improvement of phylogenies after removing divergent and ambiguously aligned blocks from protein sequence alignments. *Systematic Biology*, 56(4):564–577, 2007. ISSN 1063-5157. doi:10.1080/10635150701472164.

[132] Jordan G, Goldman N. The effects of alignment error and alignment filtering on the sitewise detection of positive selection. *Molecular biology and evolution*, 29(4):1125–39, 2012. ISSN 1537-1719. doi:10.1093/molbev/msr272.

[133] Weiss ER, Ducceschi MH, Horner TJ, Li A, Craft CM, Osawa S. Species-specific differences in expression of G-protein-coupled receptor kinase (GRK) 7 and GRK1 in mammalian cone photoreceptor cells: implications for cone cell phototransduction. *Cloning*, 21(23):9175–9184, 2001. ISSN 1529-2401.

[134] Hagberg AA, Schult DA, Swart PJ. Exploring network structure, dynamics, and function using NetworkX. In *Proceedings of the 7th Python in Science Conference*, SciPy, pages 11–15. Los Alamos National Laboratory (LANL), 2008.

[135] Shannon P, Markiel A, Ozier O, Baliga NS, Wang JT, Ramage D, Amin N, Schwikowski B, Ideker T. Cytoscape: a software environment for integrated models of biomolecular interaction networks. *Genome Research*, 13:2498–2504, 2003. doi:10.1101/gr.1239303. metabolite.

[136] Guindon S, Dufayard JF, Lefort V, Anisimova M, Hordijk W, Gascuel O. New algorithms and methods to estimate maximum-likelihood phylogenies: assessing the performance of PhyML 3.0. *Systematic Biology*, 59(3):307–321, 2010. ISSN 1076-836X. doi: 10.1093/sysbio/syq010.

[137] Wong WSW, Yang Z, Goldman N, Nielsen R. Accuracy and power of statistical methods for detecting adaptive evolution in protein coding sequences and for identifying positively selected sites. *Genetics*, 168(2):1041–1051, 2004. ISSN 0016-6731. doi: 10.1534/genetics.104.031153.

[138] Holm S. A simple sequentially rejective multiple test procedure. *Scandinavian Journal of Statistics*, 6(2):65–70, 1979.

[139] R Development Core Team. *R: A Language and Environment for Statistical Computing*. R Foundation for Statistical Computing, Vienna, Austria, 2011. ISBN 3-900051-07-0.

[140] Ames JB, Ishima R, Tanaka T, Gordon JI, Stryer L, Ikura M. Molecular mechanics of calcium-myristoyl switches. *Nature*, 389(6647):198–202, 1997. ISSN 0028-0836. doi:10.1038/38310.

[141] Lange C, Koch KW. Calcium-dependent binding of recoverin to membranes monitored by surface plasmon resonance spectroscopy in real time. *Biochemistry*, 2960(97):12019–12026, 1997.

[142] Kawamura S. Rhodopsin phosphorylation as a mechanism of cyclic GMP phosphodiesterase regulation by S-modulin. *Nature*, 362:855–857, 1993.

[143] Chen CK, Inglese J, Lefkowitz RJ, Hurley JB. Ca-dependent interaction of recoverin with rhodopsin kinase. *The Journal of Biological Chemistry*, 270(30):18060–18066, 1995.

[144] Higgins MK, Oprian DD, Schertler GFX. Recoverin binds exclusively to an amphipathic peptide at the N terminus of rhodopsin

kinase, inhibiting rhodopsin phosphorylation without affecting catalytic activity of the kinase. *The Journal of Biological Chemistry*, 281(28):19426–19432, 2006. ISSN 0021-9258. doi:10.1074/jbc.M602203200.

[145] Komolov KE, Senin II, Kovaleva NA, Christoph MP, Churumova VA, Grigoriev II, Akhtar M, Philippov PP, Koch KW. Mechanism of rhodopsin kinase regulation by recoverin. *Journal of Neurochemistry*, 110(1):72–79, 2009. ISSN 1471-4159. doi:10.1111/j.1471-4159.2009.06118.x.

[146] Hirsch JA, Schubert C, Gurevich VV, Sigler PB. The 2.8 A crystal structure of visual arrestin: a model for arrestin's regulation. *Cell*, 97(2):257–269, 1999. ISSN 0092-8674.

[147] Schubert C, Hirsch JA, Gurevich VV, Engelman DM, Sigler PB, Fleming KG. Visual arrestin activity may be regulated by self-association. *The Journal of Biological Chemistry*, 274(30):21186–21190, 1999. ISSN 0021-9258.

[148] Kiel C, Vogt A, Campagna A, Chatr-aryamontri A, Swiatek-de Lange M, Beer M, Bolz S, Mack AF, Kinkl N, Cesareni G, Serrano L, Ueffing M. Structural and functional protein network analyses predict novel signaling functions for rhodopsin. *Molecular Systems Biology*, 7(551), 2011. ISSN 1744-4292. doi:10.1038/msb.2011.83.

[149] Caruso G, Bisegna P, Andreucci D, Lenoci L, Gurevich VV, Hamm HE, Dibenedetto E. Identification of key factors that reduce the variability of the single photon response. *Proceedings of the National Academy of Sciences*, 108(19):7804–7807, 2011. doi:10.1073/pnas.1018960108/-/DCSupplemental. www.pnas.org/cgi/doi/10.1073/pnas.1018960108.

[150] Holcman D, Korenbrot JI. Longitudinal diffusion in retinal rod and cone outer segment cytoplasm: the consequence of cell structure.

Biophysical Journal, 86(4):2566–2582, 2004. ISSN 0006-3495. doi:10.1016/S0006-3495(04)74312-X.

[151] Dell'Orco D, Koch KW. A dynamic scaffolding mechanism for rhodopsin and transducin interaction in vertebrate vision. *Biochemical Journal*, 440:263–271, 2011.

[152] Dell'Orco D, Koch KW. Systems biochemistry approaches to vertebrate phototransduction: towards a molecular understanding of disease. *Biochemical Society Transactions*, 38(5):1275–1280, 2010. ISSN 1470-8752. doi:10.1042/BST0381275.

[153] Moriondo A, Rispoli G. A step-by-step model of phototransduction cascade shows that Ca2+ regulation of guanylate cyclase accounts only for short-term changes of photoresponse. *Photochem Photobiol Sci.*, 2(12):1292–1298, 2003.

[154] Krispel CM, Chen D, Melling N, Chen YJ, Martemyanov KA, Quillinan N, Arshavsky VY, Wensel TG, Chen CK, Burns ME. RGS expression rate-limits recovery of rod photoresponses. *Neuron*, 51(4):409–416, 2006. ISSN 0896-6273. doi:10.1016/j.neuron.2006.07.010.

[155] Sakurai K, Young JE, Kefalov VJ, Khani SC. Variation in rhodopsin kinase expression alters the dim flash response shut off and the light adaptation in rod photoreceptors. *Investigative Ophthalmology & Visual Science*, 52(9):6793–6800, 2011. ISSN 1552-5783. doi:10.1167/iovs.11-7158.

[156] Pepperberg D, Cornwall M, Kahlert M, Hofmann K, Jin J, Jones G, Ripps H. Light-dependent delay in the falling phase of the retinal rod photoresponse. *Visual Neuroscience*, 8(1):9–18, 1992.

[157] Gross OP, Burns ME. Control of rhodopsin's active lifetime by arrestin-1 expression in mammalian rods. *The Journal of Neuroscience*, 30(9):3450–3457, 2010. ISSN 1529-2401. doi:10.1523/JNEUROSCI.5391-09.2010.

[158] Makino CL, Dodd RL, Chen J, Burns ME, Roca A, Simon MI, Baylor DA. Recoverin regulates light-dependent phosphodiesterase activity in retinal rods. *The Journal of General Physiology*, 123(6):729–741, 2004. ISSN 0022-1295. doi:10.1085/jgp.200308994.

[159] Chen CK, Woodruff ML, Chen FS, Chen D, Fain GL. Background light produces a recoverin-dependent modulation of activated-rhodopsin lifetime in mouse rods. *The Journal of Neuroscience*, 30(4):1213–1220, 2010. doi:10.1523/JNEUROSCI.4353-09.2010.BACKGROUND.

[160] Gray-Keller MP, Polans AS, Palczewski K, Detwiler PB. The effect of recoverin-like calcium-binding proteins on the photoresponse of retinal rods. *Neuron*, 10(3):523–531, 1993. ISSN 0896-6273.

[161] Strissel KJ, Sokolov M, Trieu LH, Arshavsky VY. Arrestin translocation is induced at a critical threshold of visual signaling and is superstoichiometric to bleached rhodopsin. *The Journal of Neuroscience*, 26(4):1146–1153, 2006. ISSN 1529-2401. doi:10.1523/JNEUROSCI.4289-05.2006.

[162] Elias RV, Sezate SS, Cao W, McGinnis JF. Temporal kinetics of the light/dark translocation and compartmentation of arrestin and alpha-transducin in mouse photoreceptor cells. *Molecular Vision*, 10:672–681, 2004. ISSN 1090-0535.

[163] Strissel KJ, Lishko PV, Trieu LH, Kennedy MJ, Hurley JB, Arshavsky VY. Recoverin undergoes light-dependent intracellular translocation in rod photoreceptors. *The Journal of Biological Chemistry*, 280(32):29250–29255, 2005. ISSN 0021-9258. doi:10.1074/jbc.M501789200.

[164] Slepak VZ, Hurley JB. Mechanism of light-induced translocation of arrestin and transducin in photoreceptors: Interaction-restricted diffusion. *IUBMB Life*, 60(1):2–9, 2007. doi:10.1002/iub.7.Mechanism.

[165] Lobanova ES, Finkelstein S, Song H, Tsang SH, Chen CK, Sokolov M, Skiba NP, Arshavsky VY. Transducin translocation in rods is triggered by saturation of the GTPase-activating complex. *The Journal of Neuroscience*, 27(5):1151–1160, 2007. ISSN 1529-2401. doi:10.1523/JNEUROSCI.5010-06.2007.

[166] Kerov V, Chen D, Moussaif M, Chen YJ, Chen CK, Artemyev NO. Transducin activation state controls its light-dependent translocation in rod photoreceptors. *The Journal of Biological Chemistry*, 280(49):41069–41076, 2005. ISSN 0021-9258. doi:10.1074/jbc.M508849200.

[167] Sokolov M, Lyubarsky AL, Strissel KJ, Savchenko AB, Govardovskii VI, Pugh EN, Arshavsky VY. Massive light-driven translocation of transducin between the two major compartments of rod cells: a novel mechanism of light adaptation. *Neuron*, 34(1):95–106, 2002. ISSN 0896-6273.

[168] Buczyłko J, Gutmann C, Palczewski K. Regulation of rhodopsin kinase by autophosphorylation. *Proceedings of the National Academy of Sciences*, 88(6):2568–2572, 1991. ISSN 0027-8424.

[169] Song X, Vishnivetskiy S, Seo J, Chen J, Gurevich E, Gurevich V. Arrestin-1 expression level in rods: balancing functional performance and photoreceptor health. *Neuroscience*, 174:37–49, 2011. ISSN 1873-7544. doi:10.1016/j.neuroscience.2010.11.009.

[170] Vaz AIF, Vicente LN. A particle swarm pattern search method for bound constrained global optimization. *Journal of Global Optimization*, 39(2):197–219, 2007. ISSN 0925-5001. doi:10.1007/s10898-007-9133-5.

[171] Schmidt H, Jirstrand M. Systems Biology Toolbox for MATLAB: a computational platform for research in systems biology. *Bioinformatics*, 22(4):514–515, 2006. ISSN 1367-4803. doi:10.1093/bioinformatics/bti799.

[172] Hindmarsh A, Brown P, Grant K. SUNDIALS: Suite of nonlinear and differential/algebraic equation solvers. *ACM Transactions on Mathematical Software*, 31(3):363–396, 2005.

[173] Matthews G. Spread of the light response along the rod outer segment: An estimate from patch-clamp recordings. *Vision Research*, 26(4):535–541, 1986.

[174] Stephen R, Filipek S, Palczewski K, Sousa MC. Ca^{2+}-dependent Regulation of Phototransduction. *Photochemistry and Photobiology*, 84:903–910, 2008.

[175] Hwang JY, Koch KW. Calcium- and Myristoyl-Dependent Properties of Guanylate Cyclase-Activating Protein-1 and Protein-2. *Biochemistry*, 41:13021–13028, 2002.

[176] Peshenko IV, Olshevskaya EV, Savchenko AB, Karan S, Palczewski K, Baehr W, Dizhoor AM. Enzymatic Ppoperties and regulation of the native isozymes of retinal membrane guanylyl cyclase (RetGC) from mouse photoreceptors. *Biochemistry*, 50(25):5590–5600, 2011. ISSN 0006-2960. doi:10.1021/bi200491b.

[177] Invergo BM, Montanucci L, Koch KW, Bertranpetit J, Dell'orco D. Exploring the rate-limiting steps in visual phototransduction recovery by bottom-up kinetic modeling. *Cell Communication and Signaling*, 11(1):36, 2013. ISSN 1478-811X. doi:10.1186/1478-811X-11-36.

[178] Kolesnikov AV, Fan J, Crouch RK, Kefalov VJ. Age-related deterioration of rod vision in mice. *The Journal of Neuroscience*, 30(33):11222–11231, 2010. ISSN 1529-2401. doi:10.1523/JNEUROSCI.4239-09.2010.

[179] Muradov H, Boyd KK, Artemyev NO. Analysis of PDE6 function using chimeric PDE5/6 catalytic domains. *Vision Research*, 46(6-

7):860–868, 2006. ISSN 0042-6989. doi:10.1016/j.visres.2005.09.015.

[180] Heck M, Hofmann KP. Maximal rate and nucleotide dependence of rhodopsin-catalyzed transducin activation: initial rate analysis based on a double displacement mechanism. *The Journal of Biological Chemistry*, 276(13):10000–10009, 2001. ISSN 0021-9258. doi:10.1074/jbc.M009475200.

[181] Skiba NP, Hopp JA, Arshavsky VY. The effector enzyme regulates the duration of G protein signaling in vertebrate photoreceptors by increasing the affinity between transducin and RGS protein. *The Journal of Biological Chemistry*, 275(42):32716–32720, 2000. ISSN 0021-9258. doi:10.1074/jbc.C000413200.

[182] Koch KW, Stryer L. Highly cooperative feedback control of retinal rod guanylate cyclase by calcium ions. *Nature*, 334:64–66, 1988.

[183] Woodruff ML, Sampath AP, Matthews HR, Krasnoperova NV, Lem J, Fain GL. Measurement of cytoplasmic calcium concentration in the rods of wild-type and transducin knock-out mice. *The Journal of Physiology*, 542(3):843–854, 2002. ISSN 0022-3751. doi:10.1113/jphysiol.2001.013987.

[184] Burns ME, Mendez A, Chen J, Baylor DA. Dynamics of cyclic GMP synthesis in retinal rods. *Neuron*, 36(1):81–91, 2002. ISSN 0896-6273.

[185] Caruso G, Bisegna P, Lenoci L, Andreucci D, Gurevich VV, Hamm HE, DiBenedetto E. Kinetics of rhodopsin deactivation and its role in regulating recovery and reproducibility of rod photoresponse. *PLoS Computational Biology*, 6(12):e1001031, 2010. ISSN 1553-7358. doi:10.1371/journal.pcbi.1001031.

[186] Olson-Manning CF, Lee CR, Rausher MD, Mitchell-Olds T. Evolution of flux control in the glucosinolate pathway in Arabidopsis

thaliana. *Molecular Biology and Evolution*, 30(1):14–23, 2013. ISSN 1537-1719. doi:10.1093/molbev/mss204.

[187] Colombo M, Laayouni H, Invergo BM, Bertranpetit J, Montanucci L. Metabolic flux is a determinant of the evolutionary rates of enzyme-encoding genes. *Evolution*, 2013. doi:10.1111/evo.12262.

[188] Chelliah V, Laibe C, Novère NL. Biomodels database: A repository of mathematical models of biological processes. *Methods Mol Biol*, 1021:189–199, 2013.

[189] Jelier R, Semple JI, Garcia-Verdugo R, Lehner B. Predicting phenotypic variation in yeast from individual genome sequences. *Nature Genetics*, 43(12):1270–1274, 2011. ISSN 1546-1718. doi: 10.1038/ng.1007.

[190] Cheever ML, Snyder JT, Gershburg S, Siderovski DP, Harden TK, Sondek J. Crystal structure of the multifunctional Gβ5-RGS9 complex. *Nature Structural & Molecular Biology*, 15(2):155–162, 2008. ISSN 1545-9985. doi:10.1038/nsmb.1377.

[191] Krispel CM, Chen CK, Simon MI, Burns ME. Prolonged photoresponses and defective adaptation in rods of G$\beta5^{-/-}$ mice. *The Journal of Neuroscience*, 23(18):6965–6971, 2003. ISSN 1529-2401.

[192] Hooks SB, Harden TK. Purification and *in vitro* functional analysis of R7 subfamily RGS proteins in complex with Gβ5. *Methods in Enzymology*, 390:163–177, 2004.

[193] Rao A, Dallman R, Henderson S, Chen CK. Gβ5 is required for normal light responses and morphology of retinal ON-bipolar cells. *The Journal of Neuroscience*, 27(51):14199–14204, 2007. ISSN 1529-2401. doi:10.1523/JNEUROSCI.4934-07.2007.

[194] The International HapMap 3 Consortium. Integrating common and rare genetic variation in diverse human populations. *Nature*, 467(7311):52–58, 2010. ISSN 1476-4687. doi:10.1038/nature09298.

[195] The 1000 Genomes Project Consortium. A map of human genome variation from population-scale sequencing. *Nature*, 467(7319):1061–1073, 2010. ISSN 1476-4687. doi:10.1038/nature09534.

[196] Costanzo M, Baryshnikova A, Bellay J, Kim Y, Spear ED, Sevier CS, Ding H, Koh JLY, Toufighi K, Mostafavi S, Prinz J, St Onge RP, VanderSluis B, Makhnevych T, Vizeacoumar FJ, Alizadeh S, Bahr S, Brost RL, Chen Y, Cokol M, Deshpande R, Li Z, Lin ZY, Liang W, Marback M, Paw J, San Luis BJ, Shuteriqi E, Tong AHY, van Dyk N, Wallace IM, Whitney Ja, Weirauch MT, Zhong G, Zhu H, Houry Wa, Brudno M, Ragibizadeh S, Papp B, Pál C, Roth FP, Giaever G, Nislow C, Troyanskaya OG, Bussey H, Bader GD, Gingras AC, Morris QD, Kim PM, Kaiser Ca, Myers CL, Andrews BJ, Boone C. The genetic landscape of a cell. *Science*, 327(5964):425–431, 2010. ISSN 1095-9203. doi:10.1126/science.1180823.

[197] Schlosser G, Wagner GP. A simple model of co-evolutionary dynamics caused by epistatic selection. *Journal of Theoretical Biology*, 250(1):48–65, 2008. ISSN 0022-5193. doi:10.1016/j.jtbi.2007.08.033.

[198] Lehner B. Genotype to phenotype: lessons from model organisms for human genetics. *Nature Reviews Genetics*, 14(3):168–178, 2013. ISSN 1471-0064. doi:10.1038/nrg3404.

[199] Kang K, Bauer PJ, Kinjo TG, Szerencsei RT, Bönigk W, Winkfein RJ, Schnetkamp PPM. Assembly of retinal rod or cone Na(+)/Ca(2+)-K(+) exchanger oligomers with cGMP-gated channel subunits as probed with heterologously expressed cDNAs.

Biochemistry, 42(15):4593–4600, 2003. ISSN 0006-2960. doi: 10.1021/bi027276z.

[200] Poetsch A, Molday LL, Molday RS. The cGMP-gated channel and related glutamic acid-rich proteins interact with peripherin-2 at the rim region of rod photoreceptor disc membranes. *The Journal of Biological Chemistry*, 276(51):48009–48016, 2001.

[201] Peng C, Rich ED, Varnum MD. Subunit Configuration of Heteromeric Cone Cyclic Nucleotide-Gated Channels. *Neuron*, 42(3):401–410, 2004.

[202] Chen TY, Illing M, Molday LL, Hsu YT, Yau KW, Molday RS. Subunit 2 (or beta) of retinal rod cGMP-gated cation channel is a component of the 240-kDa channel-associated protein and mediates Ca(2+)-calmodulin modulation. *Proceedings of the National Academy of Sciences*, 91(24):11757–11761, 1994. ISSN 0027-8424.

[203] Zheng J, Trudeau MC, Zagotta WN. Rod cyclic nucleotide-gated channels have a stoichiometry of three CNGA1 subunits and one CNGB1 subunit. *Neuron*, 36(5):891–896, 2002. ISSN 0896-6273.

[204] Körschen HG, Beyermann M, Müller F, Heck M, Vantler M, Koch KW, Kellner R, Wolfrum U, Bode C, Hofmann KP, Kaupp UB. Interaction of glutamic-acid-rich proteins with the cGMP signalling pathway in rod photoreceptors. *Nature*, 400(6746):761–766, 1999. ISSN 0028-0836. doi:10.1038/23468.

[205] Kerov VS, Natochin M, Artemyev NO. Interaction of transducin-α with LGN, a G-protein modulator expressed in photoreceptor cells. *Molecular and Cellular Neuroscience*, 28:485–495, 2005.

[206] Guo L, Hajipour A, Ruoho A. Complementary interactions of the rod PDE6 inhibitory subunit with the catalytic subunits and transducin. *Journal of Biological Chemistry*, 285(20):15209–15219, 2010.

[207] Antonny B, Otto-Bruc A, Chabre M, Vuong TM. GTP hydrolysis by purified alpha-subunit of transducin and its complex with the cyclic GMP phosphodiesterase inhibitor. *Biochemistry*, 32(33):8646–8653, 1993. ISSN 0006-2960.

[208] Zhu X, Brown B, Li A, Mears AJ, Swaroop A, Craft CM. GRK1-dependent phosphorylation of S and M opsins and their binding to cone arrestin during cone phototransduction in the mouse retina. *The Journal of Neuroscience*, 23(14):6152–6160, 2003. ISSN 1529-2401.

[209] Lerea C, Bunt-Milam A, Hurley J. Alpha transducin is present in blue-, green-, and red-sensitive cone photoreceptors in the human retina. *Neuron*, 3(3):367–376, 1989.

[210] Lerea C, Somers D, Hurley J, Klock I, Bunt-Milam A. Identification of specific transducin alpha subunits in retinal rod and cone photoreceptors. *Science*, 234(4772):77–80, 1986.

[211] Lee R, Lieberman B, Yamane H, Bok D, Fung B. A third form of the G protein beta subunit. 1. Immunochemical identification and localization to cone photoreceptors. *Journal of Biological Chemistry*, 267(34):24776–24781, 1992.

[212] Ong O, Yamane H, Phan K, Fong H, Bok D, Lee R, Fung B. Molecular cloning and characterization of the G protein gamma subunit of cone photoreceptors. *Journal of Biological Chemistry*, 270(15):8495–8500, 1995.

[213] Pfister C, Chabre M, Plouet J, Tuyen V, De Kozak Y, Faure J, Kühn H. Retinal S antigen identified as the 48K protein regulating light-dependent phosphodiesterase in rods. *Science*, 228(4701):891–893, 1985.

[214] Palczewski K, McDowell JH, Hargrave PA. Rhodopsin kinase: substrate specificity and factors that influence activity. *Biochemistry*, 27(7):2306–2313, 1988. ISSN 0006-2960.

[215] Fung B, Hurley J, Stryer L. Flow of information in the light-triggered cyclic nucleotide cascade of vision. *Proceedings of the National Academy of Sciences*, 78(1):152–156, 1981.

[216] Moritz OL, Molday RS. Molecular cloning, membrane topology, and localization of bovine rom-1 in rod and cone photoreceptor cells. *Investigative Ophthalmology & Visual Science*, 37(2):352–362, 1996. ISSN 0146-0404.

[217] Chen F, Ng PS, Faull KF, Lee RH. Cone photoreceptor $\beta\gamma$-transducin: posttranslational modification and interaction with phosducin. *Investigative Ophthalmology & Visual Science*, 44(11):4622–4629, 2003. ISSN 0146-0404. doi:10.1167/iovs.03-0420.

[218] Kuo C, Taniura H, Watanabe Y, Fukada Y, Yoshizawa T, Miki N. Identification of a retina-specific MEKA protein as a 33 K protein. *Biochemical and Biophysical Research Communications*, 162(3):1063–1068, 1989.

[219] Gillespie PG, Beavo JA. Characterization of a bovine cone photoreceptor phosphodiesterase purified by cyclic GMP-sepharose chromatography. *The Journal of Biological Chemistry*, 263(17):8133–8141, 1988. ISSN 0021-9258.

[220] Hurwitz RL, Bunt-Milam AH, Chang ML, Beavo JA. cGMP phosphodiesterase in rod and cone outer segments of the retina. *The Journal of Biological Chemistry*, 260(1):568–573, 1985. ISSN 0021-9258.

[221] Deterre P, Bigay J, Forquet F, Robert M, Chabre M. cGMP phosphodiesterase of retinal rods is regulated by two inhibitory subunits. *Proceedings of the National Academy of Sciences*, 85(8):2424–2428, 1988. ISSN 0027-8424.

[222] Hurley JB, Stryer L. Purification and characterization of the gamma regulatory subunit of the cyclic GMP phosphodiesterase

from retinal rod outer segments. *The Journal of Biological Chemistry*, 257(18):11094–11099, 1982. ISSN 0021-9258.

[223] Yu QM, Cheng ZJ, Gan XQ, Bao GB, Li L, Pei G. The amino terminus with a conserved glutamic acid of G protein-coupled receptor kinases is indispensable for their ability to phosphorylate photoactivated rhodopsin. *Journal of Neurochemistry*, 73(3):1222–1227, 1999. ISSN 0022-3042.

[224] Rosenzweig DH, Nair KS, Levay K, Peshenko IV, Crabb JW, Dizhoor AM, Slepak VZ. Interaction of retinal guanylate cyclase with the α subunit of transducin: potential role in transducin localization. *Biochemical Journal*, 417:803–812, 2009. doi: 10.1042/BJ20081513.

[225] Koch KW, Duda T, Sharma RK. Photoreceptor specific guanylate cyclases in vertebrate phototransduction. *Molecular and Cellular Biochemistry*, 230(1):97–106, 2002.

[226] Yu H, Bondarenko VA, Yamazaki A. Inhibition of retinal guanylyl cyclase by the RGS9-1 N-terminus. *Biochemical and Biophysical Research Communications*, 286(1):12–19, 2001. ISSN 0006-291X. doi:10.1006/bbrc.2001.5346.

[227] Seno K, Kishigami A, Ihara S, Maeda T, Bondarenko V, Nishizawa Y, Usukura J, Yamazaki A, Hayashi F. A possible role of RGS9 in phototransduction. A bridge between the cGMP-phosphodiesterase system and the guanylyl cyclase system. *The Journal of Biological Chemistry*, 273(35):22169–22172, 1998.

[228] Hu G, Wensel T. R9AP, a membrane anchor for the photoreceptor GTPase accelerating protein, RGS9-1. *Proceedings of the National Academy of Sciences*, 99(15):9755–9760, 2002.

[229] Makino E, Handy J, Li T, Arshavsky V. The GTPase activating factor for transducin in rod photoreceptors is the complex between

RGS9 and type 5 G protein beta subunit. *Proceedings of the National Academy of Sciences*, 96(5):1947–1952, 1999.

[230] He W, Cowan C, Wensel T. RGS9, a GTPase accelerator for phototransduction. *Neuron*, 20(1):95–102, 1998.

[231] Slep KC, Kercher MA, He W, Cowan CW, Wensel TG, Sigler PB. Structural determinants for regulation of phosphodiesterase by a G protein at 2.0Å. *Nature*, 409(6823):1071–1077, 2001.

[232] Melia TJ, Cowan CW, Angleson JK, Wensel TG. A comparison of the efficiency of G protein activation by ligand-free and light-activated forms of rhodopsin. *Biophysical Journal*, 73(6):3182–3191, 1997. ISSN 0006-3495. doi:10.1016/S0006-3495(97)78344-9.

[233] Firsov ML, Kolesnikov AV, Golobokova EY, Govardovskii VI. Two realms of dark adaptation. *Vision Research*, 45(2):147–151, 2005. ISSN 0042-6989. doi:10.1016/j.visres.2004.08.005.

[234] Xu J, Dodd RL, Makino CL, Simon MI, Baylor DA, Chen J. Prolonged photoresponses in transgenic mouse rods lacking arrestin. *Nature*, 389:505–509, 1997.